จลนพลศาสตร์การย่อยสลายของ 2,6-ไดเมทิล-อนิลีนและการสร้างผลึกเหล็ก
ในกระบวนการฟลูอิดไดซ์เบดเฟนตัน

นางสาวนงลักษณ์ บุญรัตนกิจ

KINETICS OF 2,6-DIMETHYL-ANILINE DEGRADATION AND IRON
CRYSTALLIZATION IN FLUIDIZED-BED FENTON PROCESS

Miss Nonglak Boonrattanakij

A Dissertation Submitted in Partial Fulfillment of the Requirements
for the Degree of Doctor of Philosophy Program in Environmental Management
(Interdisciplinary Program)
Graduate School
Chulalongkorn University
Academic Year 2009

Thesis Title   Kinetics of 2,6-Dimethyl-aniline Degradation and Iron Crystallization
                    in Fluidized-bed Fenton Process
By   Miss Nonglak Boonrattanakij
Field of Study   Environmental Management
Thesis Advisor   Associate Professor Jin Anotai, Ph.D.
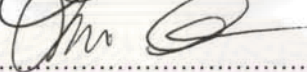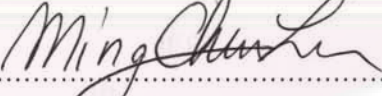Thesis Co-Advisor   Professor Ming-Chun Lu, Ph.D.

_____

Accepted by the Graduate School, Chulalongkorn University in Partial
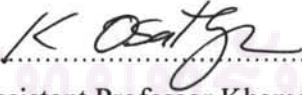Fulfillment of the Requirements for the Doctoral Degree

.... Dean of the Graduate School
(Associate Professor Pornpote Piumsomboon, Ph.D.)

THESIS COMMITTEE

.... Chairman
(Assistant Professor Manaskorn Rachakornkij, Ph.D.)

.... Thesis Advisor
(Associate Professor Jin Anotai, Ph.D.)

.... Thesis Co-Advisor
(Professor Ming-Chun Lu, Ph.D.)

.... Examiner
(Assistant Professor Khemarath Osathaphan, Ph.D.)

.... Examiner
(Assistant Professor Chakkaphan Sutthirat, Ph.D.)

.... External Examiner
(Associate Professor Duangrat Inthorn, Ph.D.)

นงลักษณ์ บุญรัตนกิจ : จลนพลศาสตร์การย่อยสลายของ 2,6-ไดเมทิล-อนิลีนและการสร้างผลึกเหล็กใน
กระบวนการฟลูอิดไดซ์เบดเฟนตัน (KINETICS OF 2,6-DIMETHYL-ANILINE DEGRADATION
AND IRON CRYSTALLIZATION IN FLUIDIZED-BED FENTON PROCESS) อ.ที่ปรึกษา
วิทยานิพนธ์หลัก: รศ.ดร.จินต์ อโณทัย, อ.ที่ปรึกษาวิทยานิพนธ์ร่วม: Prof. Ming-Chum Lu, Ph.D.,
177 หน้า.

งานวิจัยนี้ศึกษาหาค่าคงที่อัตราปฏิกิริยาระหว่าง 2,6-ไดเมทิล-อนิลีนและอนุมูลอิสระไฮดรอกซิลโดย
กระบวนการเฟนตันและเทคนิคจลนพลศาสตร์แข่งขัน ผลการทดลองพบว่าค่าคงที่อัตราปฏิกิริยาอันดับที่ 2 ระหว่าง
2,6-ไดเมทิล-อนิลีนกับอนุมูลอิสระไฮดรอกซิลที่ได้จากการทดลองภายใต้สภาวะต่างกันไม่ว่าเป็นแบบกะหรือ
แบบต่อเนื่อง มีหรือไม่มีตัวกลาง โดยปฏิกรณ์กวนสมบูรณ์หรือปฏิกรณ์ฟลูอิดไดซ์เบด มีค่าใกล้เคียงกันอยู่ในช่วง
1.59×10^{10} ถึง 1.80×10^{10} โมล่าร์$^{-1}$วินาที$^{-1}$ โดยมีค่าเฉลี่ยและช่วงความเชื่อมั่นที่ร้อยละ 95 เท่ากับ $1.70\pm0.04\times10^{10}$
โมล่าร์$^{-1}$วินาที$^{-1}$ สารกลางอะโรมาติคที่เกิดจากการออกซิเดชันของ 2,6-ไดเมทิล-อนิลีนด้วยอนุมูลอิสระไฮดรอก
ซิลประกอบด้วย 2,6-ไดเมทิล-ไนโตรเบนซิน, 2,6-ไดเมทิล-ฟีนอล, 2,6-ไดเมทิล-ไนโตรฟีนอล, 2,6-ไดเมทิล-ไฮโดร
ควิโนน, 2,6-ไดเมทิล-เบนโซควิโนน, 2,6-ไดเมทิล-3-ไฮดรอกซี-เบนโซควิโนน ชี้ให้เห็นว่าหมู่ฟังก์ชันเมทิลที่เกาะ
อยู่บนวงเบนซินมีความไวปฏิกิริยากับอนุมูลอิสระไฮดรอกซิลต่ำกว่าหมู่ฟังก์ชันอะมิโนและหมู่ฟังก์ชันไฮดรอก
ไซด์ ส่วนสารกลางกลุ่มคาร์บอกซิลิกที่พบประกอบด้วยกรดมาเลอิค กรดแลคติค กรดออกซาลิค กรดอะซิติค และ
กรดฟอร์มิค กลไกการออกซิเดชัน 2,6-ไดเมทิล-อนิลีนด้วยอนุมูลอิสระไฮดรอกซิลได้ถูกนำเสนอไว้เช่นกัน

เมื่อพิจารณาถึงการสร้างผลึกของเหล็กพบว่าเฟอร์รัสจะถูกเปลี่ยนเป็นเฟอริคทันทีหลังจากเกิดปฏิกิริยาเฟน
ตันและเฟอริคจะตกตะกอนในรูปเฟอริคไฮดรอกไซด์อย่างรวดเร็ว เนื่องจากความสามารถในการละลายน้ำต่ำ
ถึงแม้ว่าจะอยู่ในสภาวะที่เป็นกรดก็ตาม อย่างไรก็ดีถ้าการตกผลึกของเหล็กเกิดขึ้นในโซนไม่คงตัว การสร้างผลึก
ของเฟอริคไฮดรอกไซด์จะผ่านกลไกการสร้างนิวเคลียสแบบเนื้อเดียวและเกิดการเคลือบที่ผิวของตัวกลางใน
ปฏิกรณ์ฟลูอิดไดซ์เบดช้ามาก ในทางกลับกันหากการตกผลึกเกิดขึ้นในโซนกึ่งคงตัว ผลึกของเฟอริคไฮดรอกไซด์
จะถูกสร้างผ่านกลไกการสร้างนิวเคลียสแบบเนื้อผสมและเคลือบบนผิวของตัวกลางในปฏิกรณ์ฟลูอิดไดซ์เบดเร็ว
ขึ้น ซึ่งจะทำให้เหล็กถูกแยกออกจากน้ำได้อย่างมีนัยสำคัญ การตกผลึกถูกควบคุมด้วยขั้นตอนการเคลื่อนที่มากกว่า
ที่จะเป็นขั้นตอนการปฏิสัมพันธ์ที่ผิว อัตราการสร้างผลึกสามารถอธิบายได้ด้วยการรวมตัวแบบออโธไคเนติคฟล็อค
คูเลชันเมื่อมีการกวนผสมอย่างเพียงพอ อย่างไรก็ตามในสภาวะนิ่งที่ไม่มีการกวนผสม อัตราการสร้างผลึกจะอยู่
ภายใต้อิทธิพลของการแพร่แบบโมเลกุลหรือการรวมตัวแบบเพอริไคเนติคฟล็อคคูเลชันโดยขึ้นอยู่กับขนาดของ
คริสตอลไลท์ สารกลางอินทรีย์ที่สามารถสร้างสารประกอบเชิงซ้อนกับเฟอร์ริคได้จะเพิ่มความสามารถในการ
ละลายของเฟอร์ริค ทำให้รบกวนกระบวนการสร้างผลึก นอกจากนี้ยังพบว่าอัตราการสร้างผลึกบนตัวกลางลดลง
ตามเวลา จึงจำเป็นต้องมีการทดแทนตัวกลางที่ถูกเคลือบแล้วด้วยตัวกลางใหม่เพื่อให้อัตราการสร้างผลึกคงที่ ทราย
ที่ถูกเคลือบด้วยเฟอริคไฮดรอกไซด์ที่มีเหล็กร้อยละ 3.5 โดยน้ำหนักมีคะตะไลติกแอคติวิตี้เพียงร้อยละ 4 ของโก
อีไธท์

สาขาวิชาการจัดการสิ่งแวดล้อม   ลายมือชื่อนิสิต Jonglak B.
ปีการศึกษา 2552   ลายมือชื่ออาจารย์ที่ปรึกษาวิทยานิพนธ์หลัก
            ลายมือชื่ออาจารย์ที่ปรึกษาวิทยานิพนธ์ร่วม

5087809220: MAJOR ENVIRONMENTAL MANAGEMENT
KEYWORDS: ADVANCED OXIDATION PROCESSES/ HYDROXYL RADICALS/ COMPETITIVE KINETICS/ IRON CRYSTALLIZATION/ 2,6-DIMETHYL-ANILINE

NONGLAK BOONRATTANAKIJ: KINETICS OF 2,6-DIMETHYL-ANILINE DEGRADATION AND IRON CRYSTALLIZATION IN FLUIDIZED-BED FENTON PROCESS. THESIS ADVISOR: ASSOC. PROF. JIN ANOTAI, Ph.D., THESIS CO-ADVISOR: PROF. MING-CHUN LU, Ph.D., 177 pp.

This research determined the rate constant between 2,6-dimethy-aniline (2,6-DMA) and hydroxyl radicals (OH$^\bullet$) by using Fenton reaction and competitive kinetics technique. Regardless of experimental conditions either batch or continuous mode, presence or absence of media, complete suspension or fluidized-bed reactor, the intrinsic 2nd-order rate constant between 2,6-DMA and OH$^\bullet$ were found to be consistent in between 1.59×10^{10} and 1.80×10^{10} M^{-1}sec^{-1} with the average and 95% confidence interval of $1.70 \pm 0.04 \times 10^{10}$ M^{-1}sec^{-1}. Aromatic intermediates from 2,6-DMA oxidation by OH$^\bullet$ were 2,6-dimethyl-nitrobenzene, 2,6-dimethy-phenol, 2,6-dimethyl-nitrophenol, 2,6-dimethyl-hydroquinone, 2,6-dimethyl-benzoquinone, and 2,6-dimethyl-3-hydroxy-benzoquinone indicating the methyl groups on the benzene ring were less susceptible to OH$^\bullet$ attack than the amino and hydroxide groups. Maleic, lactic, oxalic, acetic, and formic acids were also identified as the carboxylic intermediates. Degradation mechanism of 2,6-DMA oxidation by OH$^\bullet$ was also proposed.

Considering iron crystallization, it was found that ferrous (Fe^{2+}) was immediately transformed to ferric (Fe^{3+}) after the initiation of Fenton reaction and sequentially precipitated out in the form of Fe(OH)$_3$ due to its low solubility even in the acidic solution. However, if precipitation occurred in the labile zone, Fe(OH)$_3$ was formed via homogeneous nucleation and crystallized very slowly onto the fluidized media. On the other hand, if it happened in the metastable zone, Fe(OH)$_3$ crystallized onto the fluidized media more rapidly via heterogeneous nucleation and iron was removed significantly from the aqueous phase. Crystallization was controlled by the transport step rather than the surface interaction step. Rate of crystal growth followed the orthokinetic flocculation when the mixing was sufficiently provided; however, it became under the influence of molecular diffusion or perikinetic flocculation depending on the crystallite size under the stagnant conditions. Presence of organic intermediates which could form complex with Fe^{3+} increased the solubility of Fe^{3+} and sequentially deteriorated the crystallization process. Crystallization rate onto fluidized media decreased with time; thus, continuously replace certain portion of coated solids with fresh media will maintain satisfactory crystallization rate. Catalytic activity of the Fe(OH)$_3$-coated sand with 3.5% iron content by weight was only equivalent to 4% of the goethite.

Field of Study: Environmental Management   Student's Signature..........Nonglak B.........

Academic Year 2009   Advisor's Signature............................

Co-Advisor's Signature............................

ACKNOWLEDGEMENTS

CONTENTS

LIST OF TABLES

Table   **Page**

.

LIST OF FIGURES

Figure   **Page**

NOMENCLATURES

AN	=	aniline
AOPs	=	advanced oxidation processes
CS	=	construction sand
2,6-DMA	=	2,4-dimethyl--aniline
n,n-DMA	=	n,n-dimethyl-aniline
2,6-DMB	=	2,6-dimethyl-benzoquinone
2,6-DMH	=	2,6-dimethyl-hydroquinone
2,6-DMN	=	2,6-dimethyl-nitrobenzene
2,6-DMP	=	2,6-dimethyl-phenol
M	=	molar
OT	=	*o*-toluidine
hr	=	hour
k	=	rate constant
mg/l	=	milligram/liter
min	=	minute
mM	=	millimolar
ml	=	milliliter
μm	=	micrometer

CHAPTER I
INTRODUCTION

1.1 Research Rationale

Nowadays, several chemicals which are highly persistent in the environment have been synthesized and used intensively and become hazardous wastes afterward. These chemicals cannot be degraded by traditional treatment processes due to their toxic and refractory property. Variation in the chemical composition leads to a need to develop a special and specific treatment method for each persistent pollutant. One group of the pollutants that is typically persistent and needs advanced treatment is the aromatic compounds.

2,6-dimethyl-aniline (2,6-DMA) is a metabolite of the xylidine group of anesthetics including lidocaine and can also be produced by the reduction of certain azo dyes by intestinal microflora. It may also enter the environment through degradation of certain pesticides. 2,6-DMA has been commercially produced and widely used as a chemical intermediate to produce many products such as pesticides, dyestuffs, antioxidants, pharmaceuticals and other products. 2,6-DMA-contaminated wastewaters from these manufacturers can pose adverse impacts in receiving waters due to its biorefractory and highly toxic properties. 2,6-DMA has been classified by International Agency for Research on Cancer (IARC) as group 2B carcinogens. As a result, appropriate and effective treatment technologies are needed to purify or clean up these contaminated wastewaters prior to discharge to the environment.

Advanced oxidation processes (AOPs) are one of the possible alternatives which can provide the destruction of refractory and hazardous organic compounds. Hydroxyl radicals (OH$^{\bullet}$), generated in the AOPs, are extremely reactive, short lived and unselective transient species which can readily oxidize organic/inorganic pollutants in water and wastewater and convert them into simple, relatively harmless substances. A number of methods can lead to the generation of OH$^{\bullet}$ including

H_2O_2/UV, O_3/H_2O_2, O_3/UV, TiO_2/UV, and Fenton's family which is of interest in this research.

Fenton process has been intensively studied for the treatment of biorefractory organic contaminants in aqueous waste streams, soils, and groundwater. The Fenton process is normally initiated by the addition of ferrous (Fe^{2+}) and hydrogen peroxide (H_2O_2) so called "Fenton's reagent". Conventional Fenton process is typically simple and effective, and requires no costly capital investment. It has been proven to be effective in treating various organic contaminants such as nitrophenol, dye, aromatic amines, polycyclic aromatic, ethers, and photographic wastewater (Ewa et al., 1991). The Fenton's reagent as an oxidant for wastewater treatment is attractive due to the facts that iron is a highly abundant and non-toxic element and H_2O_2 is easy to handle and kindly environmental making (Munter, 2001; Pignatello, 1992). This reaction is typically performed under an acidic condition to raise the iron solubility and to enhance the oxidative character of the $OH^\bullet$. A neutralization step is required after treatment to eliminate ferric ions by hydroxide precipitation and to comply with the effluent standard. This neutralization step can generate an enormous amount of ferric hydroxide sludge which requires further separation and disposal. The use of fluidized-bed reactor can overcome or lessen this problem. Ferric ions resulted from the Fenton reaction can precipitate and crystallize onto the carriers' surface; hence, significantly reducing the formation of iron puffy sludge (Chou and Huang, 1999). In addition, it was also found that these crystallized iron oxides could catalyze the decomposition of H_2O_2 to generate $OH^\bullet$ which further enhancing the removal of pollutant (Lin and Gurol, 1998).

Although the oxidation of 2,6-DMA by $OH^\bullet$ has been investigated previously by Ting et al. (2009) and Masomboon et al (2010), no intrinsic kinetic rate constant of the reaction between 2,6-DMA and $OH^\bullet$ have been reported. This constant is a very important and useful scientific and engineering parameter and is deserved to be investigated. As a result, this research project focused on the determination of the intrinsic second-order rate constant between 2,6-DMA and $OH^\bullet$. In addition, this research also characterize the iron crystallization onto the carriers in a fluidized-bed reactor in order to provide a better understanding on iron removal mechanism in the fluidized-bed Fenton process which is very valuable in field practice.

1.2 Objectives

The main objectives of this study are:

1. To characterize the kinetics of 2,6-DMA oxidation by OH$^\bullet$ using Fenton and fluidized-bed Fenton processes.
2. To characterize the iron precipitation and crystallization in the fluidized-bed Fenton process.

The first objective led to the determination of the intrinsic kinetic rate constant between 2,6-DMA and OH$^\bullet$ and the oxidation pathway of 2,6-DMA. The second objective provided the fundamental understanding on the characteristics of iron crystallization onto the carrier's surface in the fluidized-bed Fenton process as well as the catalytic ability of iron-coated media on H_2O_2 decomposition to generate OH$^\bullet$.

1.3 Hypotheses

1. Oxidation of 2,6-DMA by OH$^\bullet$ is a second-order reaction.
2. 2,6-Dimethyl-aniline decomposition by ordinary and fluidized-bed Fenton processes depends on system pH and chemical dosages.
3. Metal oxide can effectively serve as a medium for iron crystallization in the fluidized-bed Fenton process.
4. Iron concentration as well as 2,6-DMA and its intermediates have an effect on iron crystallization in fluidized-bed Fenton process.

1.4 Scope of the Research

1. Using lab scale reactors of 1.35 liter for the fluidized-bed Fenton and 0.5 liter for the ordinary Fenton.
2. Using a synthetic wastewater.
3. For the fluidized-bed Fenton process, the carriers were either silica dioxide, aluminum oxide, or construction sand.
4. Working at 25°C under room condition.
5. Operating in both batch and continuous modes.

1.5 Obtained Results

1. Intrinsic kinetic rate constant for 2,6-DMA oxidation by OH$^\bullet$.

2. Intermediates and pathway of 2,6-DMA oxidation by OH$^\bullet$.

3. Characteristics of iron crystallization onto the carriers' surface in the fluidized-bed Fenton process.

4. Catalytic ability of iron-coated media on H_2O_2 decomposition to generate OH$^\bullet$.

CHAPTER II
THEORIES AND LITERATURE REVIEWS

2.1 2,6-Dimethyl-aniline

2.1.1 General Information

2,6-dimethyl-aniline (2,6-DMA) is one of the six dimethyl-aniline isomers of which their molecular formula are $(CH_3)_2C_6H_3NH_2$. 2,6-dimethyl-aniline has two methyl groups positioned on both sides of the amino group on the benzene ring (at both ortho-positions) as shown in Figure 2.1. 2,6-dimethyl-aniline can be either obtained as a by-product in the fractional distillation of the coal tar or synthesized by heating aniline hydrochloride with methanol at 220 °C. Furthermore, 2.6-DMA is a metabolite of the xylidine group of anaesthetics including lidicaine and is produced by the reduction of certain azo dyes by intestinal microflora. It may also enter the environment through degradation of certain pesticides. 2,6-dimethyl-aniline is an aniline homologue and has similar properties of aromatic amine. 2,6-dimethyl-aniline is sparingly soluble in water but miscible with ethanol and diethyl ether and is sensitive to air and light and tends to darken on storage. 2,6-dimethyl-aniline is used to manufacture many products including pesticides, dyestuffs, antioxidants, pharmaceuticals and other products.

2,6-dimethyl-aniline damages hemoglobin, a protein that normally transports oxygen in the blood, so that oxygen cannot be transported to cells and tissues causing them to lack oxygen for their metabolisms. This condition is known as "methemoglobinemia". Methaemoglobinemia causes headache, cardiac arrhythmia, blood pressure drop, dyspnoea, spasms, and cyanosis (blue coloration of the blood). Sensitization with allergic manifestations in predisposed persons. Direct contact with 2,6-DMA can also produce skin and eye irritation. 2,6-dimethyl-aniline is released into the environmental primarily from industrial uses, and may cause long-term adverse effects in the aquatic environment (NTP, 2002).
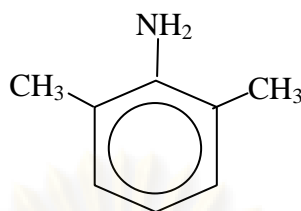
Figure 2.1 Structure of 2,6-DMA.

2.1.2 Physical and Chemical Properties

Physical state and appearance of 2,6-DMA is in a liquid form, colorless to reddish-yellow, clear liquid. It has a melting point of 11.2 °C and a boiling point of 216 °C. 2,6-dimethyl-aniline is slightly soluble in water and freely soluble in ether and alcohol. The density is 0.979 g/cm^3 at 20 °C. The substance has a flash point of 91 °C. 2,6-dimethyl-aniline is quite stable in the environment except under excessive heat exposure or contact with incompatible materials such as oxidizing agents and acids including acid chlorides, halogens, acid anhydrides, hypochlorite, and chloroformates. Addition physical and chemical properties of 2,6-DMA are presented in Table 2.1

2.1.3 Toxicology

Human can expose to 2,6-DMA via many routes. 2,6-dimethyl-aniline can be absorbed through skin, dermal contact, eye contact, inhalation and ingestion. It may cause skin irritation, eye irritation, and respiratory tract (nose and throat) irritation with coughing and/or shortness of breath. It causes gastrointestinal tract irritation with nausea, vomiting and diarrhea. Exposure through skin, inhalation and ingestion induces methemoglobinemia which affects behavior/central nervous system (CNS depression), respiration, heart, urinary system (kidneys), and blood. Symptoms of methemoglobinemia include hypoxia, apnea, cyanosis (a bluish discoloration of the skin due to deficient oxygenation of the blood), headache, fatigue, dizziness, weakness, lethargy, loss of coordination, dyspnea, coma, and death. Additional signs

Table 2.1 Physical and chemical properties of 2,6-DMA.

Property	Data
Molecular formula	$C_8H_{11}N$
Molecular weight	121.18 g/mol
Appearance	Yellow liquid, with characteristic odor and turn brown on exposure to air
Density	0.979 g/cm^3
Boiling point	216 °C
Melting point	11.2 °C
Water solubility	35 g/l @ 25°C
Specific gravity	0.9842 @ 20°C
Vapor pressure	< 0.1 kPa @ 20 °C
Ignition temperature	520°C
Flash point (closed cup)	91°C
Octanol/water partition Coefficient (log K_{ow})	1.96

and symptoms of exposure may include photophobia, visual disturbances, sluggish pupillary reaction, tinnitus, speech disturbances, anorexia, nausea, colicky pain, muscle pain, faintness, paresthesias of the extremities, tremor, seizures, cardiacarrhythmias, tachycardia, and heart block. Urinary signs and symptoms may include painful micturition, hemoglobinuria, methemoglobinuria, hematuria, oliguria, and renal insufficiency, and chocolate-brown blood. In case of chronic potential health effects, a Heinz-body hemolytic crisis may follow the development of methemoglobinemia. Heart, kidney, and liver damage may occur, possibly as secondary effects of hemolysis (NTP, 2002). In addition, 2,6-DMA may also cause mutagenic effects for bacteria and/or yeast; however, there is currently no solid evidence that 2,6-DMA is human mutagen. 2,6-DMA has been classified as group 2B carcinogens (possible for human) by International Agency for Research on Cancer (IARC).

2.1.4 First Aid Measures

In case of eye contact, immediately flush eyes with plenty of water for at least 15 minutes by warm water and get medical attention if irritation occurs. For the skin contact, wash with soap and water and cover the irritated skin with an emollient. If irritation develops or becomes worsen, the patient needs to seek for medical care. If inhaled, remove to fresh air. If not breathing, give artificial respiration. If breathing is difficult, give oxygen supply. In case of ingestion, do not induce vomiting unless directed to do so by medical personnel. Never give anything by mouth to an unconscious person. If large quantities of this material are swallowed, call a physician immediately. Loosen tight clothing such as a collar, tie, belt or waistband.

2.2 Advanced Oxidation Processes

Advanced oxidation processes (AOPs) have been known since the 1970's. The widely accepted definition for AOPs came from Glaze et al. (1987) which stated "advanced oxidation processes are defined as those which involve the generation of hydroxyl radicals ($OH^\bullet$) in sufficient quantity to affect water purification". Hydroxyl radicals is one of the most active oxidant known, it is nonselective for oxidizing compounds and able to operate at normal temperature and pressure (Tchobanoglous et al., 2003).

There are many processes able to generate the highly reactive $OH^\bullet$ species including heterogeneous photocatalytic, photo and non-photocatalytic homogeneous processes. In heterogeneous photocatalysis, $OH^\bullet$ is generated at the surface of a semiconductor (usually TiO_2) in the presence of UVA. Ozone/UV, $O_3/H_2O_2/UV$ and H_2O_2/UV are common photocatalytic combinations which can also generate $OH^\bullet$. The non-photocatalytic processes include "peroxone" (H_2O_2/O_3) and Fenton process (H_2O_2/Fe^{2+}) (Rodger and Bunce, 2001); however, this study emphasized on the latter.

2.3 Fenton Process

Fenton's reagent was discovered in 1894 by its inventor Henry J. Fenton, but its application as an oxidizing process for destroying toxic organics was applied in the late 1960s (Huang et al., 1993). Fenton reaction is one kind of AOPs used to generate $OH^{\bullet}$ for degradation of pollutants. This reaction involves chemical reagents called "Fenton's reagent", which are the combination of hydrogen peroxide (H_2O_2) and a ferrous ion (Fe^{2+}). Fenton's reagent is an effective and simple oxidant of various types of organic contaminants.

2.3.1 Hydrogen Peroxide

Hydrogen peroxide is an aqueous solution which has clear, colorless, water-like in appearance, and can be mixed with water in any proportion. It is miscible with cold water and is soluble in alcohol and ether. At high concentration, it has a slightly pungent or acidic odor. The chemical formula is H_2O_2 and it has a molecular weight of 34.015 g/mole and is non-flammable at any concentrations. Hydrogen peroxide is a diprotic acid with K_{A1} and K_{A2} equal to $10^{-11.8}$ and $<10^{-14}$, respectively.

Although pure H_2O_2 is fairly stable, it significantly decomposed into water and oxygen when heated above about 60°C or in the presence of reducing agents. Aqueous solution of H_2O_2 is mainly used for oxidation reactions, including bleaching process, chemical syntheses, and for water and wastewater treatment. In drinking water purification, Hydrogen peroxide is used to pre-oxidized organic constituents and to eliminate iron and manganese ions. Furthermore, by dissociation into oxygen and water, H_2O_2 can also supply oxygen to microorganism in biological treatment facilities and in the bioremediation of contaminated sites. It can be used as a disinfecting agent in the control of undesirable biofilm growth. Since the oxygen concentration is generally limiting factor during the in-situ biodegradation of organic contaminants, many applications using injection of H_2O_2 into the subsurface have been successfully applied to enhance the biodegradation activity. The decomposition of H_2O_2 to water and oxygen can be toward enzymatic and non-enzymatic routes.

Hydrogen peroxide also catalytically decomposes in the presence of numerous catalysts, e.g., most transition-metal ions such as Fe^{2+}, Cu^+, Cr^{2+}, Co^{2+}, or UV irradiation via different route to form a highly-oxidative $OH^\bullet$.

2.3.2 Ferrous

Iron (Fe) is the most abundant element on Earth and is the cheapest and most important of all metals. Iron is used to manufacture steel and other alloys important in construction and manufacturing. It also plays a vital role in the functioning of living organisms by transporting oxygen in blood via the hemoglobin molecule (an iron-complex organic compound). Its oxidation number varies from -2 to +6; however, most general states typically found in the environment are ferrous (Fe^{2+}) and ferric (Fe^{3+}). Iron exists in the ferrous state under reducing conditions such as those in anaerobic environment. Ferrous iron will be rapidly oxidized to ferric state when exposed to oxidizing agents; hence, it is not stable in the atmospheric environment where oxidative oxygen gas is present (21% by volume).

As mentioned previously that several transition-metal ions can catalyze the decomposition of H_2O_2 to form $OH^\bullet$, Fe^{2+} is the most preferred and environmental friendly among all transition-metal catalysts. Iron(II) sulfate is the most common form of ferrous salt commercially available in the market and can be found in various states of hydration; however, the heptahydrate or so called "green vitriol or copperas" ($FeSO_4 \cdot 7H_2O$) is the most common. This greenish crystalline compound is used as a pigment, fertilizer, medicine in the treatment of iron deficiency, coagulant for coagulation process, and catalyst in the Fenton process.

2.3.3 Hydroxyl Radicals

Hydroxyl radical is extremely reactive, short-lived, and non-selective transient species. It is a strong oxidant which has a very high oxidizing capacity equaling 2.8 V (Prengle, 1978; Masten and Davies, 1994). Table 2.2 shows the oxidation potential of $OH^\bullet$ compared to other oxidants (Parsons, 2004). It can be seen that $OH^\bullet$ is the second

Table 2.2 Oxidation potential of common oxidizing species.

Oxidant	Oxidation Potential (V)
Fluorine	3.03
Hydroxyl radical	2.80
Ozone	2.07
Hydrogen peroxide	1.78
Potassium permanganate	1.68
Chlorine dioxide	1.59
Chlorine	1.36

strongest oxidant, which is inferior only to fluorine. Hydroxyl radical can decompose the organic compounds relatively unselective with the rate constants ranging from 10^9-10^{10} $M^{-1}s^{-1}$ (Buxton, et al., 1988).

Hydroxyl radical is generated among various AOPs in the reaction mixture and has been used for achieving the treatment of a myriad of contaminated waters and industrial wastewaters. Hydroxyl radical can react in aqueous solution by different types of reactions (Eqs. 2.1 to 2.4) depending on target compounds, wastewater composition, and environmental conditions (Hoigné, 1998):

Electron transfer reaction: $OH^\bullet + M^n \Rightarrow M^{n+1} + (OH^-)_{(aq)}$ (2.1)

Hydrogen abstraction: $OH^\bullet + R\text{-}H \Rightarrow R^\bullet + H_2O$ (2.2)

Electrophilic addition: $OH^\bullet + R_2C{=}CR_2 \Rightarrow {}^\bullet CR_2\text{-}C(OH)R_2$ (2.3)

Radical interaction: $OH^\bullet + OH^\bullet \Rightarrow H_2O_2$ (2.4)
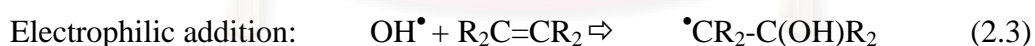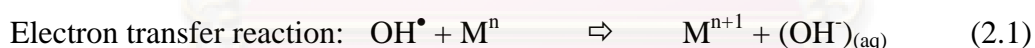
For complex or large aliphatic hydrocarbons, $OH^\bullet$ will oxidize via electrophilic addition to form carbon-center radicals which immediately further react in a bimolecular reaction with dissolved oxygen to produce peroxyl radicals and sequentially stable oxidation products. On the other hand, $OH^\bullet$ tends to react with small aliphatic compounds by the hydrogen abstraction mean in which carbon dioxide can be formed as the final product (complete mineralization). The oxidation of aromatic compounds by $OH^\bullet$ is more complex than aliphatic hydrocarbons and could

involve hydrogen abstraction, electrophilic addition, and radical interaction. Direct electron transfer normally occurs with inorganic pollutants. In addition, $OH^\bullet$ itself can react with another $OH^\bullet$ to combine or to disproportionate to form a stable product (Peres et al., 2003).

2.3.4 Fenton Reaction

Fenton process and its modified versions are being increasingly used in the treatment of contaminated water and soil. The conventional "dark" Fenton process involves the use of an oxidizing agent (usually H_2O_2) and a catalyst (usually Fe^{2+}) to generate highly reactive $OH^\bullet$. Once the Fenton's reagent is combined together, its sequential reactions are very complicated but well specified as shown in Eqs. (2.5) to (2.16) (Pignatello, 1992; Lu et al., 1999; Chen et al., 2001).

$$Fe^{2+} + H_2O_2 \rightarrow Fe^{3+} + {}^\bullet OH + OH^-; \quad k_1 = 76 \text{ M}^{-1}\text{s}^{-1} \quad (2.5)$$

$$H_2O_2 \leftrightarrow HO_2^- + H^+; \quad K_2 = 1.59 \times 10^{-12} \text{ M} \quad (2.6)$$

$$Fe^{3+} + H_2O_2 \rightarrow Fe^{2+} + HO_2^\bullet; \quad k_3 = 0.02 \text{ M}^{-1}\text{s}^{-1} \quad (2.7)$$

$$HO_2^\bullet \leftrightarrow O_2^{\bullet -} + H^+; \quad K_4 = 1.6 \times 10^{-5} \text{ M} \quad (2.8)$$

$$Fe^{2+} + {}^\bullet OH \rightarrow Fe^{3+} + OH^-; \quad k_5 = 4.3 \times 10^6 \text{ M}^{-1}\text{s}^{-1} \quad (2.9)$$

$$Fe^{2+} + O_2^{\bullet -} \rightarrow Fe^{3+} + O_2^-; \quad k_6 = 1 \times 10^7 \text{ M}^{-1}\text{s}^{-1} \quad (2.10)$$

$$Fe^{2+} + HO_2^\bullet \rightarrow Fe^{3+} + HO_2; \quad k_7 = 1.2 \times 10^6 \text{ M}^{-1}\text{s}^{-1} \quad (2.11)$$

$$H_2O_2 + {}^\bullet OH \rightarrow HO_2^\bullet + H_2O; \quad k_8 = 2.7 \times 10^7 \text{ M}^{-1}\text{s}^{-1} \quad (2.12)$$

$$HO_2^\bullet + HO_2^\bullet \rightarrow H_2O_2 + O_2; \quad k_9 = 8.3 \times 10^5 \text{ M}^{-1}\text{s}^{-1} \quad (2.13)$$

$${}^\bullet OH + {}^\bullet OH \rightarrow H_2O_2; \quad k_{10} = 5.3 \times 10^9 \text{ M}^{-1}\text{s}^{-1} \quad (2.14)$$

$$RH + {}^\bullet OH \rightarrow RH^\bullet + OH^- \rightarrow \rightarrow \rightarrow \text{ products or } CO_2 + H_2O \quad (2.15)$$

$$Fe^{3+} + 3OH^- \rightarrow Fe(OH)_{3(s)}; \quad K_{sp} = 4 \times 10^{-38} \quad (2.16)$$
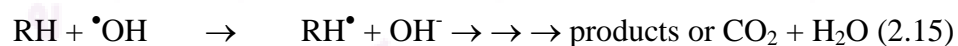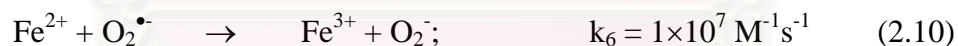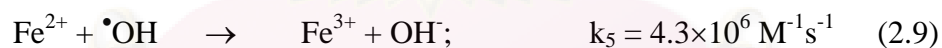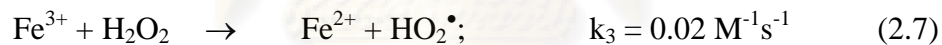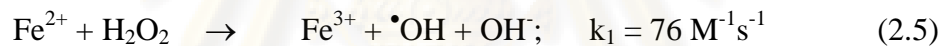
Although Fe^{2+} is acting as a catalyst in the Fenton reaction series, it can be seen that the consumption rate of Fe^{2+} in Eq. (2.5) is almost 3,800 times faster than the regeneration rate of Fe^{2+} from Fe^{3+} in Eq. (2.7). As a result, the pollutant

degradation in Fenton process typically proceeds in two sequential steps. In the first step, the pollutant disappears rapidly under sufficient Fe^{2+} leading to the $OH^\bullet$ excessive environment whereas, in the slower second step, the oxidation rate of the pollutant is controlled by Eq. (2.7) which is known as "Fenton-like process" (Lunar et al., 2000). After treatment with Fenton process, the mixture is typically neutralized to comply with the effluent standard and the ferric hydroxide will precipitate out as illustrated in Eq. (2.16). This ferric hydroxide sludge will cause a burden for further separation and disposal which is a major drawback for ordinary Fenton process.

2.4 Fluidized-bed Fenton Process

As mentioned previously, the major disadvantage of Fenton process is the production of a substantial amount of iron precipitation. To overcome and/or ease this problem, the fluidized-bed reactor (FBR) is one of the possible alternatives. The ferric ion generated from Eq. (2.5) can precipitate and crystallize onto the carriers' surface in the form of iron oxide; hence, reducing the production of puffy ferric hydroxide sludge. In FBR, several important and complicated processes occur simultaneously including: 1) homogeneous chemical oxidation (H_2O_2/Fe^{2+}); 2) heterogeneous chemical oxidation ($H_2O_2/$ iron oxide); 3) fluidized-bed crystallization; and 4) reductive dissolution of iron oxides. Factors influencing iron oxide crystallization on the surfaces of fluidized-bed carriers operated in FBR are pH, specific iron loading, H_2O_2/Fe^{2+}, and superficial velocity (Chou, et al., 2004). Figure 2.2 illustrates the fluidized-bed Fenton mechanisms in details. The Fenton's reagent can produce the non-selective oxidant $OH^\bullet$ via homogeneous reaction (a). Then, this strong oxidant attacks the aromatic hydrocarbon to initiate ring opening as reaction (b). After that, the intermediate products from previous reaction appears, these lead into further oxidation (reaction (c)). From this Fenton's reaction, Fe^{3+} is form (reaction (d)). The Fe^{3+} can be converted back to Fe^{2+} and initiate Fenton reaction further as in reaction (h). However, in the presence of solid carriers, the ferric hydrolysis product of Fenton's reaction can also crystallize and grow on the surface of the carriers (reaction(e)); hence, decreasing the precipitation of puffy ferric hydroxide forms
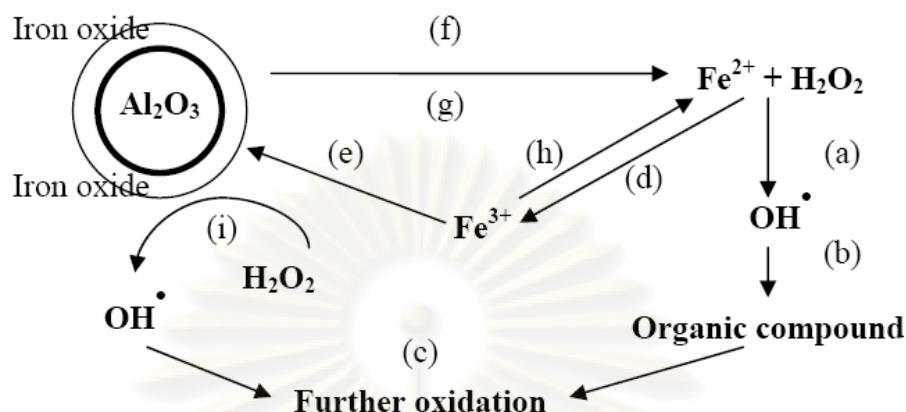
Figure 2.2 Fluidized-bed Fenton reactions.

(Chou and Huang, 1999). At the same time, the crystallized ferric oxide can also serve as a catalyst for hydrogen peroxide decomposition in a heterogeneous reaction (i) (Chou et al., 2003). Considering iron oxide on the surface carriers, it can re-dissolve via reductive dissolution (reaction (g)) and/or heterogeneous reaction (f) to form Fe^{2+}. However, these reactions which are similar to Eq. (2.7) are still slower than Eq. (2.5) (Pignatello, 1992). Key factors in the design of fluidized-bed Fenton process are: selection of carrier, including the material, specific gravity, and particle size; design of bed expansions; superficial velocity; feed mode and dosage of Fenton's reagent; and size, configuration, and recycle ratio of reactor.

2.5 Reaction Rate Constant Determination

In this research, the intrinsic second-order rate constant of the reaction between 2,6-DMA and $OH^\bullet$ was determined by using a technique of competitive kinetics between 2,6-DMA and a reference compound in the presence of $OH^\bullet$. This reference compound has to have the intrinsic rate constant with $OH^\bullet$ reported. Buxton et al. (1988) have compiled many rate constants between various organic compounds and $OH^\bullet$ some of which were used in this study. Aniline (AN) was selected as the reference compound with the rate constant with $OH^\bullet$ of 4.8×10^9 $M^{-1}sec^{-1}$ (Buxton et

al., 1988). The competitive kinetics as described later is a very useful yet simple tool to estimate the unknown rate constant of a compound without any complexity in experimental setup and equipments. It is well established that $OH^\bullet$ will react with any compound in a second-order manner. Hence, the reaction rate in a batch operation could be written as shown in Eqs (2.17) and (2.18) and could be further derived for the competition reaction manner as illustrated below:

$$\frac{d[2,6-DMA]}{dt} = -k_{2,6-DMA}[2,6-DMA][OH^\bullet] \tag{2.17}$$

$$\frac{d[AN]}{dt} = -k_{AN}[AN][OH^\bullet] \tag{2.18}$$

$$\frac{Eq(2.16)}{Eq(2.17)} = \frac{\dfrac{d[2,6-DMA]}{dt}}{\dfrac{d[AN]}{dt}} = \frac{-k_{2,6}[2,6-DMA][OH^\bullet]}{-k_{AN}[AN][OH^\bullet]} \tag{2.19}$$

$$\frac{\dfrac{1}{[2,6,DMA]}d[2,6-DMA]}{\dfrac{1}{[AN]}d[AN]} = \frac{k_{2,6-DMA}}{k_{AN}} \tag{2.20}$$

$$\frac{\displaystyle\int_0^i \frac{1}{[2,6,DMA]}d[2,6-DMA]}{\displaystyle\int_0^i \frac{1}{[AN]}d[AN]} = \frac{k_{2,6-DMA}}{k_{AN}} \tag{2.21}$$

$$\frac{\ln[2,6-DMA]_i - \ln[2,6-DMA]_0}{\ln[AN]_i - \ln[AN]_0} = \frac{k_{2,6-DMA}}{k_{AN}} \tag{2.22}$$

$$\frac{\ln\dfrac{[2,6-DMA]_i}{[2,6-DMA]_0}}{\ln\dfrac{[AN]_i}{[AN]_0}} = \frac{k_{2,6-DMA}}{k_{AN}} \tag{2.23}$$

$$\ln\left(\frac{[2,6-\text{DMA}]_i}{[2,6-\text{DMA}]_0}\right) = \frac{k_{2,6-\text{DMA}}}{k_{\text{AN}}} \ln\frac{[\text{AN}]_i}{[\text{AN}]_0} \qquad (2.24)$$

where $[2,6\text{-DMA}]_0$, $[\text{AN}]_0$, and $[2,6\text{-DMA}]$, $[\text{AN}]$ are concentrations of 2,6-DMA, AN before and after the reaction, respectively; $[\text{OH}^\bullet]$ is concentration of the hydroxyl radical; $k_{2,6\text{-DMA}}$, k_{AN} are the rate constants of $\text{OH}^\bullet$ reacting with 2,6-DMA and AN, respectively. This final equation is similar to the one used by Shen et al. (2008) in the determination of the rate constant between *p*-chloronitrobenzene and $\text{OH}^\bullet$. According to the Eq. (2.24), the plot between $\ln([2,6\text{-DMA}]_i/[2,6\text{-DMA}]_0)$ versus $\ln([\text{AN}]_i/[\text{AN}]_0)$ should result in a linear relationship and the slope will represent the ratio of the rate constant between aniline and 2,6-DMA.

In addition to the batch study, this research also determined the intrinsic rate constant of 2,6-DMA in the continuous mode in order to confirm the results. The reaction rate equations between 2,6-DMA and $\text{OH}^\bullet$ under the continuous mode could be derived as follows:

$$\frac{d[2,6-\text{DMA}]}{dt} = -k_{2,6-\text{DMA}}[2,6-\text{DMA}][\text{OH}^\bullet] + Q\left([2,6-\text{DMA}]_{\text{in}} - [2,6-\text{DMA}]_{\text{out}}\right)$$
$$(2.25)$$

$$\frac{d[\text{AN}]}{dt} = -k_{\text{AN}}[\text{AN}][\text{OH}^\bullet] + Q\left([\text{AN}]_{\text{in}} - [\text{AN}]_{\text{out}}\right) \qquad (2.26)$$

At steady state $\Rightarrow$ $\dfrac{d[2,6-\text{DMA}]}{dt} = 0$, $\dfrac{d[\text{AN}]}{dt} = 0$

$$\frac{k_{2,6-\text{DMA}}[2,6-\text{DMA}][\text{OH}^\bullet]}{k_{\text{P}}[\text{AN}][\text{OH}^\bullet]} = \frac{Q\left([2,6-\text{DMA}]_{\text{in}} - [2,6-\text{DMA}]_{\text{out}}\right)}{Q\left([\text{AN}]_{\text{in}} - [\text{AN}]_{\text{out}}\right)} \qquad (2.27)$$

$$\frac{k_{2,6-\text{DMA}}}{k_{\text{AN}}} = \frac{\left([2,6-\text{DMA}]_{\text{in}} - [2,6-\text{DMA}]_{\text{out}}\right)}{\left([\text{AN}]_{\text{in}} - [\text{AN}]_{\text{out}}\right)} \cdot \frac{[\text{AN}]}{[2,6-\text{DMA}]} \qquad (2.28)$$

where $[2,6\text{-DMA}]_{\text{in}}$, $[\text{AN}]_{\text{in}}$, and $[2,6\text{-DMA}]_{\text{out}}$, $[\text{AN}]_{\text{out}}$ are influent and effluent concentrations of 2,6-DMA, AN at the steady state, respectively; $[\text{OH}^\bullet]$ is concentration of the hydroxyl radical; $k_{2,6\text{-DMA}}$ and k_{AN} are the rate constant of $\text{OH}^\bullet$

reacting with 2,6-DMA and AN, respectively; and Q is the flow rate in and out of the reactor.

2.6 Precipitation and Crystallization

2.6.1 Rational

Precipitation phenomenon is very important in both water and wastewater treatment processes. It is the formation of a solid in a solution and involves several physical and chemical processes. Reverse process of precipitation is called "dissolution." Since these two processes are reversible but sometimes progress very slowly, both equilibrium and kinetics considerations are important. Knowledge of equilibrium relationships permits the calculation of equilibrium concentrations of cation(s) and anion(s) from the dissolution/precipitation of any salts. Nonetheless, in some heterogeneous systems, the equilibrium calculation may only provide the boundary conditions of the system rather than the situation that truly exists because the equilibrium is slowly established. In such cases, the kinetics consideration which is more complicated will play a major role in predicting the system behavior.

2.6.2 Nucleation

Once the product of cation(s) and anion(s) according to the solubility equation exceeds the dissociation constant, the solution will be oversaturated and a solid phase will be simultaneously formed. Various processes are involved in the solid formation; however, only three steps are believed to control the overall process. The first step is the interaction between ions or molecules leads to the formation of a critical cluster or nucleus or so called "nucleation" as shown in Eqs. (2.29) to (2.32). These nuclei can serve as the centers from which spontaneous growth of crystals can occur. The nucleation process determines the size and distribution of crystal produced. The second step is the formation of crystallites (crystal growth) as a result from sequential deposition of material on the nuclei formed from the first step as shown in Eq. (2.33).

The last step is the formation of large crystals from the crystallites by a process called "ripening" as shown in Eq. (2.34)

$$X + X \quad \leftrightarrow \quad X_2 \tag{2.29}$$

$$X_2 + X \quad \leftrightarrow \quad X_3 \tag{2.30}$$

$$X_{j-1} + X \leftrightarrow \quad X_j \text{ (critical cluster)} \tag{2.31}$$

Nucleation: $\qquad X_j + X \quad \leftrightarrow \quad X_{j+1}$ $\hspace{3cm}$ (2.32)

Crystallite formation: $\qquad X_j + X \quad \leftrightarrow \quad X_{j+1} \rightarrow \text{crystal growth}$ (2.33)

Crystal formation: $\qquad X_{j+1} + X \leftrightarrow \quad X_{j+1} \rightarrow \text{crystal ripening}$ (2.34)
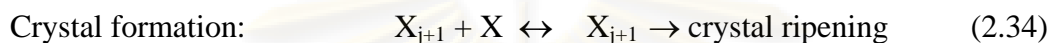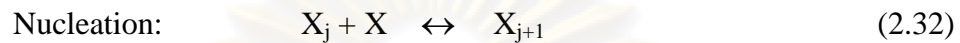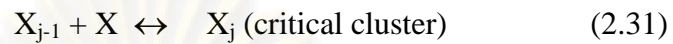
Nucleation can be divided into two types, i.e., homogeneous and heterogeneous nucleation, depending on the number of phases during the initial step of solid formation. Figure 2.3 shows the schematic solubility isotherm of a solid electrolyte, where "S" is the saturation ratio (a/a_0), "a" is the actual concentration, and "a_0" is the concentration at solubility equilibrium of the solutes that characterize the solubility. Line "S = 1" divided the graph into two areas, i.e., undersaturated (no precipitation occurs) and oversaturated zones (precipitation should occur theoretically). Within the oversaturated zone, "S_M" is the minimum supersaturation ratio in which the precipitation could occur simultaneously without a need for the surface-catalytic seeds which called "homogeneous nucleation." In other word, solid precipitation will proceed spontaneously within the labile zone (above the "S_M-line"). Between the unsaturation and labile zones is a metastable zone where the nucleation rate is virtually zero or extremely slow even though the solution is already oversaturation; hence, the solutes can be stable for long periods without precipitation.

2.6.2.1 Homogeneous Nucleation

If the concentration of a solution is gradually increased until exceeding the solubility product with respect to a solid phase, the new solid phase will be theoretically formed. Nonetheless, in real practice, the new solid phase will not be formed within a specific amount of time until a certain degree of supersaturation has been achieved and accelerate the precipitation process. This phenomenon can be explained by chemical thermodynamics principle.
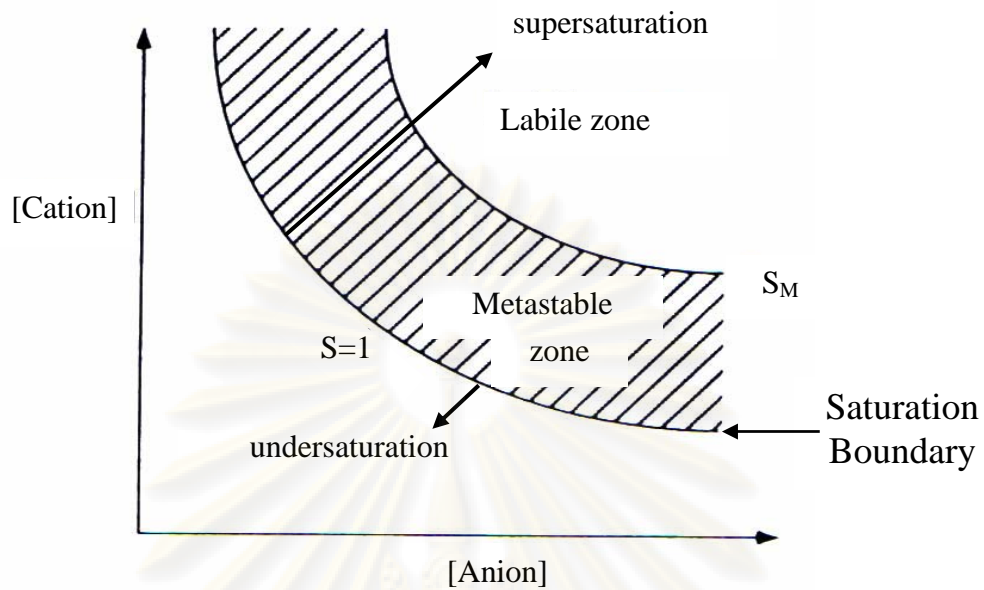
Figure 2.3 Schematic solubility isotherm of a solid electrolyte (Adapted from Stumm and Morgan, 1996).

A nucleus will be formed if total Gibb's free energy of the system decreases as a result from the formation of a new solid phase from an aqueous phase. In other word, the change in free energy of the formation of a nucleus (ΔG_f) has to be negative. The "ΔG_f" is the summation of free energy in the system which has two parts, i.e., free energy from bulk phase (ΔG_{bulk}) and free energy from solid phase ($\Delta G_{surface}$). The "ΔG_{bulk}" is a function of supersaturation degree in the aqueous phase and is always negative for a supersaturation solution. On the other hand, the "$\Delta G_{surface}$" is related to the interfacial energy between the surface of the solid being formed and the solvent; hence, is always positive. Then, the "ΔG_f" will be negative if the negative quantity of "ΔG_{bulk}" is greater than the positive quantity of "$\Delta G_{surface}$" and; thus, the nucleus formation can be thermodynamically favorite. As a result, a large supersaturation must be exceeded before the pure solid nucleus can be formed from the homogeneous oversaturated solution by itself or so called "homogeneous nucleation".

2.6.2.2 Heterogeneous Nucleation

Heterogeneous nucleation is in many cases the predominant formation process for crystals in natural waters. In the presence of foreign solid particles, the "$\Delta G_{surface}$" is reduced due to the interference of the interfacial energy of the external seeds (should match well with the crystal to be formed), thus reducing the formation free energy, and sequentially allow the nucleation to proceed more easily (Figure 2.4). In other words, these foreign solids are serving as the catalyst to reduce the energy barrier of the nucleation process similar to chemical catalysts which reduce the activation energy for chemical reaction. Theoretically, with proper matching between the foreign solid and the crystal to be precipitate, the nucleation may take place at a lower saturation ratio (in the metastable zone in Figure 2.3) on the solid surface than in solution (homogeneous nucleation).

In fluidized-bed Fenton process, the media, normally SiO_2 or construction sands, will be fluidized in the reactor and serve as the foreign solids on which the iron oxide can precipitate; hence, the nucleation process follows the heterogeneous mechanism. According to the nucleation principle mentioned previously, to optimize iron crystallization onto the media in fluidized-bed Fenton process, the saturation ratio has to be maintained within the metastable zone of Figure 2.3.

2.6.3 Crystal Growth

After the nucleation process (i.e., the initial formation of solid nuclei), spontaneous growth of crystal will occur. The attachment of a molecule/nucleus to another nucleus to form a solid lattice which includes the transportation of materials to the surface of these nuclei and surface deposition will become very important and should follow the mechanism of solid-solution interface at the molecular level. Four steps are believed to get involve in the attachment of solutes/nuclei to the solid surface of foreign particles or other nuclei as shown in Figure 2.5: 1) diffusion through the bulk solution and the water layer adjacent to nuclei (bulk diffusion); 2) adsorption-desorption reaction on the solid surface; 3) migration on the surface to or
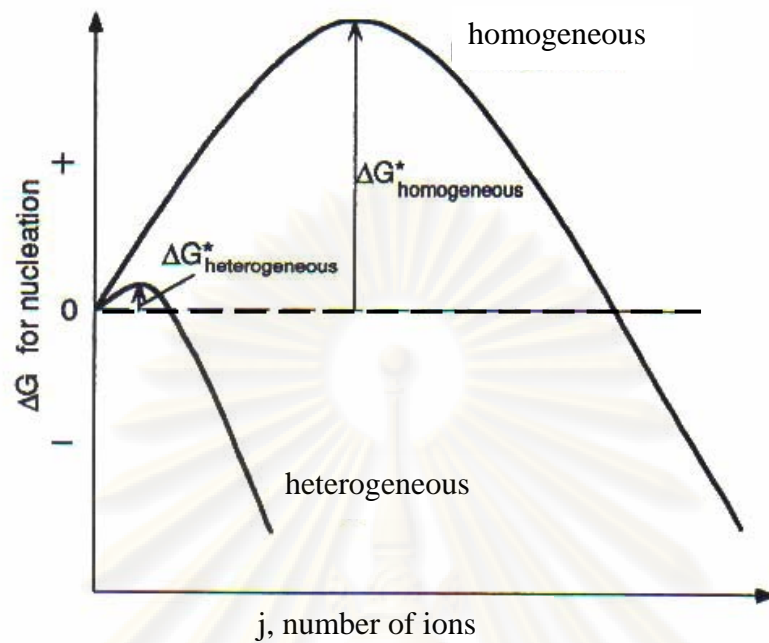
Figure 2.4 Schematic representation of the ability of a solid substrate to catalyze the nucleation (Stumm and Morgan, 1996).
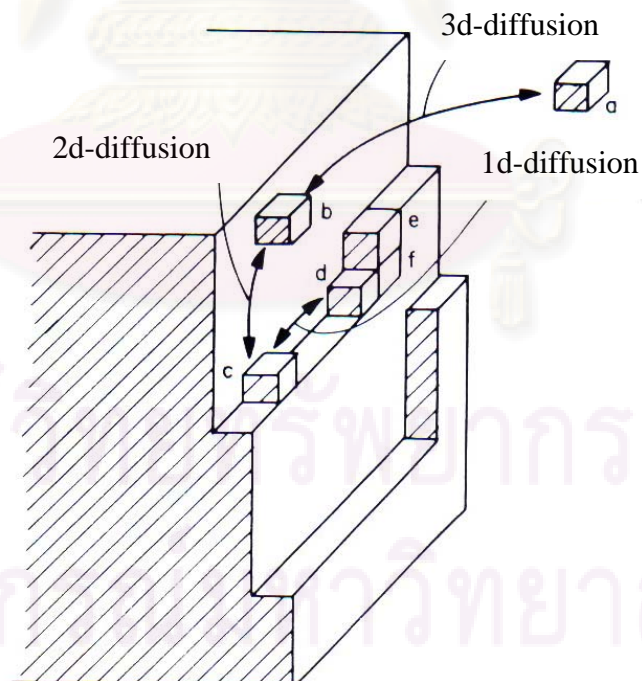
Figure 2.5 Attachment and detachment of an ion or molecule to and from a solid lattice (Morel and Hering, 1993).

from a step edge (surface diffusion); and 4) migration along a step edge to or from a kink (edge diffusion). Considering on the precipitation part, the ion or molecule will be more stable (lower free energy) as it embeds deeper into the solid matrix: a < b < c < d < e < f. If step 1 only is limiting, the kinetics are said to be diffusion or transport controlled. In this case, there is a concentration gradient in a liquid layer adjacent to the solid surface as shown in Figure 2.6. The liquid-film thickness depends on the mixing condition. On the other hand, if step 2, 3 and/or 4 only are limiting, the kinetics are said to be surface-interaction control and there will be no concentration gradient in the liquid adjacent to the solid surface. If the growth of crystal is controlled by the surface interaction; then, a zero-order rate law could be applied if the steady-state conditions at the surface prevail (Stumm and Morgan, 1996):

$$\frac{dC}{dt} = -k_S A \qquad (2.35)$$

where "k_S" is the surface-reaction rate constant normalized to solid surface area and "A" is the surface area of the solid. On the other hand, for transport control mechanism, Stumm and Morgan (1996) proposed a parabolic rate law for the diffusion at the solid interface at the ionic or molecular level as:

$$\frac{dC}{dt} = -k_p t^{-\frac{1}{2}} \qquad (2.36)$$

where k_p is the rate constant. Integrating equation (2.36) will yield:

$$C = C_0 - 2k_p t^{\frac{1}{2}} \qquad (2.37)$$

Since, this research used a 0.22-μm membrane filter to differentiate the soluble species from the particulate species, the solutes may not be in the molecular level but can be in the colloidal particles with the diameters less than 0.22 μm. In other word, due to the limitation in measurement procedure, the iron particles with the sizes less than 0.22 μm such as the crystallites would be considered as soluble iron. According to literatures, diameters of colloids can vary from 0.001 to 100 μm which also cover the range of crystallite size. Therefore, the agglomeration or reduction of these

(a) diffusion control   (b) surface-interaction control
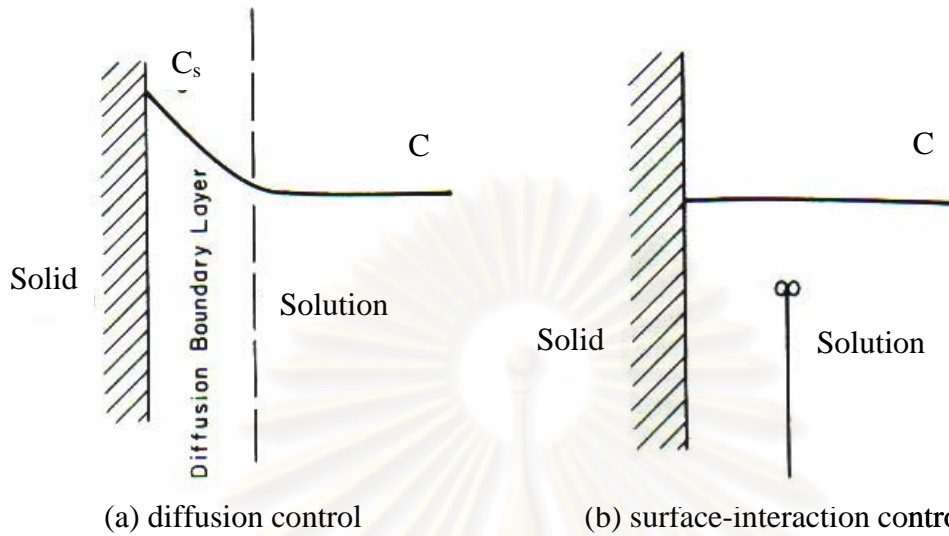
Figure 2.6 Concentration gradient in liquid phase for extreme cases of diffusion control and surface-interaction control (Morel and Hering, 1993).

crystallites during the crystal growth stage as a result from colloidal transport and collision could be described by the second-order rate law as proposed by O'Melia and Tiller (1993), who studied on the aggregation of colloids as follows:

$$\frac{dN}{dt} = -k_a N^2 \qquad (2.38)$$

or

$$\frac{1}{N} = \frac{1}{N_0} + k_a t \qquad (2.39)$$

where "N" is the number concentration of particles in suspension at time "t" and "k_a" is a second-order rate constant which is a function of physical and chemical properties of the system including mass transport coefficient and collision efficiency factor. The second-order rate law of Eq. (2.38) is comparable to the very well-known rate of change in the concentration of colloidal particles during the flocculation process both in perikinetic (random diffusion control) and orthokinetic (movement of solvent or velocity gradient control) manners.

In this study, both transport equations (Eqs. (2.36) and (2.38)) were used to characterize the behavior of crystal formation in order to provide a better understanding on the crystallization process.

2.7 Literature Reviews

2.7.1 Competitive Kinetics Technique

Leitner and Roshani (2010) determined the rate constant of benzotriazole (BT) by the reaction of direct ozonation and $OH^\bullet$ at different pH. They accessed the kinetics information by 2 approaches, i.e., the log-reduction of BT in the case which ozone was present in excess (1st-model) and the competition kinetic technique in the case which a reference compound was co-existed (2nd–model). The results showed that the 2nd order rate constant of BT with molecular ozone at pH 2 by the 1st-model was 36.4±3.8 $M^{-1}s^{-1}$ as compared to 18.4±0.8 $M^{-1}s^{-1}$ for the 2nd-model. With the 2nd-model, the 2nd order rate constant at pH 5 was found to be 22.0±0.2 $M^{-1}s^{-1}$. In a second stage, the reaction of BT and $OH^\bullet$ was carried out by using the 2nd–model involving 2 probe compounds during the ozonation at pH values ranging from 2 to 10.2. They found that the 2nd order rate constant of BT and $OH^\bullet$ were found to vary from $6.2\times10^9\,M^{-1}s^{-1}$ at pH 10.2 to $1.7\times10^{10}\,M^{-1}s^{-1}$ at pH 2.

Balci et al. (2009) investigated the kinetic and mechanism of atrazine degradation by in-situ electrochemically generated Fenton's reagent. They found the intrinsic rate constant of the reaction between atrazine and $OH^\bullet$ by competition kinetics technique to be $2.54\pm0.22\times10^9\,M^{-1}s^{-1}$. The atrazine disappearance rate and solution mineralization efficiency were very rapid at the beginning of the reaction, but became slow down as the reaction proceeded. High mineralization rate of 82% was obtained by TOC and IC analysis. The oxidation pathway of atrazine degradation by $OH^\bullet$ was also proposed.

Kwon et al. (2009) determined the second order rate constants of $OH^\bullet$ with 14 organics and inorganic solutes such as chloride, carbonate, sulfate, bromide, etc., by using a simple competitive kinetics in a continuous flow system in the UV/H_2O_2 process. *p*-Nitroso-dimethyl-aniline (PNDA) was selected as the reference probe. They found that the $OH^\bullet$ rate constants obtained for 14 solutes selected in this study

were consistent with values reported in the literatures using the more complicated pulse radiolysis method.

Shen et al. (2008) investigated the kinetics and mechanism of p-chloronitrobenzene (pCNB) degradation by ozone. With reference compounds, nitrobenzene (NB) and chlorobenzene (CB), the reaction rate constants of pCNB with O_3 and $OH^\bullet$ were measured by means of competition kinetics (mixture of pCNB and NB, or pCNB and CB) and found to be 1.6×10^9 and 2.6×10^9 $M^{-1}s^{-1}$, respectively. The increases in chloride and nitrate concentrations nearly equaled to the decrease in pCNB concentration. The degradation pathway for the ozonation of pCNB was also proposed.

Mazellier et al. (2007) investigated the degradation of fenuron by hydroxyl and carbonate radicals in aqueous solution by using the competitive method. Photolysis of H_2O_2 at 254 nm was used to generate $OH^\bullet$ and carbonate radicals were generated by the photolysis of $Co(NH_3)_5CO_3^+$ at 254 nm. Atrazine was used as the reference compound for both processes. The results found that the 2nd order rate constant of fenuron with $OH^\bullet$ and carbonate radicals were found to be $7\pm1\times10^9$ $M^{-1}s^{-1}$ and $7-12\pm3\times10^6$ $M^{-1}s^{-1}$, respectively. The intermediates of fenuron oxidized by hydroxyl and carbonate radicals were also identified by LC-MS.

Einschlag et al. (2003) determined the rate constant of a set of nitroaromatic compounds with $OH^\bullet$ using competition experiment in the UV/H_2O_2 process. For a given pair of substrates S_1 and S_2, the relative reactivity β (defined as k_{S1}/k_{S2}) was calculated from the slope of the plot between $ln[S_1]$ VS $ln[S_2]$. This method allows a better estimation of the relative reactivity than the plot of $ln[S_1]$ and $ln[S_2]$ against time. The rate constants of nitroaromatic substrates with $OH^\bullet$ were found to be in between 0.33×10^9 and 8.6×10^9 $M^{-1}s^{-1}$.

Spanggord et al. (2000) examined the kinetics of aminodinitrotoulenes (2-amino-4,6-dinitrotoluene (2-ADNT) and 4-amino-2,6-dinitrotoluene (4-ADNT)) by

using the competition kinetics in a peroxone (ozone and H_2O_2) oxidizing system where both $OH^\bullet$ and ozone are important oxidants. The results found that the rate constant of 2- and 4-ADNT with ozone by using resorcinol as a reference compound were around 1.45×10^5 and 1.8×10^5 $M^{-1}s^{-1}$, respectively. For $OH^\bullet$ oxidation, determined using p-nitoracetophenone (PNAP) as the reference compound, the rate constants were found to be 1.6×10^9 and 1.9×10^9 $M^{-1}s^{-1}$ for 2-, and 4-ADNT, respectively. Although rate constants for $OH^\bullet$ oxidation were much higher than those for ozone, the kinetics modeling revealed that ozone was the dominant oxidant for ADNTs oxidation in the peroxone mixture, except when the ADNTs were below 1 μM (200 ppb).

2.7.2 Degradation of 2,6-Dimethyl-aniline by AOPs

Masomboon et al. (2010) determined the oxidation of 2,6-DMA be electro-Fenton process at pH 2. They found that 1 mM of Fe^{2+}, 20 mM of H_2O_2 and current density of 15.89 Am^{-2} were the optimum operating parameters for completely degrading 1 mM of 2,6-DMA. Furthermore, the degradation pathway of 2,6-DMA was also proposed.

Masomboon et al. (2009) investigated the effect of reaction conditions including the dosages of Fenton's reagent and initial pH on 2,6-DMA degradation and COD removal. They found that 70% removal efficiency was achieved under the optimum conditions of 2 mM of Fe^{2+}, 20 mM of H_2O_2 and pH 2 after 3 hrs. Moreover, they also proposed the intermediates and pathway of 2,6-DMA degradation.

Ting et al. (2009) investigated the kinetics of 2,6-DMA oxidation by photoelectron-Fenton process using different electrochemical cells. Effect of initial pH, Fe^{2+} concentration, H_2O_2 loading, and current density were explored to validate the kinetics model. The results showed that when pH was higher than 2, amorphous $Fe(OH)_{3(s)}$ was generated and the degradation of 2,6-DMA increased with increasing of Fe^{2+} and current density from 1.0 to 1.5 mM and 3.5 to 10.6 A/m^2, respectively,

and the optimal H_2O_2 concentration for 2,6-DMA oxidation under the studied condition was 25 mM.

2.7.3 Removal of Organic Compounds in Heterogeneous Catalysis by H_2O_2

Flores et al. (2008) demonstrated that H_2O_2 could be activated in the presence of a heterogeneous catalyst (Fe^{3+}-containing ashes) to generate a powerful radical oxidant. The result from leaching test indicated that more of the 99 % by weight of the iron ion still stayed in the solid catalysts and the presence of H_2O_2 did not alter this relation. It is concluded that radical species ($HO_2\bullet$) are formed and could be further transformed to $OH^\bullet$ when the H_2O_2 was activated by the immobilized Fe^{3+}. The results showed that it was possible to oxidize reactive black 5 dye using a stoichiometric amount of H_2O_2. After 2 hours of treatment, reactive dye solutions were effectively decolorized and 80% of the original COD was removed.

Zelmanov and Semiat (2008) investigated the catalytic behavior of iron-based nano-catalysts on ethylene glycol and phenol treatment in the advanced oxidation processes. The results showed that the Fenton-like reaction using iron (III) oxide-based nano-catalysts in the presence of H_2O_2 could degrade both substances efficiently.

Dantas et al. (2006) evaluated the use of new composites as the adsorbents and/or heterogeneous catalysts for Fenton process to treat textile wastewater. The efficiency of the process was explored as a function of the experimental parameters: pH, H_2O_2 concentration and iron oxides content. The composites with high iron oxide content could effectively adsorb the contaminants in textile wastewater, and the adsorptive capacity increased with the iron content. These solids were also applied as the catalyst in the heterogeneous Fenton reaction and found to be very effective at pH 3.0 with the consumption of H_2O_2 lower than those required by the homogeneous Fenton process.

Baldrian et al. (2006) used the heterogeneous catalysts based on magnetic mixed iron oxides to decolorize several synthetic dyes. All the catalysts could catalyze H_2O_2 to produce highly reactive $OH^\bullet$ which able to decolorize the synthetic dyes effectively. The most effective catalyst was $FeO.Fe_2O_3$ which provided more than 90% decolorization. The fastest decomposition proceeded during the first hour of the reaction. In addition to dye decolorization, all the catalysts also caused a significant decrease in COD. These catalysts were active in the pH range of 2–10 depending on their structures and able to perform sequential catalytic cycles with low metal leaching.

Christopher et al. (2005) studied Fenton-mediated oxidation in the presence and absence of oxygen. The experiment showed that the oxidation of formic acid could occur effectively under a variety of experiment conditions by Fenton process. The intermediates generated during formic acid oxidation were found to increase the oxidation efficiency, especially at high initial organic concentrations, by contributing in the redox cycling of iron. In the presence of oxygen, however, such improvement was attenuated through competition for the organic intermediates.

Lu et al. (2002) investigated how surface dissolution of goethite affected 2-chlorophenol oxidation in the goethite/H_2O_2 process. The results showed that ligand and reductant could enhance the dissolution rate of goethite which was a surface-controlled mechanism. Furthermore, the result from this study indicated that 2-chlorophenol could be effectively degraded by Fenton-liked reaction using the goethite as a catalyst at acidic pH. The extent of 2-chlorophenol degradation increased with increasing goethite dosage which providing more surface sites for the reductive dissolution.

Huang et al. (2001) examined the catalyzed decomposition of H_2O_2 and 2-chlorophenol in the presence of iron oxides. The catalytic activity for H_2O_2 decomposition was the highest for ferrihydrite, less for goethite, and much less for hematite based on mass and surface area basis. However, hematite exhibited the

highest activity in catalyzing 2-chlorophenol oxidation. The oxidation efficiency of 2-chlorophenol corresponded with the inverse sequence of specific area and pH_{pzc} of the iron oxides.

Lu (2000) investigated the effect of goethite particle size, goethite dosage, Fe^{2+} and Fe^{3+} concentrations on the 2-chlorophenol oxidation. It was found that 2-chlorophenol could be decomposed with H_2O_2 catalyzed by goethite and the oxidation rate increased with decreasing goethite particle size. 2-Chlorpheol degradation was almost retarded with 0.8 g/l of goethite because Fe^{2+} could not be produced at this condition. Addition of Fe^{2+} and Fe^{3+} can enhance the oxidation efficiency in the presence of goethite and H_2O_2. In conclusion, the essential mechanisms of goethite catalyzing H_2O_2 to decompose 2-chlorophenol may be due to the catalysis of ferrous ion and goethite surface. The reaction mechanisms are shown in Eqs. (2.40) to (2.42):

$$\alpha\text{-}FeOOH_{(s)} + 2H^+ + \tfrac{1}{2}H_2O_2 \rightarrow Fe^{II} + \tfrac{1}{2}O_2 + 2H_2O \qquad (2.40)$$

$$Fe^{II} + H_2O_2 \rightarrow Fe^{III} + OH^\bullet + OH^- \qquad (2.41)$$

$$Fe^{III} + H_2O + OH^- \rightarrow \alpha\text{-}FeOOH_{(s)} + 2H^+ \qquad (2.42)$$
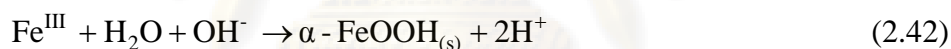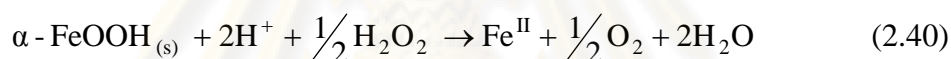
Chou and Huang (1998) studied on the oxidation of benzoic acid (BA) via Fenton-liked reaction using an innovative supported γ-FeOOH catalyst. Oxidation of BA by H_2O_2 was performed to understand the effects of initial pH and H_2O_2 dosage. The removal efficiency of BA at an initial pH of 3.2 was higher than at initial pH of 6.0 and 10.0; this result can be partly explained by reductive dissolution of γ-FeOOH. Therefore, the extent of heterogeneous catalysis was evaluated and found that the majority of mineralization of BA takes place on the catalyst surface while some occur in the aqueous phase due to iron dissolution of the catalyst.

Lin and Gurol (1998) described the kinetics, mechanism, and implication on the catalytic decomposition of H_2O_2 with granular size goethite ($\propto$-FeOOH) particles in aqueous solution. The results showed that the decomposition rate of H_2O_2 over goethite surface can be explained by the 2nd-order kinetic expression and the apparent

reaction rate was dominated by the intrinsic reaction rates on the oxide surface rather than the mass transfer rate of H_2O_2 to the surface. The reaction mechanism for the decomposition of H_2O_2 on goethite surface was proposed on the basis of the fundamental reactions explaining the surface complexation chemistry for iron oxide and interaction of H_2O_2 with the surface sites as shown in Eqs. (2.43) to (2.47):

$$\equiv Fe^{III}OH + H_2O_2 \leftrightarrow (H_2O_2)_s \qquad (2.43)$$

$$(H_2O_2)_s \rightarrow \equiv Fe^{II} + H_2O + HO_2^\bullet \qquad (2.44)$$

$$\equiv Fe^{II} + H_2O_2 \rightarrow \equiv Fe^{III}OH + OH^\bullet \qquad (2.45)$$

$$HO_2^\bullet \rightarrow H^+ + O_2^{\bullet -} \qquad (2.46)$$

$$\equiv Fe^{III}OH + HO_2^\bullet/O_2^{\bullet -} \rightarrow \equiv Fe^{II} + H_2O/OH^- + O_2 \qquad (2.47)$$

Lin et al. (1996) investigated on the possibility of using mixture of H_2O_2 and iron oxide (goethite, α-FeOOH) particles as a chemical oxidant for wastewater treatment by using BuCl as a studied compound. The oxidation rate of BuCl was closely related with degradation rate of H_2O_2. The results showed that BuCl was oxidized effectively by $OH^\bullet$ generated from the interaction of H_2O_2 with FeOOH particles.

2.7.4 Iron Crystallization in Fluidized-bed Fenton Reactor

Hsueh et al. (2006) used a novel supported iron oxide, prepared in a fluidized-bed reactor (FBR), as a catalyst for the heterogeneous photo-assisted Fenton degradation of azo-dye Reactive Black 5 (RB5). This catalyst was much cheaper than Nafion-based catalysts, and could markedly accelerate the degradation of RB5 under irradiation by UVA (@ 365 nm). The effects of the molar concentration of H_2O_2, the pH of the solution and the catalyst loading on the degradation of RB5 were elucidated. A simplified mechanism of RB5 decomposition which was consistent with the experimental findings for a solution with the pH of up to 7.0 was proposed. Approximately 70% decolorization was obtained and 45% of the total organic carbon

was eliminated on the surface of the iron oxide at pH 7.0 after 480 minutes in the presence of 0.055 mM RB5, 5.0 g iron oxide/L, 29.4 mM H_2O_2, under 15W UVA.

Chou et al. (2004) determined the effect of operational pH, superficial velocity, specific iron loading, and influent H_2O_2 concentration on the crystallization efficiency of FeOOH. Two types of FeOOH catalysts were synthesized: FeOOH I was prepared at pH 3.5 (70% amorphous FeOOH and 30% γ-FeOOH), and FeOOH II was formed by aging FeOOH I at pH 13 (30% amorphous FeOOH and 70% γ-FeOOH). The results demonstrated that all these parameters were found to significantly influence the crystallization efficiency. The FeOOH II catalyst presented higher reactivity to ward H_2O_2 but lower stoichiometric efficiency in oxidizing benzoic acid than FeOOH I, similar to the result from the commercial goethite. Furthermore, the performance of catalytic oxidation was significantly depended on the crystalline property.

Chou et al. (2001) applied a novel supported γ-FeOOH catalyst to oxidize benzoic acid (BA) in a circulating fluidized-bed reactor by H_2O_2 and to determine the effects of homogeneous and heterogeneous catalysis. They found that the degradation rate of H_2O_2 was proportional to its concentration and the BA decomposition depended on both BA and H_2O_2. Conclusively, although heterogeneous catalysis contributed primarily to the oxidation of BA at pH 4.4-7.0, the homogeneous catalysis was of increasing importance below pH 4.4.

Chou and Huang (1999) investigated on the effect of Fe^{2+} on the catalytic oxidation of benzoic acid (BA) in the FBR applying supported γ-FeOOH as the carrier. They found that both mineralization of organics and crystallization of Fe^{3+} were simultaneously well performed under proper condition. Moreover, the reductive and the crystallization of γ-FeOOH as well as the oxidation of BA was proposed based on the experiment results. The reaction mechanism is shown in Figure 2.7
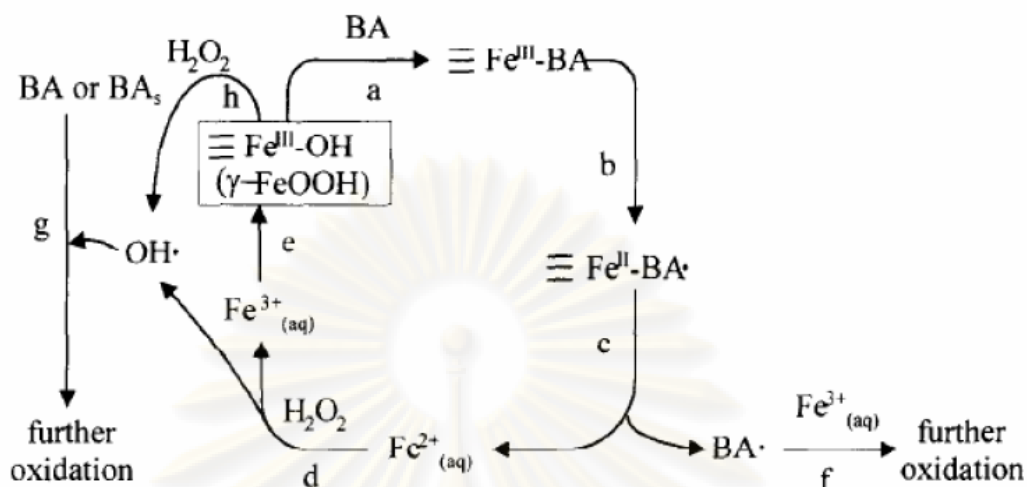
Figure 2.7 Reaction mechanism of benzoic acid (BA) oxidation by the fluidized-bed Fenton process: (A) reductive dissolution: reactions a, b, and c; (B) synthesis of Fe(III) hydroxide: reactions d and e; (C) oxidation of BA: reactions f, g, and h; BAx(5) denotes the surface complex of BA and γ-FeOOH (Chou and Huang, 1999).

Tai (1999) studied the crystal growth kinetics of a two-step growth process in liquid fluidized-bed crystallizers. A reliable method has been proposed to determine the parameters of the two-step growth. For sparingly soluble salts, the growth process was more complicated, but the two-step model could still be applied successfully under a similar environment of pH, ionic strength, and species ratio.

CHAPTER III
METHODOLOGY

3.1 Materials and Chemicals

3.1.1 Chemicals

2,6-DMA, n,n-dimethyl-aniline (n,n-DMA), aniline (AN), 2,6-dimethyl-phenol (2,6-DMP), 2,6-dimethyl-nitrobenzene (2,6-DMN), 2,6-dimethyl-benzoquinone (2,6-DMB), $FeSO_4 \cdot 7H_2O$, H_2O_2, and all chemical substances used in this work were analytical reagent grade. Fluidized media were quartz sand (SiO_2), construction sand (CS), and aluminum oxide (Al_2O_3). Except stated otherwise, the diameter sizes of SiO_2 and CS were 0.42 to 0.59 mm by using the sieves #30 & #40 (passing #30 but retained on #40) whereas the size of Al_2O_3 was 2.5 mm which was the smallest size commercially available. All media were soaked in HCl solution at pH 1 for 24 hours, washed with de-ionized water until the solution pH was 7, and then oven dried at 103°C (Lo and Chen, 1997). De-ionized water from a Millipore system with a resistivity of 18.2 $M\Omega$/cm was used for preparing all solutions.

3.1.2 Batch Reactor

For the batch experiments both for 2,6-DMA degradation kinetics study and iron precipitation/crystallization study, a 0.5-liter Pyrex beaker in a water bath for temperature control at 25±0.2°C was used as the reactor (as shown in Appendix A).

3.1.3 Fluidized-bed Reactor

A 1.35-liter glass-cylinder reactor with an inlet, outlet, and a recirculation pump as shown in Figure 3.1 was used as the fluidized-bed reactor (FBR). The carrier used in this study was either quartz sand, construction sand, or aluminum oxide. The
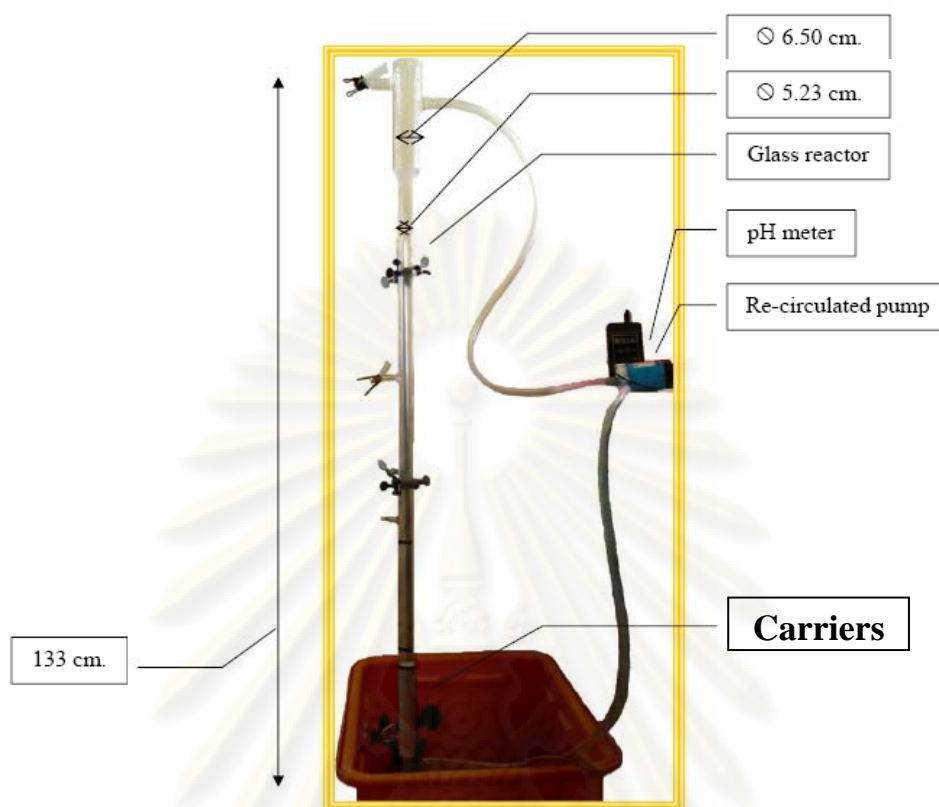
Figure 3.1 Fluidized-bed reactor.

bed expansion was kept constant at 50% from the original bed level by adjusting the internal recirculation rate. The FBR was controlled at 25±0.2°C by air recirculation from 2 air conditioners.

3.2 Experimental Procedures

3.2.1 Kinetics of 2,6-Dimethyl-aniline Degradation

3.2.1.1 Completely Mixed Reactor

For the batch study, the synthesis wastewater was prepared in the beaker using reagent grade chemicals diluted with de-ionized water to the desired concentration. A calculated amount of $FeSO_4 \cdot 7H_2O$ was added as the source of Fe^{2+}. Next, the stirrer was turned on to mix the solution and completely dissolve the ferrous salt. After that,

the pH was adjusted to 3.0 ± 0.1 by 1+3 H_2SO_4. H_2O_2 solution was added and the reaction was simultaneously started. At selected time interval, an appropriate amount of aliquot was taken from the reactor for analysis. To stop further Fenton reaction, an appropriate amount of 0.1 N NaOH was added to the sample to raise the pH to alkaline range. After that, the solution was filtered by a 0.22-μm cellulose acetate membrane filter to separate precipitated iron before analysis. Solution pH was controlled constantly by the addition of 1+3 H_2SO_4 or 1 or 6 N NaOH whenever necessary. All experimental activities are described in Figure 3.2.

For the continuous study, the synthetic wastewater with Fe^{2+} dissolution and H_2O_2 solution were separately, but continuously and equally (18 ml/min), fed into the 0.5-liter beaker by a peristaltic pump. The effluent characteristics were monitored until the steady state has been reached. All other procedures were similar to the batch study.

3.2.1.2 Fluidized-bed Reactor

For fluidized-bed Fenton experiment, the synthetic wastewater with desired Fe^{2+} concentration was prepared in a beaker before pouring into the FBR. After that, 300 gm (300 g per 1.3 L) of carriers was filled into the reactor. The internal recirculation pump was switched on to mix the solution and suspend the carrier at 50% bed expansion. The pH was adjusted to 3.0 ± 0.1 by 1+3 H_2SO_4. Next, H_2O_2 solution was added and the reaction was simultaneously started. Solution pH was controlled constantly by the addition of 1+3 H_2SO_4 or 1 or 6 N NaOH whenever necessary. At selected time interval, an appropriate amount of aliquot was taken from the FBR for analysis. Pretreatment step was similar to the case of Fenton experiment. Experimental steps are summarized in Figure 3.2.

3.2.2 Iron Crystallization

All experimental procedures and setup for completely mixed reactor and fluidized-bed reactor in this part were similar to those in the kinetics study.

Filling with synthetic wastewater and Fe^{2+}/Fe^{3+} solution into the 0.5 L beaker (completely mixed reactor) and 1.35 L FBR (fluidized-bed reactor)

⇩

Filling the carriers into the reactor (fluidized-bed reactor)

⇩

Turning on the stirrer (completely mixed reactor) or the recycle pump to suspend the carriers and mix the solution (fluidized-bed reactor)

⇩

Adjusting pH by 1+3 H_2SO_4 or 1 or 6 N NaOH

⇩

Adding H_2O_2 to the solution and start the reaction (Fenton experiment)

⇩

Taking the sample to analyze (At selected time interval)

⇩   ⇩

pH measurement
H_2O_2 residual
Ferrous ion
Soluble iron analysis
Total iron analysis

Adding 0.1 N NaOH

⇩

GC analysis
TOC analysis
IC analysis
Intermediate identifications

Figure 3.2 Experimental scheme for Fenton and fluidized-bed Fenton processes.

3.3 Experimental Scenarios

This research study was divided mainly into two parts. The first part aimed to determine the kinetics and mechanism of 2,6-DMA degradation by $OH^{\bullet}$. Various experimental scenarios, including batch and continuous modes, with and without solid media, were performed to determine the intrinsic 2nd-order rate constant between 2,6-DMA and $OH^{\bullet}$ to ensure the accuracy of the obtained values. For mechanism determination, several extra experiments were performed using the initially identified aromatic intermediates, i.e., 2,6-DMP, 2,6-DMN and 2,6-DMB, as the target compounds for cross-checking purpose. In the second part, the behavior of the iron precipitation and crystallization onto the media in the FBR was investigated.

3.3.1 Kinetics of 2,6-Dimethyl-aniline Degradation

To determine the intrinsic 2nd-order rate constant between 2,6-DMA and $OH^{\bullet}$, 6 experimental scenarios (Scenarios B to G) were set up and carried out. In addition, one control experiment was also performed for system control (Scenario A).

Scenario A

Determination of the effect of volatilization and H_2O_2 on the disappearance of 2,6-DMA, n,n-dimethylaniline, and aniline in a batch reactor under the conditions as shown in Table 3.1. This experiment was conducted to observe the reactivity of all target compounds with H_2O_2 as well as their ability to volatile to the atmosphere under the studied conditions.

Table 3.1 Conditions for the determination of H_2O_2 oxidation and volatilization of target compounds.

2,6-DMA (mM)	AN (mM)	n,n-DMA (mM)	H_2O_2 (mM)	pH
1	1	1	20	3

Scenario B

Determination of the effect of H_2O_2 on the degradation of o-toluidine in a batch reactor with the condition as shown in Table 3.2. This experiment aimed to verify the H_2O_2–resistivity of the o-toluidine which was used as an internal standard for GC analysis.

Table 3.2 Conditions for the determination of o-toluidine oxidation by H_2O_2.

o-toluidine (mM)	H_2O_2 (mM)	pH
0.1	2	11

Scenario C

Verification of the competitive rate technique in a batch reactor with the conditions as shown in Table 3.3. This part aimed to verify the feasibility and accuracy of the competition rate technique in determining the reaction rate constant by using two organics, i.e., AN and n,n-DMA of which the rate constants with $OH^\bullet$ have been already reported.

Table 3.3 Conditions for verification of the competitive rate technique.

n,n-DMA (mM)	AN (mM)	Fe^{2+} (mM)	H_2O_2 (mM)	pH	Number of run
1	1	1	20	3	3

Scenario D

Determination of intrinsic rate constant by ordinary Fenton process in a batch reactor in the absence of solid carriers with the conditions as shown in Table 3.4. This part aimed to determine the 2nd-order rate constant between 2,6-DMA and $OH^\bullet$ by the competitive rate technique using AN as a reference compound.

Table 3.4 Conditions for the rate constant determination under the batch operation.

2,6-DMA (mM)	AN (mM)	Fe^{2+} (mM)	H_2O_2 (mM)	pH	Number of run
1	1	1	20	3	3
0.5	1	1	20	3	1
1	0.5	1	20	3	1
0.5	0.5	1	20	3	1
1	1	1.5	30	3	1
1	1	2	40	3	1
1	1	1	30	3	1

Scenario E

Determination of intrinsic rate constant by ordinary Fenton process in the presence of SiO_2 in the batch reactor with the conditions as shown in Table 3.5. This part aimed to investigate the effect of solid media on the disappearance rate and rate constant of 2,6-DMA simulating of those occurred the fluidized-bed Fenton process.

Table 3.5 Conditions for the rate constant determination in the presence of solid media.

2,6-DMA (mM)	AN (mM)	Fe^{2+} (mM)	H_2O_2 (mM)	pH	SiO_2 (g/l)
1	1	1	20	3	37.04

Scenario F

Determination of intrinsic rate constant by fluidized-bed Fenton process with the conditions as shown in Table 3.6. This part aimed to investigate the effect of FBR operation on the oxidation rate and rate constant of 2,6-DMA.

Table 3.6 Conditions for rate constant determination by the fluidized-bed Fenton process.

2,6-DMA (mM)	AN (mM)	Fe^{2+} (mM)	H_2O_2 (mM)	pH	CS (g/l)	Number of run
1	1	1	20	3	230.77	2

Scenario G

Determination of intrinsic rate constant by ordinary Fenton process in the continuous mode with the conditions as shown in Table 3.7. The objective of this part was similar to those of Scenario D; however, the operation was changed from a batch mode to continuous mode.

Table 3.7 Conditions for the rate constant determination under the continuous operation.

2,6-DMA (mM)	AN (mM)	Fe^{2+} (mM)	H_2O_2 (mM)	pH	Number of run
1	1	1	20	3	2

3.3.2 Mechanism of 2,6-Dimethyl-aniline Oxidation

To determine the oxidation pathway of 2,6-DMA by $OH^\bullet$, the Fenton reaction of 2,6-DMA and its potential intermediates was studied in the batch reactor.

Scenario H

Determination of the mechanism of 2,6-DMA oxidation by $OH^\bullet$ with the conditions as shown in Table 3.8.

Table 3.8 Conditions for oxidation pathway determination.

2,6-DMA (mM)	2,6-DMB (mM)	2,6-DMN (mM)	2,6-DMP (mM)	Fe^{2+} (mM)	H_2O_2 (mM)	pH
10	-	-	-	10	200	3
-	10	-	-	5	100	3
-	-	10	-	5	100	3
-	-	-	10	5	100	3

3.3.3 Iron Precipitation and Crystallization

Since the precipitation and crystallization of solid particles occur simultaneously and simultaneously, this research decided to investigate all the conditions involving in these two processes.

Scenario I

Preliminary study on the effect of pH on iron solubility with the conditions as shown in Table 3.9. Since Fe^{2+} is one of the Fenton's reagent and Fe^{3+} is the oxidize product from Fenton reaction, it is important to determine the aqueous solubility of both iron species. This can ensure that all $FeSO_4 \cdot 7H_2O$ being added could completely dissolve in the water and the precipitation of Fe^{3+} can be understood.

Table 3.9 Conditions for iron solubility study.

Iron (mM)	pH	$NaClO_4$ (M)
1 mM of Fe^{2+}	1-12	-
		0.1
1 mM of Fe^{3+}	1-12	0.1

Scenario J

Determination the effect of iron concentration on iron solubility at different pH with the condition as shown in Table 3.10. This part aimed to provide a better understanding in the solubility behavior of Fe^{2+} and Fe^{3+} in aqueous phase.

Table 3.10 Conditions for the effect of iron concentration.

Iron	pH	NaClO$_4$ (M)
1 & 2 mM Fe^{2+}	1-12	0.1
1 & 2 mM Fe^{3+}		

Scenario K

Determination of Fe(OH)$_3$ crystallization with the conditions as shown in Table 3.11. The behavior of Fe(OH)$_3$ crystallization onto solid media under supersaturated was investigated in this part which can lead to a better understanding on the removal of iron in the fluidized-bed Fenton process.

Table 3.11 Conditions for the Fe(OH)$_3$ crystallization characterization in FBR.

Fe^{3+} (mM)	pH	CS (g/l)	SiO$_2$ (g/l)	Al$_2$O$_3$ (g/l)
1	7	230.77	-	-
1	7	-	230.77	-
1	7	-	-	230.77
1	3	230.77	-	-

Scenario L

Determination of crystallization under Fenton reaction with the conditions as shown in Table 3.12. This part aimed to determine the natural behavior of iron crystallization in the fluidized-bed Fenton process in the absence of organic matters.

Table 3.12 Conditions for the crystallization in fluidized-bed Fenton process.

Fe^{2+} (mM)	H_2O_2 (mM)	pH	CS (g/l)	SiO_2 (g/l)
1	20	3	230.77	-
			-	230.77
			230.77 (passing #30)	-

Scenario M

Determination of effect of $Fe(OH)_3$ crystallites on crystallization process with the conditions as shown in Table 3.13. In this part, the Fenton reaction was allowed to proceed in a completely mixed reactor (CMR) for 1 hour without any medium before transferring into the FBR for crystallization for 3 hours (1-hr pre-CMR+FBR). This scenario was different from previous in term of the crystallite formation. In previous scenario, the iron crystallites were formed and the crystallization onto the sand surface occurred simultaneously. On the other hand, the crystallites were allowed to ripen for 1 hour (the crystals became larger) before the crystallization in the FBR could happen.

Table 3.13 Conditions for the effect of $Fe(OH)_3$ crystallites.

Fe^{2+} (mM)	H_2O_2 (mM)	pH	CS (g/l)	Operating Mode
1	20	3	230.77	fully FBR
				1-hr pre-CMR+FBR
3	60	3	230.77	5-min pre-CMR+FBR

Scenario N

Determination of effect of iron concentration on iron crystallization with the conditions as shown in Table 3.14. As the iron concentration increased, the supersaturated condition became more prevailed even though the pH was the same; hence, the effect of supersaturation on iron crystallization could be obtained without

compromising the effect of pH. In this part, various Fe^{2+} concentrations were used to observe the behavior of iron crystallization both under the typical FBR mode and 1-hr pre-CMR+FBR mode.

Table 3.14 Conditions for the effect of iron concentration on crystallization.

Fe^{2+} (mM)	H_2O_2 (mM)	pH	CS (g/l)	Operating Mode
1	20			fully FBR
				1-hr pre-CMR+FBR
2	40	3	230.77	fully FBR
				1-hr pre-CMR+FBR
3	60			fully FBR
				1-hr pre-CMR+FBR

Scenario O

Determination of effect of mixing on crystal growth with the conditions as shown in Table 3.15. This part aimed to provide a better understanding on the mechanism of crystallite formation and crystal growth.

Table 3.15 Conditions for the effect of mixing on crystal growth.

Fe^{3+} (mM)	pH	Operating Conditions
3	3	Purging with air in cylinder
		Purging with O_2 in cylinder
		Purging with N_2 for 15 min and kept in BOD bottle
		Fenton process

Scenario P

Determination of effect of organo-ferric complex on Fe^{3+} solubility and crystallization in FBR. This scenario consisted of 2 parts. The first part studied under constant organo-ferric complex concentration without Fenton's reagent in FBR (Table

3.16), the type and concentration of carboxylic acids being used simulated from the conditions found during the oxidation of 1 mM of 2,6-DMA. The second part aimed to investigate under the dynamic condition in the fluidized-bed Fenton process (Table 3.17).

Table 3.16 Conditions for the effect of organo-ferric complex on Fe^{3+} solubility/crystallization in FBR.

Fe^{3+} (mM)	Formic acid (mM)	Acetic acid (mM)	Oxalic acid (mM)	pH	CS (g/l)
1	2.0	0.5	2.0	3	230.77
	-	-	-		

Table 3.17 Conditions for the effect of organo-ferric complex on Fe^{3+} solubility/crystallization under dynamic state in fluidized-bed Fenton process.

2,6-DMA (mM)	AN (mM)	Fe^{2+} (mM)	H_2O_2 (mM)	pH	CS (g/l)	Operating Mode
0.1	0.1	1	20	3	230.77	fully FBR
						1-hr pre-CMR+FBR
1	1					fully FBR
						1-hr pre-CMR+FBR

Scenario Q

Determination of the reusability of iron-coated CS for iron crystallization with the conditions as shown in Table 3.18. This part aimed to investigate the capability of CS to serve as the fluidized medium for iron crystallization.

Table 3.18 Conditions for the reusability of iron-coated CS for iron crystallization.

Fe^{2+} (mM)	H_2O_2 (mM)	pH	CS (230.77 g/l)
1	20	3	Cycle 1st – Cycle 5th
2	40		Cycle 6th – Cycle 101st

Scenario R

Determination of the catalytic ability of iron-coated CS in comparison with the goethite in Fenton reaction with the conditions as shown in Table 3.19. Since iron oxide can serve as a catalyst in Fenton process, this study part aimed to determined the catalytic activity of the iron-coated CS obtained from the fluidized-bed Fenton process and compared with the commercial goethite. The test was performed in a batch mode due to the cost limitation of expensive goethite.

Table 3.19 Experimental scenarios for the catalytic ability of iron-coated construction sand on the oxidation of 2,6-DMA and AN.

2,6-DMA (mM)	AN (mM)	H_2O_2 (mM)	pH	Catalyst
1	1	20	3	75 g/l iron-coated CS
				0.075 g/l goethite
				0.75 g/l goethite
				1.0 g/l goethite
				7.5 g/l goethite
				75 g/l goethite

3.4 Analytical Methods

3.4.1 Measurement of Aromatic Compounds

After raising the pH by 0.1 N NaOH addition and filtered by cellulose acetate membranes with 0.22 μm pore size to separate precipitated iron, the sample was analyzed for residual organic compounds and its intermediates by using a GC-17A gas chromatograph equipped with a flame ionization detector and HP-5 capillary column (Hewlett-Packard) with 0.53-mm in inside diameter and 15-m length. Exactly 1.0 μl of sample was injected into the injection port. The column temperature was initially set at 85°C for 3 minutes, then increased by 65°C per minute to 200°C and maintained at this temperature for the final 5 minutes. Injector and detector temperatures were set at 250 and 280°C, respectively. *o*-toluidine was used as the internal standard. Chromatogram of all aromatic compounds used in this study is shown in Figure 3.3 and the standard curves are shown in Appendix B.
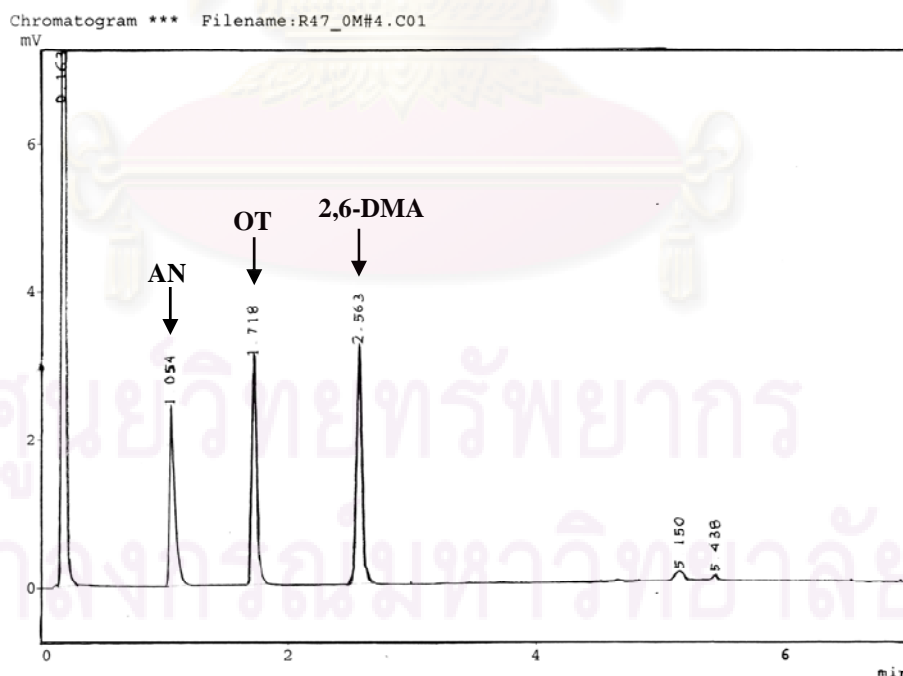
Figure 3.3 Gas chromatography chromatogram.

3.4.2 Measurement of Iron

Concentration of iron species, Fe^{2+}, soluble and total iron, were performed immediately after sampling without alkaline addition in order to prevent the precipitation of $Fe(OH)_2$. For ferrous analysis, the sample was analyzed by light absorbance measurement at 510 nm after being complexed with 1,10-phenanthroline using UV-vis spetophotometer (Genesys 20, ThermoSpectronic, USA) following the Standard Methods (APHA, 1992). The DI water mixed with the sample without phenanthroline was used as a blank for every sample. For total and soluble iron analysis, the samples were digested by concentrated hydrochloric acid (HCl) and hydroxylamine as the reductant to transform Fe^{3+} to Fe^{2+}. Then, the samples were formed a colored complex with 1,10-phenanthroline following to the ferrous analysis.

3.4.3 Measurement of Hydrogen Peroxide Residual

Similar to Fe^{2+} analysis, the sample was analyzed for H_2O_2 immediately after sampling. The concentration of hydrogen peroxide residual was determined by standard iodometric method in which the potassium iodide and sodium thiosulfate were used as the reactant and titrant, respectively, as described in Appendix C.

3.4.4 Measurement of Total Organic Carbon

Mineralization of the effluent was determined by a mean of total organic carbon using SHIMADZU TOC-V_{CPH} (Japan). Before the analysis, the Fenton reaction was stopped by 6 N NaOH at the ratio of 1:10 (20 ml NaOH to 200 ml sample), and then the solution was filtered with 0.22-µm microfilter to separate iron sludge from the solution.

3.4.5 Identification and Measurement of Carboxylic Intermediates

Carboxylic acids were determined by the Ion Chromatograph (SHIMADSU) equipped with SCL-10A VP system controller, DGU-20A$_3$ degasser, LC-20AD VP

liquid chromatograph, CTO-20A column oven, CDD-10A VP conductivity detector, Shim-pack IC-GA3 guard column and Shim-pack IC-A3 analytical column (4.6 mm $\phi \times 15$ cm). The mobile phase was 8.0 mM p-hydroxybenzoic acid and 3.2 mM bis(2-hydroxyethyl)iminotris(hydroxymethyl)methane. The flow rate and temperature were set at 1.2 ml min^{-1} and 40 °C, respectively. Exactly 10 μl of the alkaline sample after NaOH addition was injected into the injecting port.

3.4.6 Identification of Aromatic Intermediates

To identify the aromatic intermediates from 2,6-DMA oxidation by OH$^\bullet$, 4 ml of the sample after stopping Fenton reaction was injected into an extraction tube containing 2 ml of n-hexane. The tube was then shaken by hand 100 times, followed by 15 minutes of sonication, and then centrifuged at 4,000 rpm for 5 minutes. The upper-layer of n-hexane was withdrawn as much as possible into a 5-ml analyzing tube. The remaining mixture in the extraction tube was then re-extracted twice more following the same procedure. At the third extraction, the upper-layer of n-hexane was pulled out and filled the analyzing tube up to the 5-ml mark. A small amount of anhydrous Na_2SO_4 was added to remove moisture before GC analysis. One μl of the extraction solvent into the Agilent Technologies 6890N Network GC System equipped with a J&W DB-5MS capillary column (0.25 mm × 30 m) and connected with the 5973 Network Mass Selective Detector. The GC temperature program was as follows: 40°C for 2 min, followed by a 15 °C min^{-1} ramp to 280 °C, then hold for 5 min.

3.4.7 Solid Characterization

Iron oxide coated media were characterized for their surface properties, including specific surface area, pore volume, and pore size, and iron oxide species by BET surface analyzer (Autosorb-1 from Quantachrome) and XRD analyzer (D8 Discover from Bruker AXS.), respectively.

CHAPTER IV
RESULTS AND DISCUSSION

4.1 Kinetics of 2,6-Dimethyl-aniline Degradation

4.1.1 Experimental Control

4.1.1.1 2,6-Dimethyl-aniline, n,n-Dimethyl-aniline and Aniline Oxidation by H_2O_2 and Volatilization

This experimental part (Scenario A) aimed to determine the oxidation of 2,6-dimethyl-aniline (2,6-DMA), n,n-dimethyl-aniline (n,n-DMA) and aniline (AN) by H_2O_2 as well as their volatilization. The results demonstrated that H_2O_2 did not have any significant impact on degradation of these three compounds as shown in Figure 4.1 (raw data are shown in Appendix D). In addition, volatilization of these three compounds could be neglected within the experimental period. From these results, it believed that the target compound (2,6-DMA) and the reference compounds could not be degraded effectively and rapidly without an involvement of hydroxyl radicals under the studied conditions.

4.1.1.2 o-Toluidine Oxidation by H_2O_2

In this study, *o*-toluidine (OT) was used as the internal standard for gas chromatograph analysis to obtain accurate concentrations of the compounds. As a result, it is necessary to assure that *o*-toluidine would not be degraded under the conditions in GC vial in which the pH was adjusted to 11 to stop Fenton reaction and the sample was diluted 10 times (Scenario B). Figure 4.2 exhibits that *o*-toluidine concentration was not significantly decreased in the presence of H_2O_2, so it means that *o*-toluidine can serve very well as the internal standard.
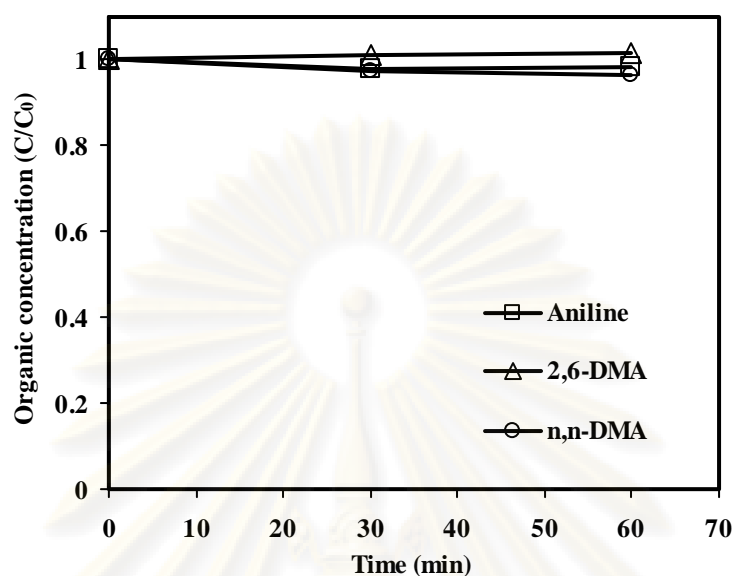
Figure 4.1 Control experiment for direct H_2O_2 oxidation and volatilization with the initial conditions as follows: 1 mM of 2,6-DMA, n,n-DMA and AN, 20 mM of H_2O_2 at pH 3 and 25°C.
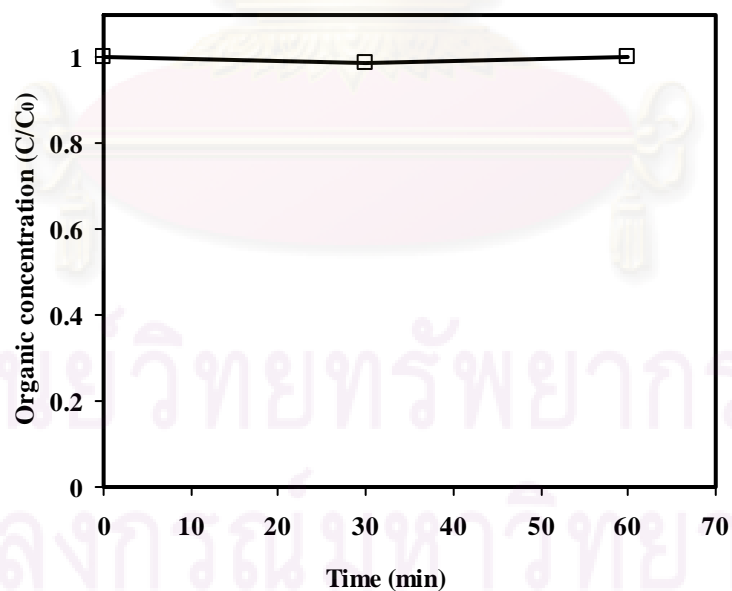
Figure 4.2 Control experiment for direct H_2O_2 oxidation of the internal standard (OT) with the initial conditions as follows: 0.1 mM of OT, 2 mM of H_2O_2 and pH 11.

4.1.2 Verification of Competitive Kinetics Technique

A preliminary study was conducted to verify the accuracy of this competitive kinetics technique by monitoring the degradation rate of aniline with the rate constant with $OH^\bullet$ of 4.8×10^9 $M^{-1}sec^{-1}$ in the presence of n,n-DMA of which its second-order rate constant with $OH^\bullet$ is also known (2.9×10^9 $M^{-1}sec^{-1}$) as shown in Scenario C. Data repeatability and reliability were also conducted as shown in Figure 4.3 as an example case in which the Fenton experiment was carried out in triplicate. It can be seen from the figure that the data obtained from three different runs with similar conditions were almost the same; hence, verifying the consistency of experimental set up and procedure. Considering on the aniline and n,n-DMA removal efficiencies from Figure 4.3(a), it can been seen that aniline was removed faster than n,n-DMA because aniline molecular structure was simpler than n,n-DMA which has a dimethylamino group attached to a phenyl group. This is in agreement with the reported rate constants where the second-order rate constant with $OH^\bullet$ of aniline was greater than n,n-DMA. Figure 4.3(b) is the plot between $\ln([n,n\text{-}DMA]/[n,n\text{-}DMA]_0)$ versus $\ln([AN]/[AN]_0)$ shows a linear relationship and the slope will represent the ratio of the rate constants between aniline and n,n-DMA. The average slope of 0.65 was obtained which was very close to the theoretical value of 0.60; hence, this competitive kinetics technique employed in this research is valid.

4.1.3 Intrinsic Rate Constant of 2,6-Dimethyl-aniline with Hydroxyl Radical

4.1.3.1 Batch Study in the Absence of Media

The intrinsic rate constant of 2,6-DMA was determined by using the similar procedure in a batch reactor similar to the case of technique verification, Data repeatability was repeatedly obtained as shown in Figure 4.4 as an example case. Figure 4.4(a) showed that the removal efficiency of aniline was slower than 2,6-DMA. It can expected that the second order rate constant of 2,6-DMA with $OH^\bullet$ will
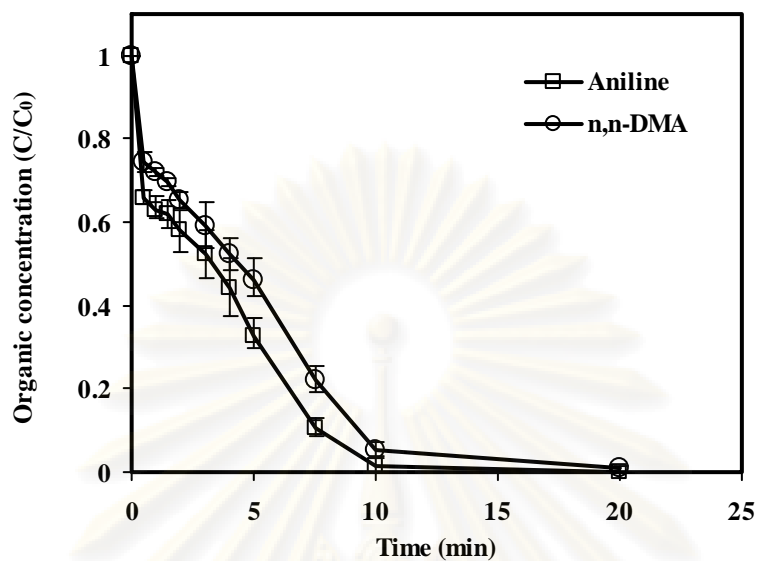
(a) Profile of AN and n,n-DMA
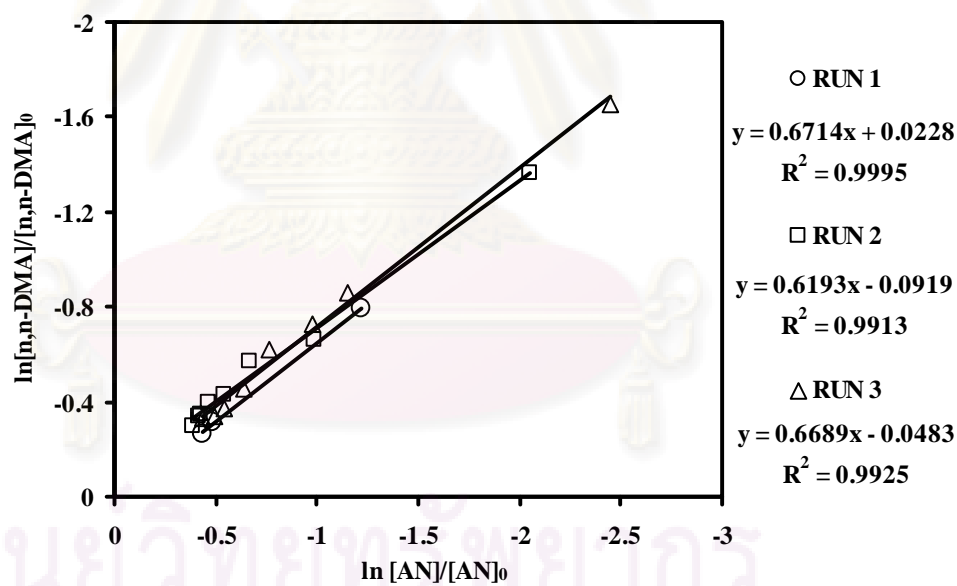
(b) Relationship between $\ln([n,n\text{-DMA}]/[n,n\text{-DMA}]_0)$ versus $\ln([AN]/[AN]_0)$

Figure 4.3 Verification of competitive technique with the initial conditions as follows: 1 mM of AN, 1 mM of n,n-DMA, 1 mM of Fe^{2+}, 20 mM of H_2O_2 at pH 3 and 25°C.
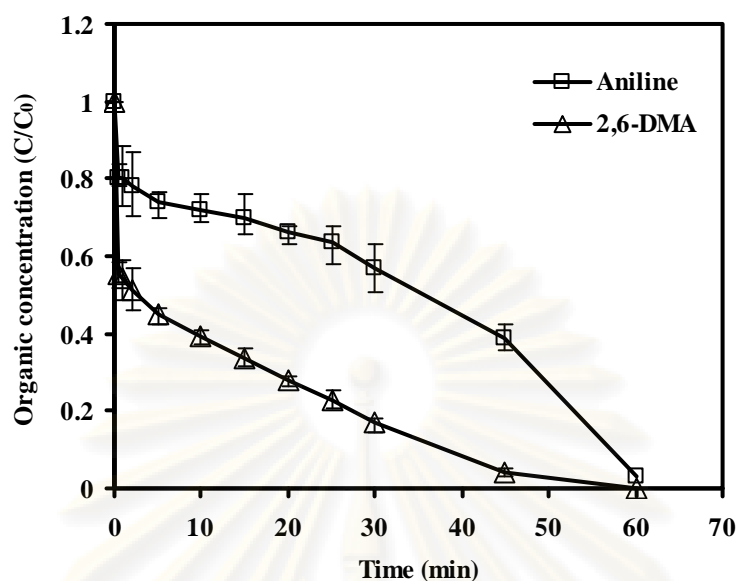
(a) Profile of AN and 2,6-DMA
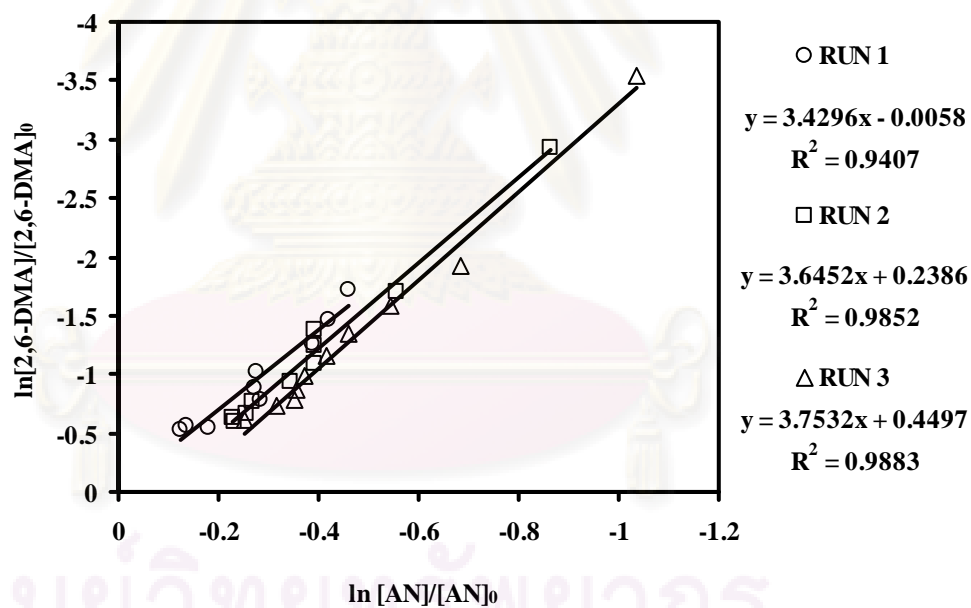
(b) Relationship between $\ln([2,6\text{-DMA}]/[n2,6\text{-DMA}]_0)$ versus $\ln([AN]/[AN]_0)$

Figure 4.4 Intrinsic rate constant determination of 2,6-DMA in batch mode with the initial conditions as follows: 1 mM of AN, 1 mM of 2,6-DMA, 1 mM of Fe^{2+}, 20 mM of H_2O_2 at pH 3 and 25°C.

be greater than aniline. Following the experimental triplications from Figure 4.4(b), the results showed that the ratios of the rate constant between 2,6-DMA and aniline by the Fenton process under the condition of 1 mM of 2,6-DMA, 1 mM of aniline, 1 mM of Fe^{2+}, 20 mM of H_2O_2, pH 3, and 25°C were quite steady with an average of 3.61. The rate constants were estimated to be in the range of 1.65×10^{10} to 1.80×10^{10} $M^{-1}sec^{-1}$ as shown in Table 4.1. Furthermore, under other conditions as described in Scenario D, the rate constants between 2,6-DMA and $OH^{\bullet}$ in the Fenton reaction were found to be quite steady between 1.59×10^{10} and 1.80×10^{10} M^{-1} sec^{-1} as summarized in Table 4.1 (graphical determinations are shown in Appendix E). By averaging the values in Table 4.1, the second-order intrinsic rate constant between 2,6-DMA and $OH^{\bullet}$ obtained from the batch study without media was 1.71×10^{10} $M^{-1}sec^{-1}$.

4.1.3.2 Batch Study in the Presence of Media

In this section, the intrinsic rate constant of 2,6-DMA with $OH^{\bullet}$ was determined in a silica-suspension batch reactor to simulate a fluidized-bed reactor (Scenario E). Figure 4.5(a) shows the time profiles of aniline and 2,6-DMA in the presence of SiO_2. As compared to ordinary Fenton process without SiO_2 (Figure 4.4a), it can be seen that both removal rate and efficiency in the presence of SiO_2 were significantly lower. This is possibly due to the limitation of Fe^{2+} in the presence of SiO_2 suspension as a result from surface complexation which should be similar to the condition which occurs in the fluidized-bed Fenton reactor. Certain portion of added Fe^{2+} was adsorbed onto the surface of SiO_2; hence, reduced the amount of free Fe^{2+} to catalyze the decomposition of H_2O_2 to generate the powerful $OH^{\bullet}$. As a result, the disappearance rates of aniline and 2,6-DMA were decelerated as compared to in the absence of SiO_2. Nonetheless, the results showed that the ratio of the rate constants between 2,6-DMA and aniline obtained from the SiO_2-suspension reactor which simulating the fluidized-bed Fenton reactor of 3.34 (Figure 4.5(b)) which is corresponding to the value of the rate constant of 1.6×10^{10} M^{-1} sec^{-1} (Table 4.1) was comparable to the results from previous part.

Table 4.1 Intrinsic rate constants of 2,6-DMA obtained from various experimental conditions.

Operating Condition	AN (mM)	2,6-DMA (mM)	Fe^{2+} (mM)	H_2O_2 (mM)	Media (g/l)	k ($M^{-1}sec^{-1}$)
Batch without media	1	1	1	20	-	1.65×10^{10}
	1	1	1	20	-	1.75×10^{10}
	1	1	1	20	-	1.80×10^{10}
	1	0.5	1	20	-	1.73×10^{10}
	0.5	1	1	20	-	1.59×10^{10}
	0.5	0.5	1	20	-	1.59×10^{10}
	1	1	1.5	30	-	1.74×10^{10}
	1	1	2	40	-	1.77×10^{10}
	1	1	1	30	-	1.76×10^{10}
	average					1.71×10^{10}
Batch with media	1	1	1	20	37.04 (SiO_2)	1.60×10^{10}
Batch in fluidized-bed Reactor	1	1	1	20	230.77 (CS)	1.67×10^{10}
	1	1	1	20	230.77 (CS)	1.75×10^{10}
	average					1.71×10^{10}
Continuous without media	1	1	1	20	-	1.70×10^{10}
	1	1	1	20	-	1.71×10^{10}
	average					1.71×10^{10}
Overall average						1.70×10^{10}
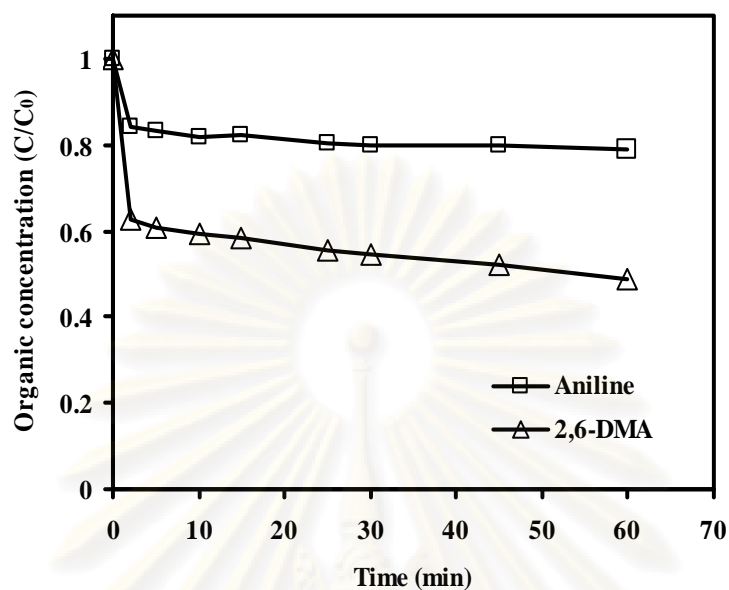
(a) Profile of AN and 2,6-DMA
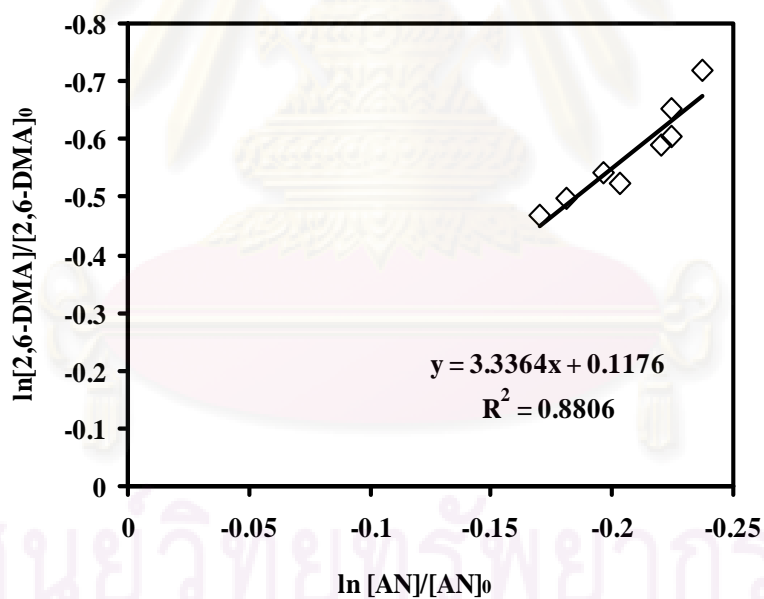
(b) Relationship between $\ln([2,6\text{-DMA}]/[n2,6\text{-DMA}]_0)$ versus $\ln([AN]/[AN]_0)$

Figure 4.5 Intrinsic rate constant determination between 2,6-DMA and OH$^\bullet$ in a SiO$_2$-suspension reactor with following conditions: 1 mM of AN, 1 mM of 2,6-DMA, 1 mM of Fe^{2+}, 20 mM of H$_2$O$_2$, 37.04 g/l of SiO$_2$ at pH 3 and 25°C.

4.1.3.3 Batch Study in the Fluidized-bed Reactor

In this experiment, the second-order rate constants of 2,6-DMA with OH$^\bullet$ was determined in the real fluidized-bed Fenton process (Scenario F). From Figure 4.6(a), the data repeatability of the fluidized-bed Fenton process was also confirmed. It can be seen that the data obtained from two different runs with similar conditions were almost the same; thus, it can verify the consistency of experimental set up and procedure. The outcomes for the slopes of Figure 4.6(b) found that the average rate constant was 1.71×10^{10} M^{-1} sec^{-1} (Table 4.1) which was very close to the results from previous two cases. This could verify the reliability of the rate constant obtained in this study.

4.1.3.4 Continuous Study in the Absence of Media

The continuous study was also carried out to examine the intrinsic rate constant of 2,6-DMA (Scenario G). From Figure 4.7, the repeatability of the continuous study was also assured. It can been seen from the figure that the data obtained from two different runs with similar conditions under the steady state were almost the same; hence, verified the consistency of experimental set up and procedure. Moreover, the oxidation of aniline was slower than 2,6-DMA similar to the batch study. The concentrations of aniline and 2,6-DMA reached the equilibrium within 30 minutes. It means that within the experimental period for 2.5 hours, both of these compounds were quite steady. The second-order intrinsic rate constant from this continuous experiment could be determined by following Eq. 2.28 and found to be with the average of 1.71×10^{10} M^{-1}sec^{-1} as shown in Table 4.1. In addition, since the influent flow rates were also known, the concentrations of OH$^\bullet$ at the steady state could be estimated and were found to be in the range of 4.85×10^{-10} to 6.82×10^{10} mM. Due to its high reactivity and short lifetime the concentration of OH$^\bullet$ in aqueous solution can be expected as very low depending on the presence of reactants, scavengers, organic compounds, and environmental conditions.
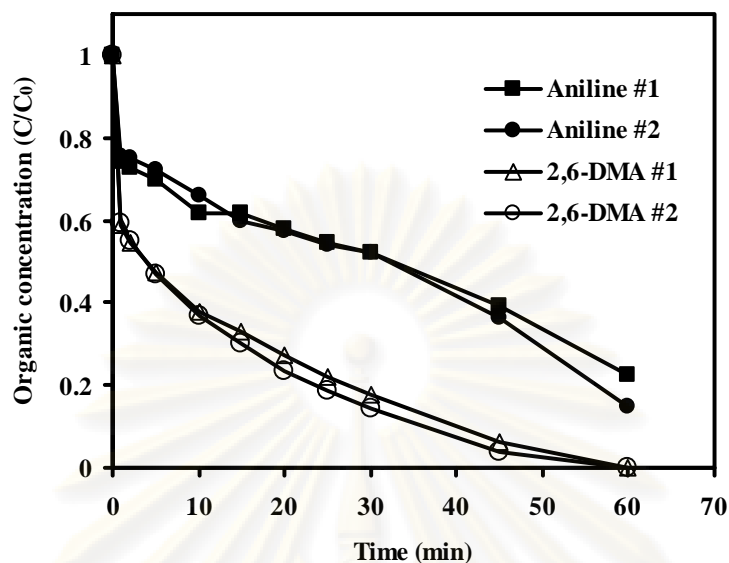
(a) Profile of AN and 2,6-DMA
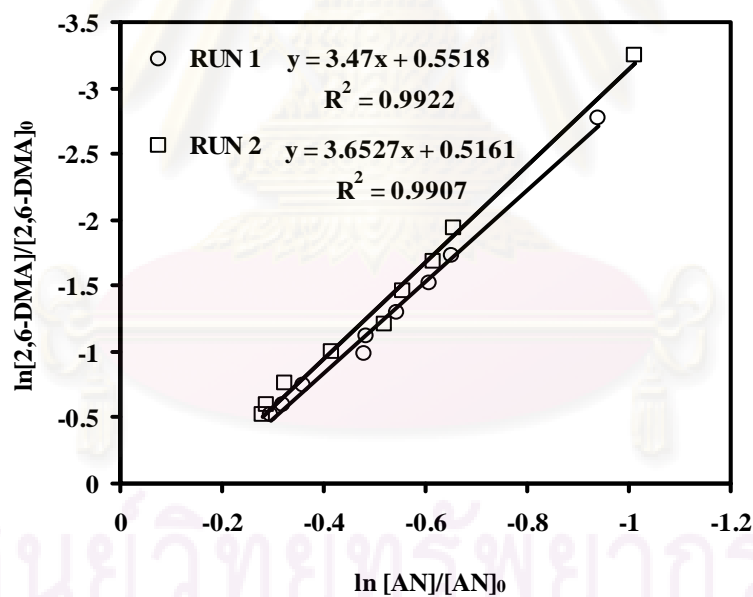
(b) Relationship between ln([2,6-DMA]/[n2,6-DMA]$_0$) versus ln([AN]/[AN]$_0$)

Figure 4.6 Instrinsic rate constant determination between 2,6-DMA and OH$^\bullet$ in a batch fluidized-bed reactor with following conditions: 1 mM of AN, 1 mM of 2,6-DMA, 1 mM of Fe^{2+}, 20 mM of H$_2$O$_2$, 230.77 g/l of CS at pH 3 and 25°C.
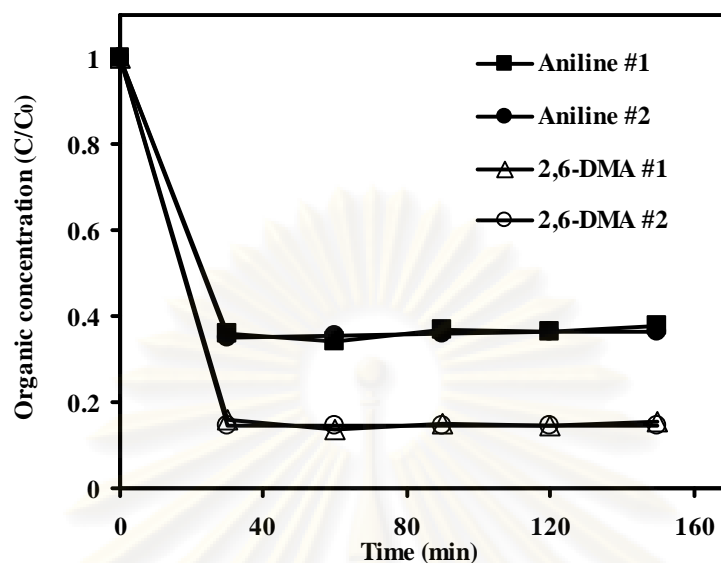
Figure 4.7 Time-profile of 2,6-DMA and AN in continuous mode with the initial conditions as follows: 1 mM of AN, 1 mM of 2,6-DMA, 1 mM of Fe^{2+}, 20 mM of H_2O_2 at pH 3 and 25°C.

4.1.3.5 Overall Rate Constant and Confidence Interval

Average intrinsic second-order rate constant between 2,6-DMA and $OH^\bullet$ from 14 runs was 1.70×10^{10} M^{-1} sec^{-1} as shown in Table 4.1. An attempt has been made to determine the confidence interval for this rate constant mean. By assuming that the measured data were normally distributed and the population variance was unknown, the confidence intervals had to be estimated by using the "t-distribution" instead of the "standard normal distribution" since the data size was less than 30 (Daniel, 1991). The calculation result revealed that the average and 95 percent confidence interval of the intrinsic second-order rate constant between 2,6-DMA and $OH^\bullet$ was $1.70 \pm 0.04 \times 10^{10}$ M^{-1} sec^{-1}.

4.1.4 Effect of Fenton's Reagent on Organic Degradation

Concentrations of the Fenton's reagent, Fe^{2+} and H_2O_2, have a major impact on Fenton reaction not only because they generate the $OH^\bullet$ but also act as the scavengers for $OH^\bullet$. It is interesting to investigate the effect of Fenton's reagent on

the degradation of 2,6-DMA and AN (using the data obtained from Scenario D). Figure 4.8 shows the degradation profiles of 2,6-DMA and AN concurrently present in the Fenton process. It can be seen that when the Fe^{2+}:H_2O_2 ratio was kept constant at 1:20, the disappearance rate of both target compounds increased as the concentration of Fenton's reagent increased. This implies that, for the 2,6-DMA and AN solution at 1 mM each, the amounts of Fe^{2+} and H_2O_2 being added in this study were still under
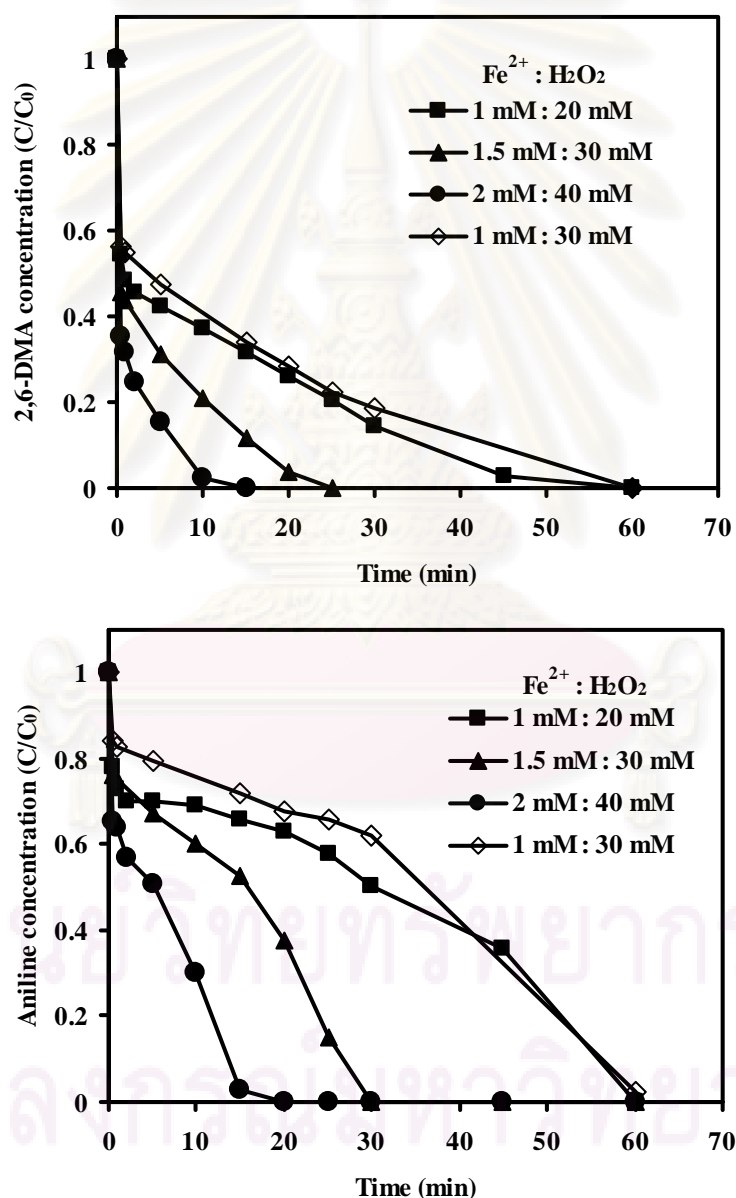
Figure 4.8 Effect of Fenton's reagent on the degradation of 2,6-DMA and AN in a batch mode without media with the initial conditions as follows: 1 mM of AN, 1 mM of 2,6-DMA at pH 3 and 25°C.

the optimum doses; hence, scavenging effect from Fe^{2+} and H_2O_2 was minimal. Decreasing the Fe^{2+}:H_2O_2 ratio from 1 mM : 20 mM to 1 mM : 30 mM did not provide any significant impact on the degradation process indicating that H_2O_2 was not the limiting recipe under the studied conditions; however, increasing the Fe^{2+}:H_2O_2 ratio from 1 mM : 30 mM to 1.5 mM : 30 mM notably accelerated the oxidation rate. This indicates that Fe^{2+} was the principal variable in this case.

4.1.5 Degradation Intermediates and Pathway

The mechanism of 2,6-DMA oxidation by $OH^{\bullet}$ was also investigated in this study (Scenario H). The concentrations of 2,6-DMA and Fenton's reagent were increased 10 times in order to raise the intermediate concentrations to a level that could be accurately identified by the GC/MS and IC. In addition, several extra experiments were also performed using the identified aromatic intermediates as the target compounds to identify their respective oxidation products in order to cross-check the results. The aromatic intermediates found with 80% matching quality or greater were 2,6-DMN, 2,6-DMP, 2,6-DMB, 2,6-dimethyl-hydroquinone (2,6-DMH), 2,6-dimethyl-nitrophenol, and 2,6-dimethyl-3-hydroxy-benzoquinone as shown in Table 4.2. According to the MSDS, only 2,6-DMP is more toxic than the mother compound, 2,6-DMA; nonetheless, its toxicity could be neglected as will be discussed later. This indicated that the methyl group on the aromatic ring was less sensitive to

Table 4.2. Identified aromatic intermediates of 2,6-DMA oxidation by $OH^{\bullet}$.

Retention Time (min)	Chemical formula	Q^a (%)
8.000	$C_8H_8O_2$ (2,6-dimethyl-benzoquinone)	83
8.097	$C_8H_{10}O$ (2,6-dimethyl-phenol)	97
8.943	$C_8H_9NO_2$ (2,6-dimethyl-nitrobenzene)	98
9.046	$C_8H_8O_3$ (2,6-dimethyl-3-hydroxy-p-benzoquinone)	80
10.046	$C_8H_{10}O_2$ (2,6-dimethyl-hydroquinone)	81
10.674	$C_8H_9NO_3$ (2,6-dimethyl-nitrophenol)	90

[a]Q is the matching quality when compared with the mass spectrum in the Wiley7n database.

OH• attack than amine- and nitro-functional groups. In addition to the aromatic intermediates, several carboxylic acids were also detected; including maleic, lactic, oxalic, acetic, and formic acids. The pathway of 2,6-DMA oxidation by OH• is proposed as shown in Figure 4.9. The proposed mechanism is quite similar to those of aniline oxidation by OH• either in the Fenton processes (Brillas et al., 1998) or in the catalytic ozonation (Sauleda and Brillas, 2001) or by oxygen in the wet air oxidation (Oliviero et al., 2003). This is understandable since the methyl group on the aromatic ring of 2,6-DMA was not susceptible to OH• attack as mentioned previously; therefore, OH• would attack other sites around the benzene ring of 2,6-DMA (either at the amine or hydrogen positions) as if it was AN. In addition, several identified species obtained from this study were also in agreement with Skoumal et al. (2008) who studied the oxidation of chloroxylenol by electrochemical advanced oxidation processes. They found OH• attacked at the chlorine position to form 2,6-DMH, which was further oxidized to 2,6-DMB and several carboxylic acids similar to the observation in this study. Moreover, the ring-cleavage C-3 or lower compounds identified in this work were corresponding very well with the reaction network for the catalytic wet air oxidation of maleic acid proposed by Oliviero et al. (2001).

The time profiles of the major products are illustrated in Figure 4.10(a), which reveals that the concentrations of the aromatic intermediates were very low (i.e., less than 0.015 mM) even though 80% of 10 mM 2,6-DMA have been already transformed. This indicates that the aromatic ring was rapidly ruptured to form open-chain products. Hence, the toxicity impact of these aromatic intermediates could be neglected since 2,6-DMP which is more toxic than 2,6-DMA was accumulated at the very low concentrations of around 0.014 mM or less and disappeared rapidly when the oxidation process proceeded. Acetic and formic acids, which are the most successive organic products prior to conversion to CO_2, were accumulated in the solution. This implies that under the studied conditions within 60 minutes of reaction time, 2,6-DMA could not be completely mineralized to CO_2. This is in agreement with the total organic carbon profile as shown in Figure 4.10(b) in which only 35% of initial organic carbon was converted to CO_2. Considering the carbon balance at the end of the reaction period, it can be seen that approximately 70% of the organic carbon could be quantified from the identified intermediates.
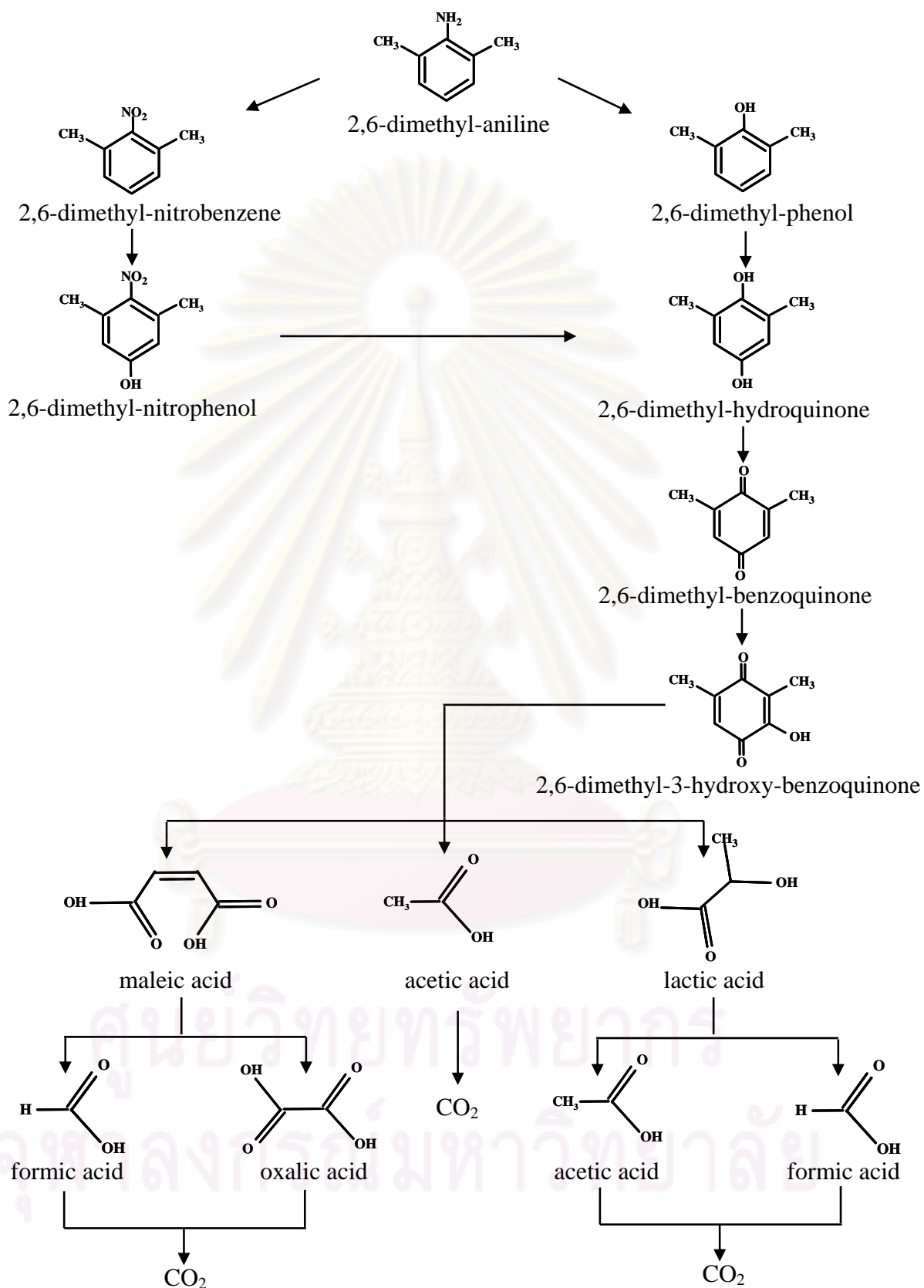
Figure 4.9 Proposed reaction pathway for the mineralization of 2,6-DMA by OH•.
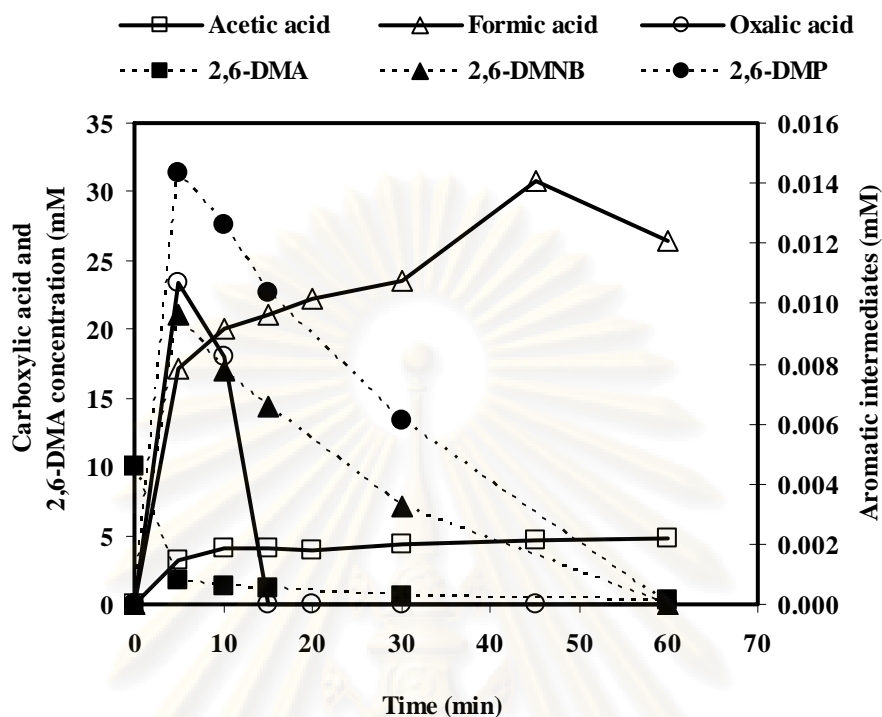
(a) Concentration profile
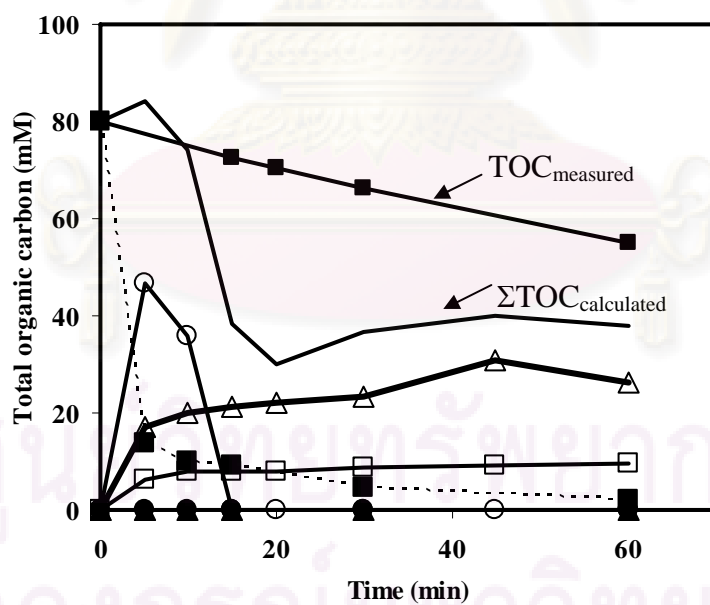
(b) Total organic carbon profile

Figure 4.10 Intermediate products and TOC profiles of 10 mM of 2,6-DMA degradation by Fenton reaction with 10 mM of Fe^{2+} and 200 mM of H_2O_2 at pH 3 and 25 °C.

4.2 Iron Crystallization

4.2.1 Iron Solubility

In this section, the aqueous solubility of Fe^{2+} and Fe^{3+} which are the major iron species in water was determined within the pH range of 2 and 12 with the conditions mentioned in Scenarios I and J. Figure 4.11(a) shows that Fe^{2+} dissolved very well in water when the pH was less than 5 but became less soluble as the pH increased toward pH 12. The precipitation was expected to be in the form of $Fe(OH)_2$.
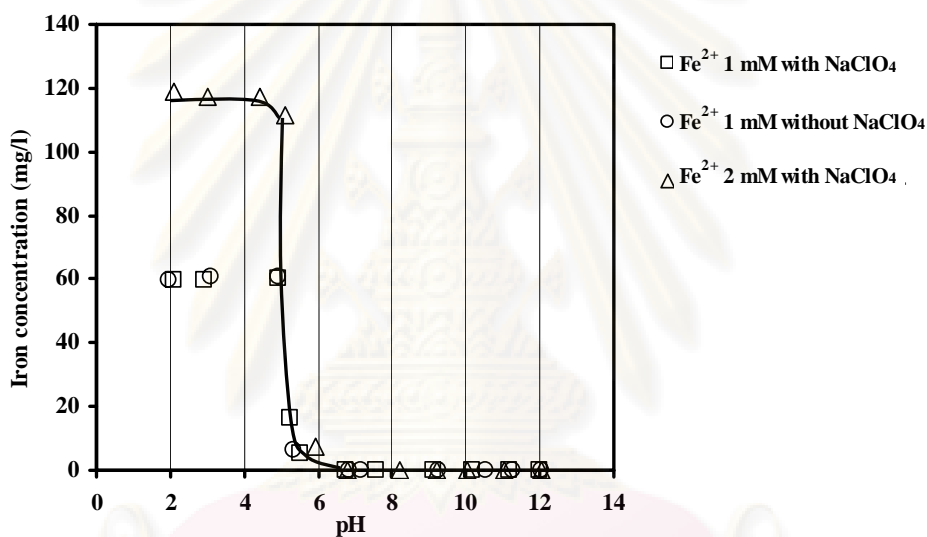
(a) Fe^{2+} solubility
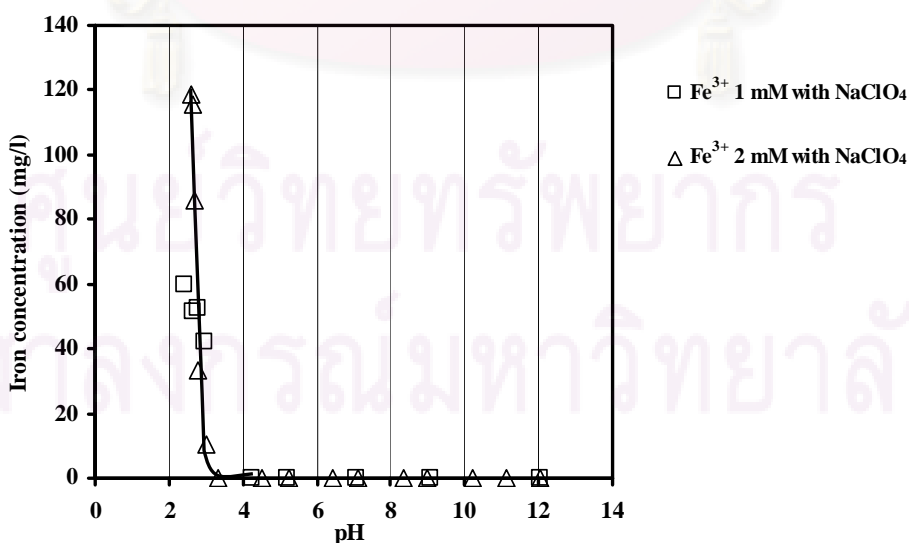
(b) Fe^{3+} solubility

Figure 4.11 Effect of ionic strength and pH on iron solubility at 25°C.

On the other hand, Fe^{3+} which was the product from Fe^{2+} oxidation by H_2O_2 in Fenton reaction was much less soluble than Fe^{2+}, i.e., only 10 mg/l dissolved at pH 3 and became lessen as the pH increased as shown in Figure 4.11(b). These results suggest the Fe^{3+} should continuously precipitate out in the form of $Fe(OH)_3$ during the Fenton reaction at pH greater than 3 since the concentration of Fe^{2+} being used was typically higher than 10 mg/l. These results are in agreement with the theoretical principle as shown in Figure 4.12. The lines which representing the concentrations of various ferric-hydroxo complexes as a function of pH are calculated based on theoretical principle of ferric-hydroxo complexes and ferric hydroxide precipitation at 25°C in ideal solution (neglecting the ionic strength). Details for the calculation are shown in Appendix F. The points were the solubility data observed from the experiments. The difference might be due to the effect of ionic strength in the real solution. The data at pH greater than 3 could not be detected accurately because they were lower than the detection limit of the Phenanthroline method.

In order to ensure that the solid ferric phase precipitated out was $Fe(OH)_3$ rather than other ferric oxide species, a test was performed in the absence of oxygen gas by purging with nitrogen gas during the dissolution and placing into the BOD bottle (Scenario O). The results in Figure 4.13 show that the solubility of Fe^{3+} gradually decreased with time and the soluble Fe^{3+} was approaching the value
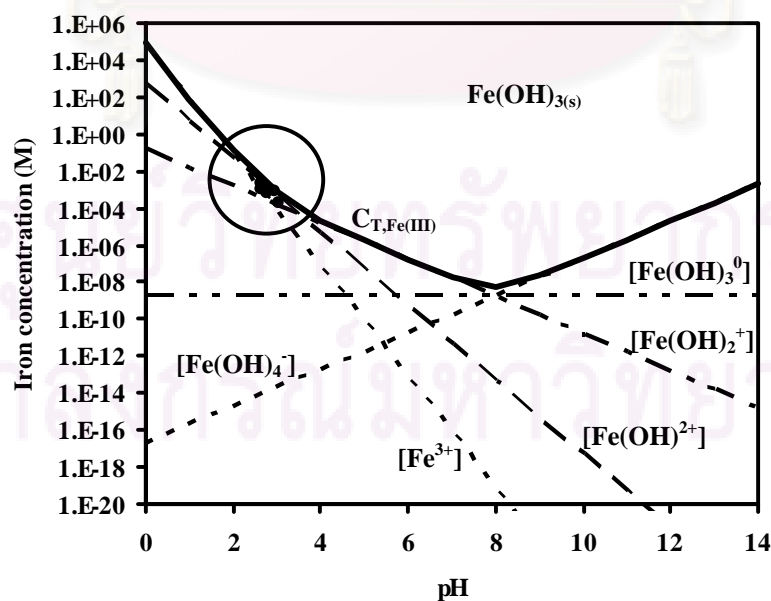
Figure 4.12 Theoretical Fe^{3+} solubility in an ideal solution.
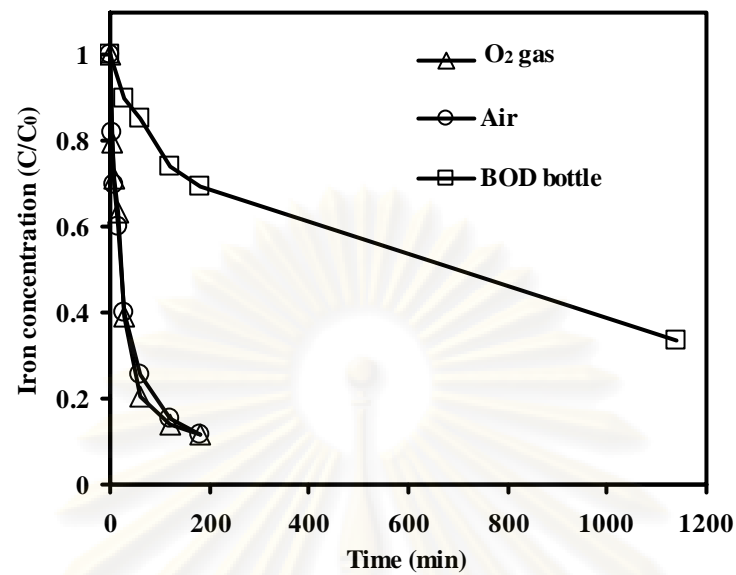
Figure 4.13 Ferric precipitation under different dissolved oxygen levels and turbulence condition (purging with O_2 and air versus stagnant condition in BOD bottle) with the initial conditions as follows: 1 mM of Fe^{3+} at pH 3 and 25°C.

obtained from the solubility test under O_2 gas and air purging (Scenario O) indicating that oxygen did not directly involve in the precipitation process. These iron precipitates should have a potential to crystallize onto the solid particles existing in the fluidized bed reactor under proper environments. Nonetheless, it is important to note that the physical appearance of ferric precipitates at acidic pH was significantly different from those precipitated at neutral pH. At low pH, the solids were dark yellow with discrete particle appearance whereas were orange to red with agglomerate puffy-floc appearance at neutral pH (See Figure A.7). The difference in crystalline structure/color might be due to the pH dependency of the crystalline formation rate. At low pH, the OH^- concentration is very low, resulting in a slower crystallization rate than at high pH where OH^- is dominated. It is very interesting to observe that the color of iron particles in the solution at pH 3 in the BOD bottle gradually changed from dark yellow to orange and red similar to those of pH 7 at the end of 19 hours. This observation supports the statement that the color of the $Fe(OH)_3$ precipitates depends largely on the ripening or aging period of the crystals. According to Stumm and Morgan (1996), there is a metastable zone within which the crystal formation/growth is possible at a lower saturation ratio on a solid surface than in

solution. The crystallization can occur without the concomitant nucleation stage if the solution is seeded with crystallites or foreign particles which could provide their surfaces for nucleation or so called "heterogeneous nucleation". These differences in solid properties also impacted the crystallization onto fluidized-bed media as will be discussed later.

It is important to note that the iron solutions prepared at pH 2 to 12 would significantly have different ionic strength due to acid/alkaline addition for pH adjustment. The difference in ionic strength might affect the solubility of iron due to activity dissimilarity. As a result, another test (Scenario I) was conducted by buffering the ionic strength of the solutions at different pH with 0.1 M of $NaClO_4$. Figure 4.11(a) shows that the effect of ionic strength on ferrous solubility. Between pH 5.4 and 5.8, the ionic strengths of Fe^{2+} solution with and without $NaClO_4$ were approximately 2.0×10^{-6} (mainly from SO_4^{2-}) and 1.0×10^{-1} M (mainly from Na^+ and ClO_4^-), respectively. It can be seen that the effect was diminutive and could be neglected even though the ionic strengths of these solutions were almost 50 times different. This was possible due to the accuracy of the phenanthroline method at very low Fe^{2+} concentration; i.e., the remaining Fe^{2+} concentration might be lower than the detectable limit for 1 cm light path. Nonetheless, the ionic strength of the solution was buffered by 0.1 M $NaClO_4$ in the case of Fe^{3+} solubility test.

4.2.2 Fe(OH)$_3$ Crystallization in Fluidized-bed Reactor

In this part (from Scenario K), Fe^{3+} was precipitated out in the form of $Fe(OH)_3$ at pH 7 in the absence of H_2O_2 to simulate the neutralization condition after Fenton treatment. Under this condition, the concentration product of Fe^{3+} and OH^- was much higher than the solubility product of $Fe(OH)_3$ implying a supersaturated solution. It was very interesting to found that $Fe(OH)_3$ very poorly crystallized onto the fluidized media including SiO_2, Al_2O_3, and CS as shown in Figure 4.14. It is believed that the formation of $Fe(OH)_3$ at pH 7 is very rapid; hence, the mechanism mainly followed the homogeneous crystallization rather than the heterogeneous crystallization. $Fe(OH)_3$ cluster or nucleus was rapidly formed from the supersaturated solution and serving as nuclei for further material deposition to
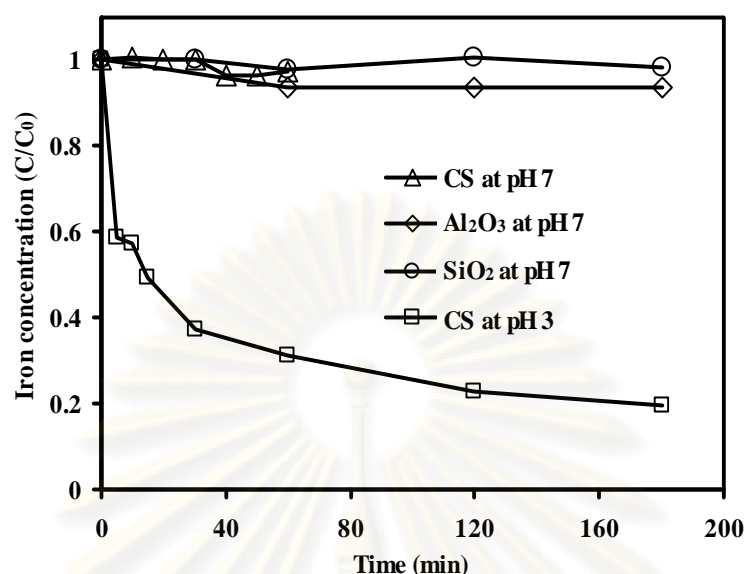
Figure 4.14 Effect of pH and fluidized-bed material on total iron removal with the initial conditions as follows: 1 mM of Fe^{3+}, 230.77 g/l of media at 25 °C.

form crystallites which sequentially ripening to form crystals. The role of fluidized-bed media was minute by the overwhelmingly nucleus formation. In other word, the $Fe(OH)_3$ crystals could be effectively formed and grown by themselves without foreign solids. This suggests that crystallization of iron in fluidized-bed Fenton process could not performed rapidly and effectively after neutralization. In order to verify this hypothesis, Fe^{3+} solution at pH 3 was circulated in the FBR with construction sands under the same operating conditions. The result revealed that iron could efficiently crystallize onto the sand surface with the removal efficiency of 78% in 3 hours. At pH 3, the OH^- concentration was 10^4 times lower than at pH 7; hence, the precipitation occurred within the metastable zone where foreign particles could effectively stimulate the crystallization by providing their surface for heterogeneous nucleation.

4.2.3 Fe(OH)₃ Crystallization in Fluidized-bed Fenton Process

From previous section, it was found that Fe^{3+} could effectively crystallize onto the sand surface at pH 3. This section investigated into more details by simulating the real fluidized-bed Fenton process (Scenario L). Fe^{2+} and H_2O_2 were added

simultaneously into the FBR with either CS or SiO_2 serving as the fluidized materials at pH 3. In this scenario, the experiment with CS was duplicated to determine the reliability and repeatability of the experimental setup and procedure. It can be seen from Figure 4.15 that these two duplicated runs provided very close results which implied that the experimental setup and procedure were reliable and accurate. Regarding on the type of fluidized material, it was found that the iron crystallization onto the CS was faster than onto the SiO_2 even though the iron removal efficiencies at 180 minutes were comparable. This may be due to the impurity on the CS surface and/or surface property of the CS. To verify this hypothesis, CS with different size distribution, i.e., passing sieve #30 but retained on sieve #40 (0.42 mm $< \phi <$ 059 mm) versus passing sieve #30 ($\phi <$ 059 mm), were tested and the results were shown in Figure 4.15. It can be seen that the iron crystallization rate and efficiency of both sets were comparable indicating that the size of CS did not have any significant impact on iron crystallization under the studied conditions. It is well documented that most of Fe^{2+} is simultaneously transformed to Fe^{3+} after the initiation of the Fenton reaction. Data from this study confirmed with this statement as shown in the Table D.30, i.e., Fe^{2+} disappeared instantly within the first 5 minutes to form Fe^{3+}. Most of
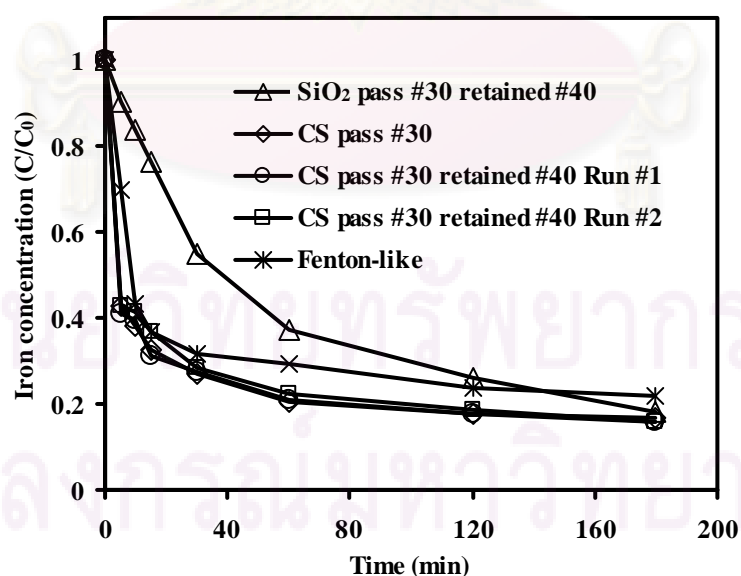
Figure 4.15 Total iron removal in the fluidized-bed Fenton process with various solid materials and sizes with the initial condition as follows: 1 mM of Fe^{2+} or Fe^{3+}, 20 mM of H_2O_2, 230.77 g/l of media at pH 3 and 25 °C.

Fe^{3+} being formed precipitated out and sequentially crystallized onto the CS surface leaving only a small portion of soluble Fe^{3+} in the solution as representing by the soluble iron concentration. It is also interesting to observe that iron reduction in the Fenton-like process with 1 mM Fe^{3+} and similar H_2O_2 concentration was comparable to those of Fenton process as shown in Figure 4.15. This implies that H_2O_2 did not play a major role on iron crystallization, instead the species of iron and its precipitation/crystallization environment primarily controlled the crystallization process.

4.2.4 Effect of Fe(OH)$_3$ Crystallites

To better understand the crystallization mechanism occurred in the fluidized-bed Fenton process, a set of experiment was performed. Fenton reaction was allowed to proceed in a completely mixed reactor (CMR) in the absence of sand for 60 minutes before switching to the fluidized-bed reactor using CS as the media (Scenario M). By doing this, significant amount of $Fe(OH)_3$ crystallites should be formed prior to contact with sand whereas in real fluidized-bed reactor, the $Fe(OH)_3$ nuclei were formed and simultaneously contact with sand. The results for 1 mM of Fe^{2+} and 20 mM of H_2O_2 were shown in Figure 4.16(a) indicating that the crystallization rate was faster in the real fluidized-bed reactor than in the 1-hr pre-CMR+FBR run although the iron removal efficiencies were comparable. As the iron content increased from 1 mM to 2 and 3 mM (Scenario N), the crystallization rate in the 1-hr pre-CMR+FBR mode became worsen and worsen, respectively, when compared to those of real FBR mode as shown in Figures 4.16(b) and 4.16(c). This is because the formation of the crystallites and crystals became ripened and ripened as the iron concentration increased resulting in more homogeneous crystallization than heterogeneous pathway. This implies that newly formed nuclei could adsorb and crystallize onto the sand surface more rapidly and effectively than the matured crystallites. To determine the impact of ripening time on crystallization, another experiment was performed in the CMR for 5 minutes before switching to the fluidized-bed reactor and the results are shown in Figure 4.16(c). As compared to the 1-hr pre-CMR+FBR, it was found that
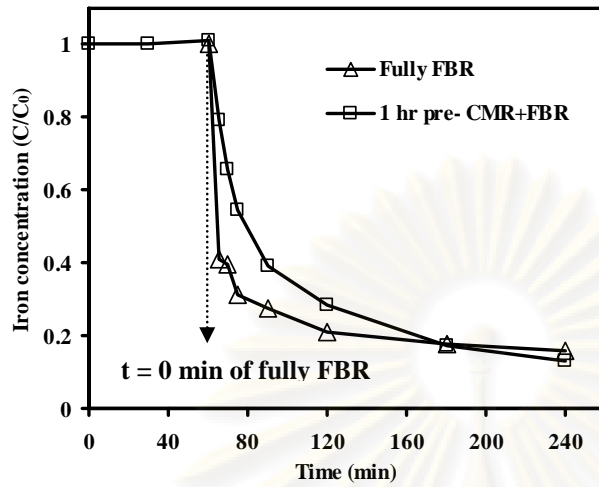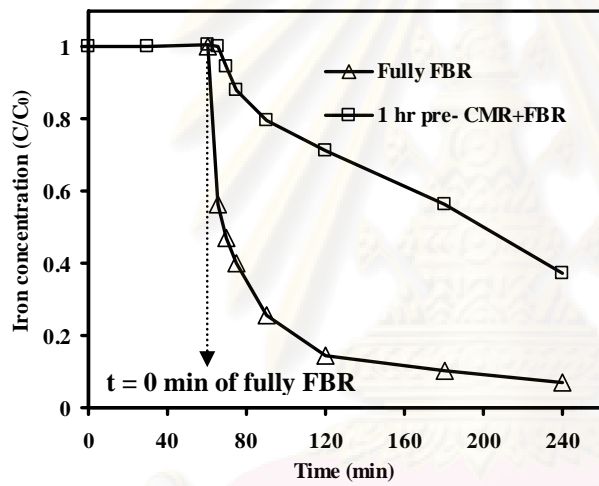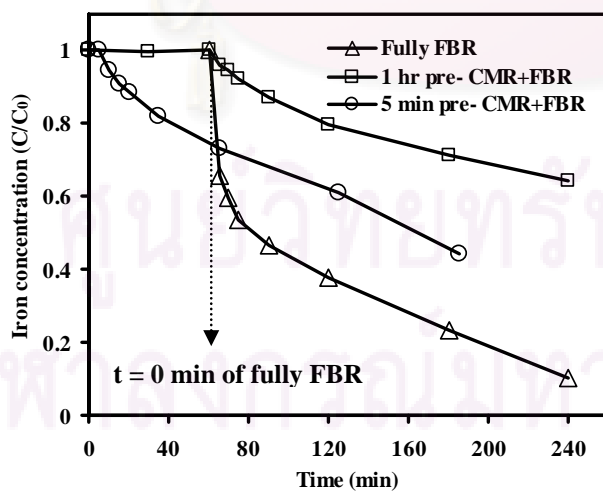
Figure 4.16 Comparison between fully FBR and pre-CMR+FBR operations on total iron removal with the initial conditions as follows: 230.77 g/l of CS at pH 3 and 25°C.

the crystallization rates were comparable indicating that the ripening step happened very fast and should mainly depend on iron concentration. The results from this part suggest that for crystallization optimization in field practice, the crystallization should begin as soon as possible in the fluidized-bed reactor.

4.2.5 Effect of Iron Concentration

As mentioned earlier, the crystallization onto the sand surface or heterogeneous crystallization will occur primarily within the metastable zone. Thus, to optimize the iron removal performance, a low saturation ratio on a solid surface has to be maintained. Therefore, it can be expected that when the iron content increases, the solution would move toward intense supersaturated condition since the concentration product would be much higher than the solubility product of the concerned solid phase. The results of this part (Scenario N) are summarized in Figure 4.17. It can be seen that total iron remaining at 180 minutes was quite constant regardless on initial iron concentration. This observation is understandable since the solubility of $Fe(OH)_3$ was mainly controlled by the solution pH. Since the pH was maintained constantly at 3.0, the soluble iron should also be constant at the equilibrium as governed by the solubility product. In addition, the soluble irons at 30 minutes of all three runs were almost the same regardless on initial iron concentration. This implies that the rate of crystal growth increased as the initial iron increased from 1 mM to 2 and 3 mM, respectively. This observation was opposite to those in the study of pH effect even though both scenarios increased the degree of supersaturation of the $Fe(OH)_3$, i.e., increased Fe^{3+} and OH^- concentration, respectively. This is because in this part the iron concentration was increased only 3 times as compared to an increase of 10^4 times in OH^- concentration when pH increased from 3 to 7. In addition, according to the solubility product formula, OH^- concentration has the power of three whereas the Fe^{3+} has only the power of one; hence, the influence of OH^- concentration is much more drastic than those of Fe^{3+}. The phenomenon happened in the FBR was similar to those in the case of 1-hr pre-CMR before FBR (Scenario N) as shown in Figure 4.18. The soluble irons at 30 minutes for all three
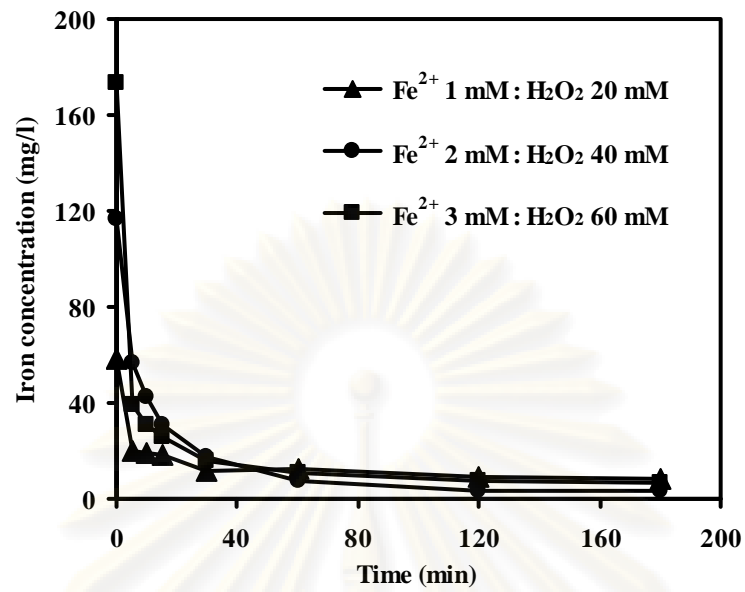
(a) Soluble iron
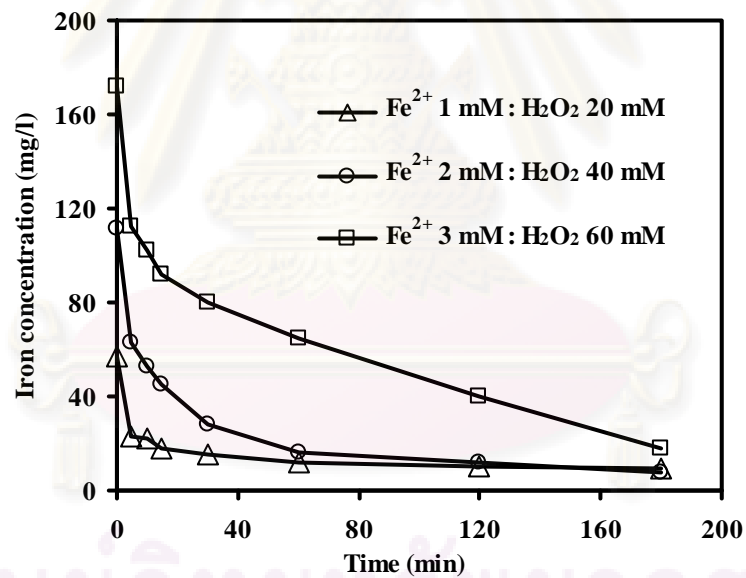
(b) Total iron

Figure 4.17 Effect of Fe^{2+} concentration on iron removal in the fluidized-bed Fenton process under constant $Fe^{2+}:H_2O_2$ ratio scenario with the initial conditions as follows: 230.77 g/l of CS at pH 3 and 25°C.
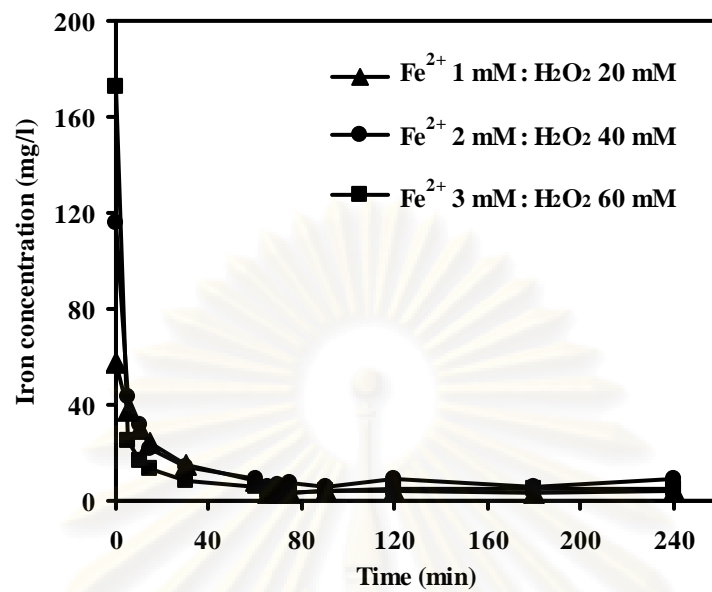
(a) Soluble iron
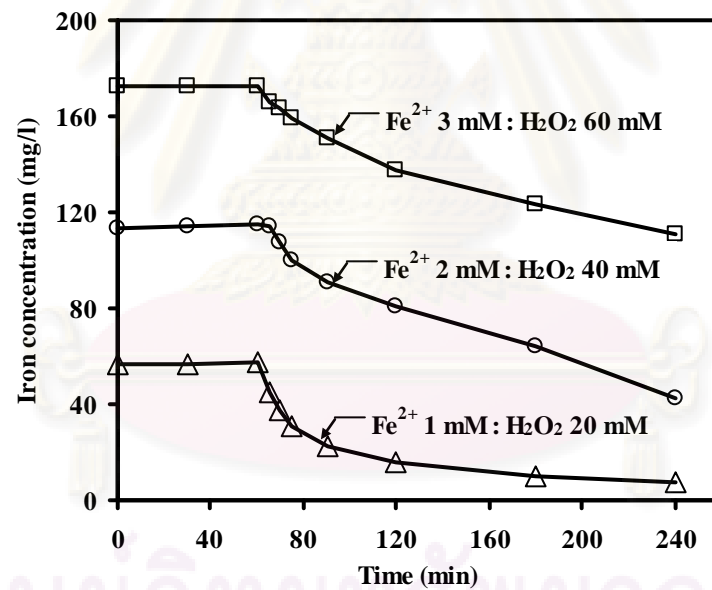
(b) Total iron

Figure 4.18 Effect of Fe^{2+} concentration on iron removal in the 1-hr pre-CMR+FBR under constant $Fe^{2+}:H_2O_2$ ratio scenario with the initial conditions as follows: 230.77 g/l of CS at pH 3 and 25°C.

initial iron concentrations were comparable indicating that the rate of crystal growth also increased with iron concentration.

4.2.6 Effect of Turbulence

After the nucleation process (i.e., the initial formation of solid nuclei), spontaneous growth of crystal will occur. The attachment of a molecule/nucleus to another nucleus to form a solid lattice which includes the transportation of materials to the surface of these nuclei and surface deposition will become very important and should follow the mechanism of solid-solution interface at the molecular level. To understand the mechanism of iron crystallization, a set of experiment was performed. Ferric solution at 1 mM was prepared at pH 3 and vigorously purging with either air or O_2 (Scenario O). The results show that soluble iron decreased at the same pace for both conditions as shown in Figure 4.19. In addition, the reduction of soluble iron in
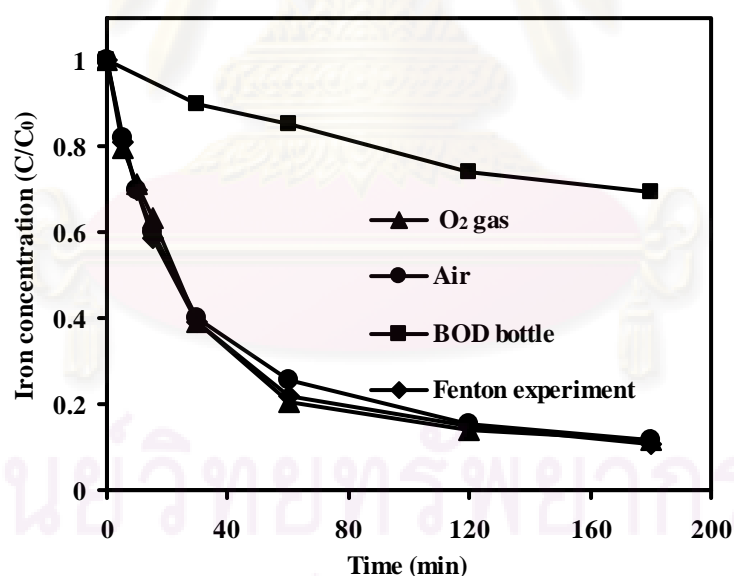
Figure 4.19 Ferric precipitation under turbulence condition by purging with O_2 and air, and stagnant condition in BOD bottle (replotted of Figure 4.13 for 180 minutes) with the initial conditions as follows: 1 mM of Fe^{3+} at pH 3 and 25°C as compare to those in Fenton experiment with the initial conditions as follows: 1 mM of Fe^{2+}, 20 mM of H_2O_2 at pH 3 and 25°C.

the Fenton experiment performed in a beaker with sufficient mixing with Fe^{2+} concentration of 1 mM also followed the similar pattern. It is important to note that Fe^{2+} should be rapidly transformed to Fe^{3+} by Fenton reaction (measured residual Fe^{2+} was negligible). However, if in the stagnant environment where no mixing was provided (1 mM Fe^{3+} solution in the BOD bottles and sacrificed one bottle per sampling), the soluble iron decreased very slowly as seen in Figure 4.19. These results indicated that when the mixing was sufficiently provided, the agglomeration of nuclei resulting in the crystal growth was similar regardless on mixing type and the oxygen gas did not chemically involved in the process. It is interesting to observe that the iron profiles in Figure 4.19 did not show a linear relationship implying that the crystallization process was not controlled by surface reaction as mentioned in Section 2.6.3. Further analysis to verify the effect of molecular transport on the crystal growth by constructing a relationship between iron concentration and the square root of time (plot of C vs $t^{1/2}$) was shown in Figure 4.20(a). It can be seen that only the data from the BOD-bottle experiment under a stagnant condition had a linear relationship. This indicates that the molecular/nucleus diffusion step controlled the crystallization process in this case whereas was not the rate-limiting step under the turbulence condition (either in the O_2-supplied, air-supplied, or Fenton experiment). This was understandable since the mixing would homogenize the iron oxide molecules in the solution and eliminate the concentration gradient at the molecular/nucleus level. To determine the real mechanism other than the molecular/nucleus diffusion and surface reaction which controlling the crystallization process under turbulence condition, another plot of the reciprocal iron with time following the second-order kinetics (plot of 1/C vs time) was constructed as shown in Figure 4.20(b) and found to have the linear relationship for all cases. Hence, the crystallization was controlled by the transport/ collision of the crystallites/ crystals in the mixture via colloidal behavior. In addition, the crystallization should be controlled by orthokinetic flocculation in the case of turbulence environment whereas by perikinetic flocculation in the case of stagnant environment. This conclusion was in agreement with previous observation that the molecule/ nucleus transport was also the rate-controlled step under the stagnant environment. This is because the perikinetic flocculation will become more predominant as the size of colloids is smaller.
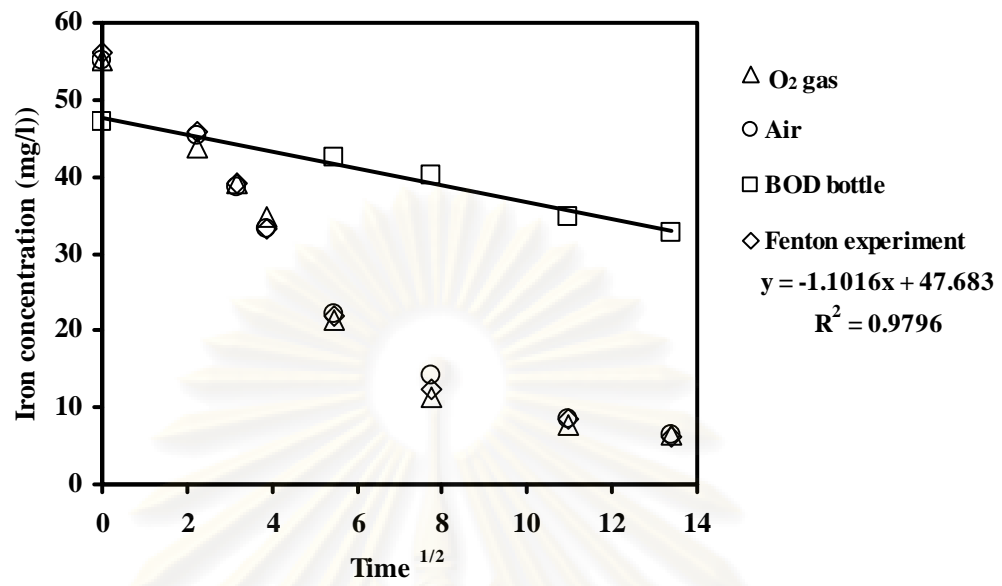
(a) Molecular transport control
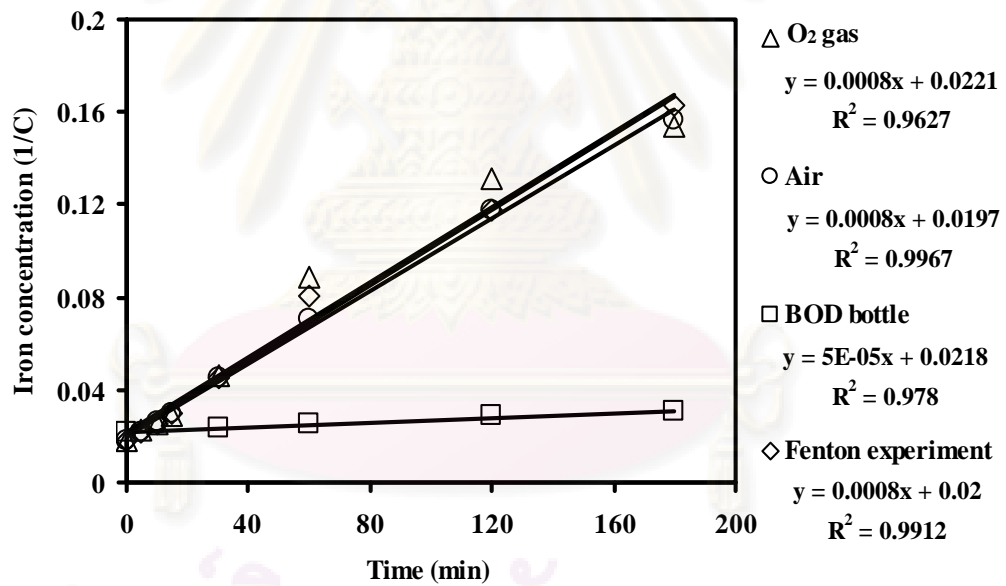
(b) Crystallite transport control

Figure 4.20 Determination of the rate-limiting step controlling the crystallization process.

4.2.7 Effect of Organic Compounds

Some organic intermediates from $OH^\bullet$ oxidation such as oxalic acid can significantly form complex with ferric ion. These ferro-organic complexes will increase the solubility of iron in the system and sequentially deteriorate the iron crystallization process. To verify the effect of ferro-organic complexes on iron crystallization, oxalic, acetic, and formic acids which have been identified as the intermediates from 2,6-DMA oxidation in Section 4.1.5 were added into the Fe^{3+} solution at pH 3 to determine Fe^{3+} solubility (Scenario P). The data as shown in Figure 4.21 indicating that the solubility of Fe^{3+} significantly increased in the presence of volatile fatty acids and as a result the crystallization of iron on the CS became minimal. The results from this part supported with the hypothesis mentioned above. In addition, the experiments under true fluidized-bed Fenton process also confirmed with this observation. Figure 4.22 shows that iron removal was the best in the absence of organic matters followed by in the presence of 0.1 and 1.0 mM of both 2,6-DMA and AN, respectively. It is very interesting to observe a re-emerging of total iron in the experiment with 1.0 mM organics, i.e., total iron decreased considerably in
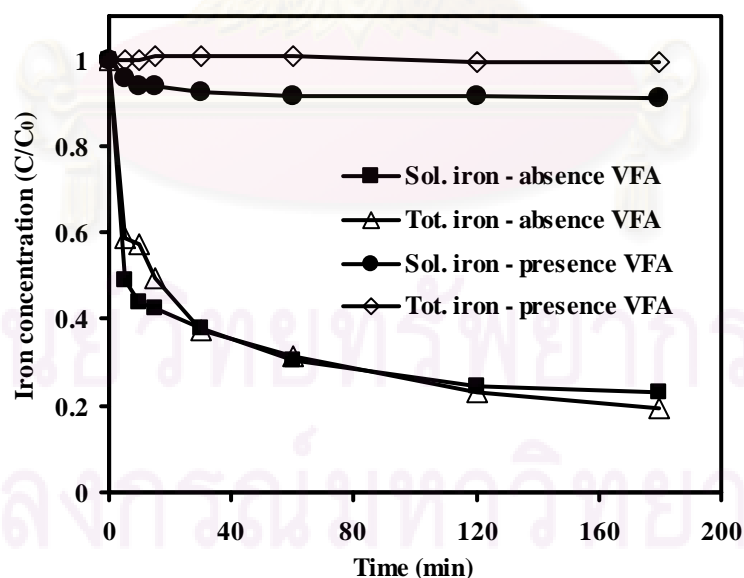
Figure 4.21 Effect of organo-ferric complex on iron crystallization in FBR with the initial conditions as follows: 1 mM of Fe^{3+}, 230.77 g/l of CS at pH 3 and 25°C, VFA consisted of 2 mM of formic acid, 0.5 mM of acetic acid and 2 mM of oxalic acid.
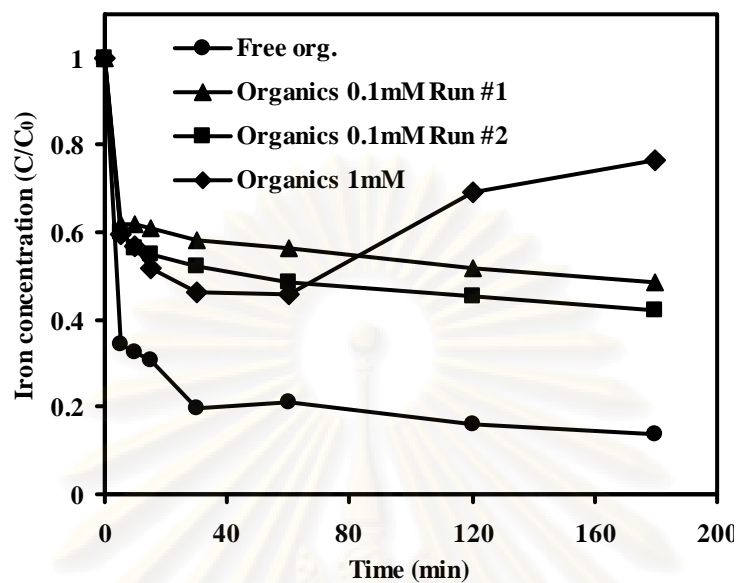
(a) Soluble iron
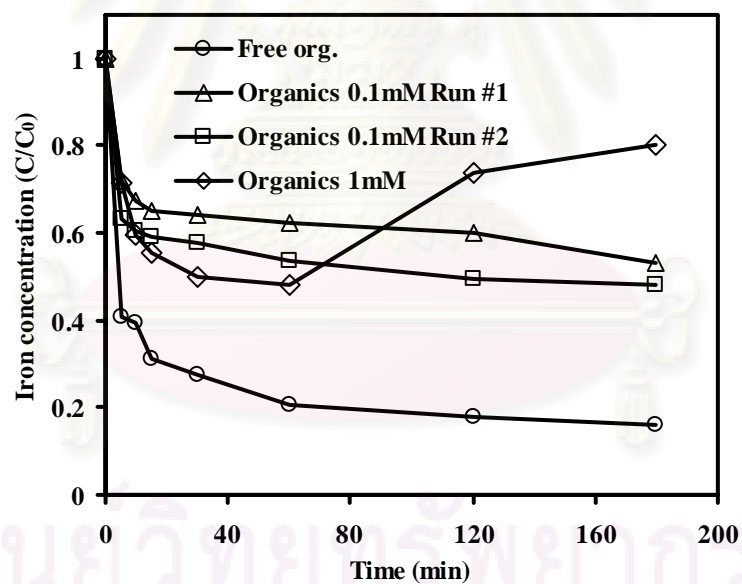
(b) Total iron

Figure 4.22 Effect of organo-ferric complex on iron crystallization in fluidized-bed Fenton process in the presence of 2,6-DMA and AN with the initial conditions as follows: 1 mM of Fe^{2+}, 20 mM of H_2O_2, 230.77 g/l of CS at pH 3 and 25°C.

the first 60 minutes but increased again afterward. This can be explained that after 60 minutes, the volatile fatty acids such as oxalic acid were generated which could form complex with ferric and increased the solubility of ferric in the solution. If the Fenton reaction was allowed to proceed for 1 hour before the FBR started (1-hr pre-CMR+FBR), it still observed the similar trend as in the case of FBR, i.e., the iron could be removed most efficiently in the absence of organics followed by 0.1 and 1.0 mM of both 2,6-DMA and AN, respectively. Another interesting point regarding on the effect of organics is the comparison between fully FBR and 1-hr pre-CMR+FBR as shown in Figures 4.23 and 4.24. These 2 runs were carried out under the same conditions except for the 1-hr pre-CMR+FBR allowed the Fenton reaction to proceed in a batch reactor for 1 hour before switching to FBR mode. In this manner, 2,6-DMA and AN were more completely transformed to several products including the ferric-complexable species. Hence, very limited iron was crystallized onto the sand surface. On the other hand, when the system was operated in fully FBR mode, it can be seen that total iron decreased in the first 60 minutes due to crystallization onto sand surface; however, as the reaction period proceeded, the ferric-complexable organics were formed and sequentially deteriorated the crystallization process. Observing from the trend, it can be expected that the total iron would continuously increased and eventually should be at the same level as in the case of 1-hr pre-CMR+FBR. The results from this part are very valuable for FBR operation. It implies that the removal of iron via crystallization will be promising if the Fenton reaction could remove most of the volatile fatty acids. Or in other word, iron removal will follow the organic removal efficiency. It also implies that fluidized-bed Fenton process is suitable for diluted wastewater or using for the polishing purpose. By this way, the process will be very effective for both pollutant and iron removals

4.2.8 Reusability of Iron-coated Construction Sand for Iron Crystallization

This part aimed to evaluate the capability of CS to serve as media for iron crystallization in the fluidized-bed Fenton process (Scenario Q). The iron crystallization was performed for 101 cycles and the results are shown in Figure 4.25.
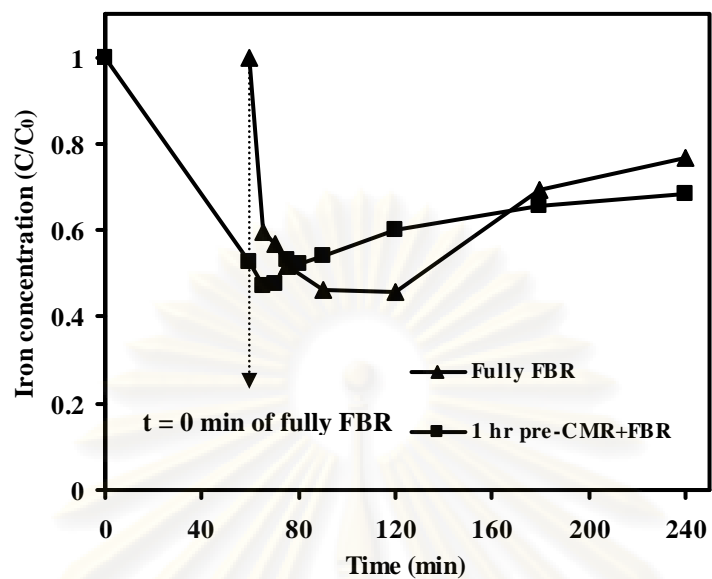
(a) Soluble iron
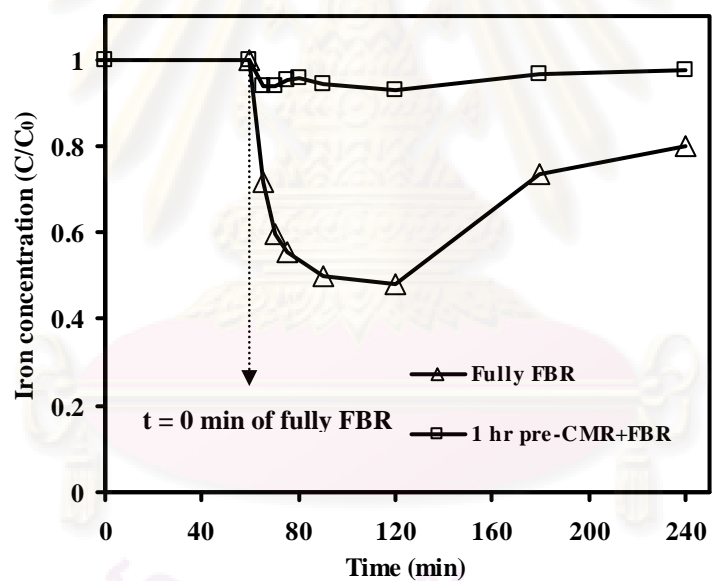
(b) Total iron

Figure 4.23 Effect of organo-ferric complex on iron crystallization of 1 mM of 2,6-DMA and 1 mM of AN with the initial conditions as follows:, 1 mM of Fe^{2+}, 20 mM of H_2O_2, 230.77 g/l of CS at pH 3 and 25°C.
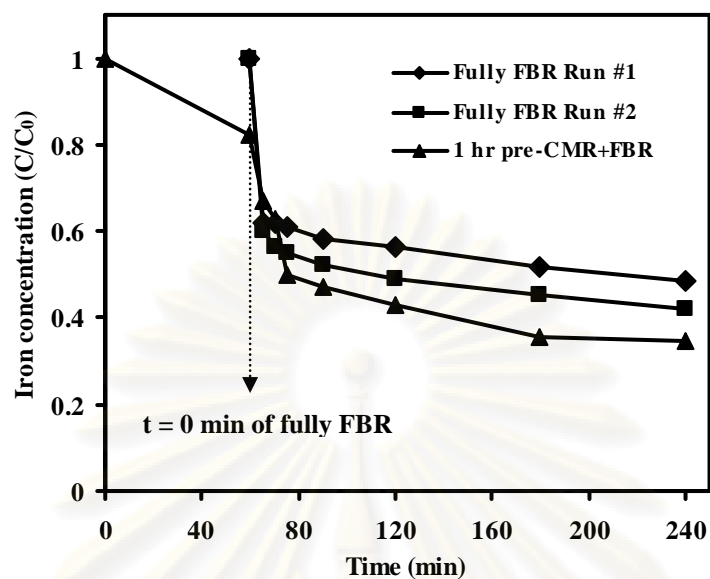
(a) Soluble iron
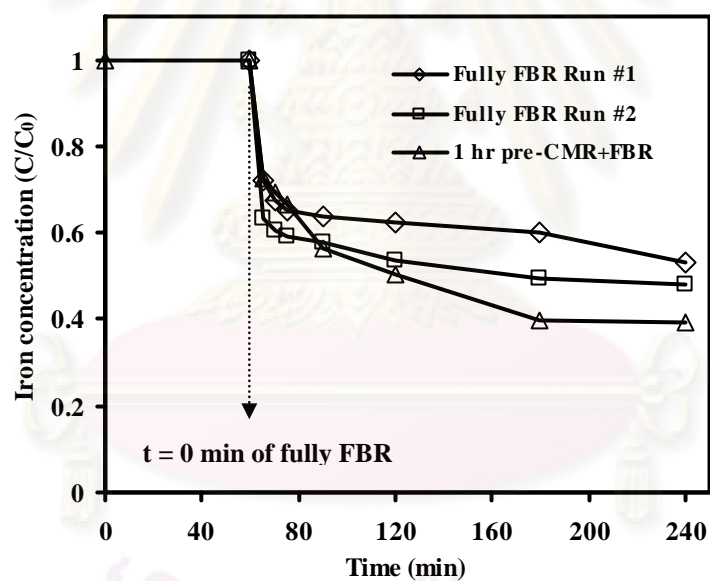
(b) Total iron

Figure 4.24 Effect of organo-ferric complex on iron crystallization of 0.1 mM of 2,6-DMA and 0.1 mM of AN with the initial conditions as follows: 1 mM of Fe^{2+}, 20 mM of H_2O_2, 230.77 g/l of CS at pH 3 and 25°C.
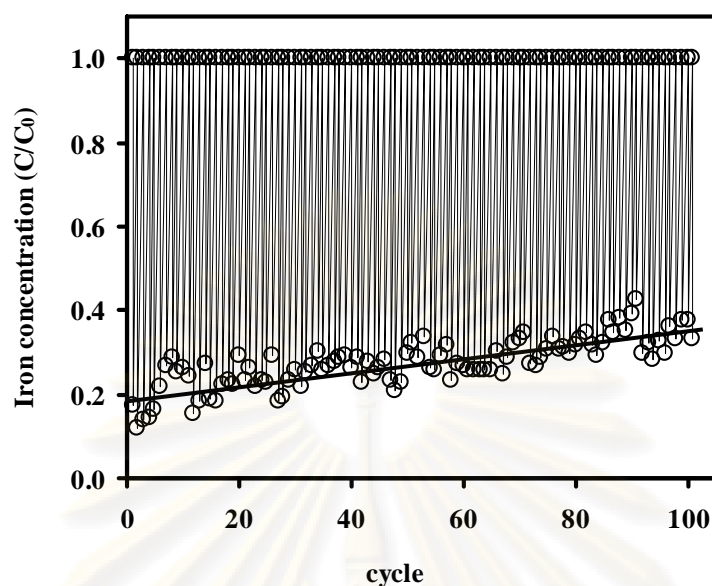
Figure 4.25 Reusability of iron-coated CS for iron crystallization with the initial conditions as follows: 230.77 g/l of CS, pH 3 at 25°C and 1 mM of Fe^{2+} and 20 mM of H_2O_2 for cycle 1 to 5 and 2 mM of Fe^{2+} and 40 mM of H_2O_2 for cycle 6 to 101.

It can be seen that the iron crystallization efficiency in 1 hour decreased gradually from 80% in the first cycle to 65% in the 101st cycle. This is believed to be due to the decreasing in the crystallization rate of iron crystallites onto the interaction sites on the iron-coated CS as the $Fe(OH)_3$ accumulating on the surface. Exhaustion of effective sites for crystallization was not believed to be the main cause because the reduction in iron still proceeded after 3 hours as shown in the profile plot of the 101st cycle as compared to the first cycle (Figure 4.26). It is very interesting to observe that the reduction of soluble iron in the 101st cycle was more rapid than those in the first cycle whereas the reduction of total iron turned to the opposite direction. This implies that the $Fe(OH)_3$ coated on the CS could somehow accelerate the formation of iron nuclei and crystallites; however, retard the crystallization rate of those crystallites onto the sand surface. The results from this part reveal that the iron crystallization performance in the real fluidized-bed Fenton reactor will be gradually deteriorated or decelerated with time. Hence, to maintain the high iron removal performance, it is wisely to continuously and constantly replace a portion of iron-coated CS in the FBR with the similar amount of fresh CS. To characterize the iron oxide coated on the CS surface, the 101st-cycle CS sample was analyzed by the XRD analyzer to determine
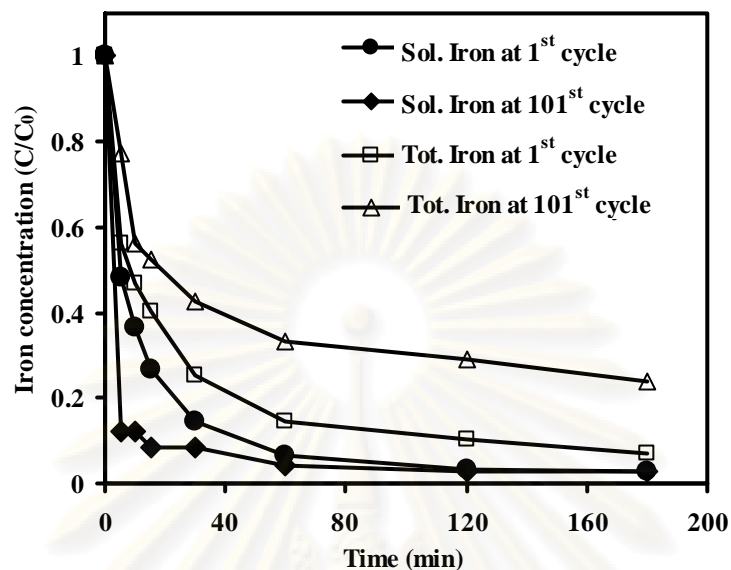
Figure 4.26 Comparison of iron profile between the 1st- and 101st –cycles with the initial conditions as follow: 2 mM of Fe^{2+}, 40 mM of H_2O_2, 230.77 g/l of CS at pH 3 and 25°C.

the iron oxide species coated on the surface. The result from XRD analysis as shown in Figure 4.27 revealed that only SiO_2 was detected. According to the calculation of iron removal from aqueous phase, the amount of iron coated on the CS surface should be more than 3.5% by weight and its catalytic activity was observed as will be discussed in the next part. Physical appearance between fresh CS and the 101st-cycle iron-coated CS was very distinguished from each other as shown in Figures A5 and A6, respectively. Despite of that, it can be expected that the iron oxide coated on the surface of CS should be $Fe(OH)_3$ since the results from the solubility study were consistent with the values calculated based on the presence of $Fe(OH)_3$ precipitates. In addition, Homanee (2005) characterized the iron oxide which crystallized on the SiO_2 in the fluidized-bed Fenton process at pH 6.5 within 5 hr and found to be $Fe(OH)_3$.

4.2.9 Catalytic Activity of Iron-coated Construction Sand

Iron oxides in various forms are believed to have catalytic activity which can stimulate H_2O_2 decomposition to generate $OH^•$. The objective of this part was to
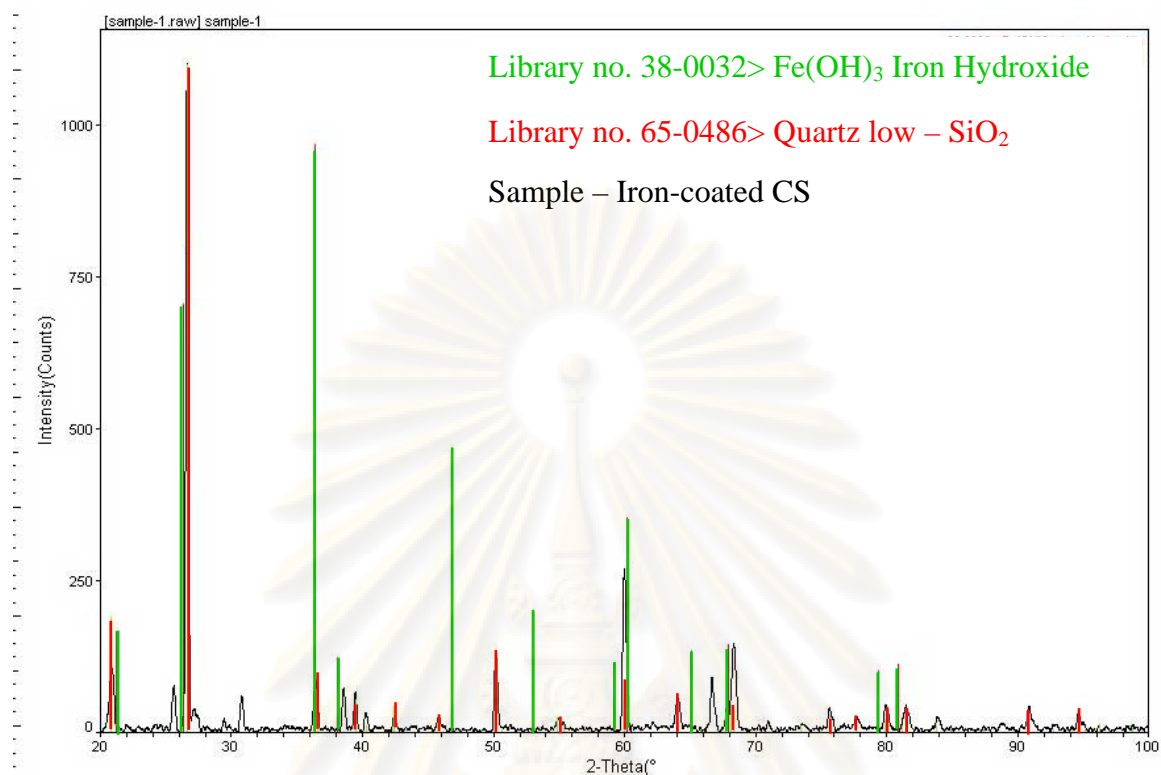
Figure 4.27 XRD analysis of the 101st-cycle iron-coated CS.

determine the catalytic activity of iron-coated CS and compare with those of commercial goethite (Scenario R). The results show that the 75 g of the 101st-cycle iron-coated CS had the catalytic activity approximately equivalent to 3 g of goethite in terms of AN and 2,6-DMA oxidations as shown in Figure 4.28. It is important to note that goethite had higher BET surface than iron-coated CS (8.63 versus 13.51 m^2/gm) which might affect the catalytic activity of these two iron oxides since the reactions involved surface interaction. In spite of surface difference, other factors such as iron oxide species should have more impact on the catalytic activity since the difference in surface area between these two iron oxides was only 1.6 time but the difference in reactivity was enormous, i.e., 75 g/l of iron-coated CS could remove only 30 and 40% of 1 mM of AN and 2,6-DMA, respectively, at 180 minutes whereas the same amount of goethite could completely remove both compounds in just 15 minutes. It was well documented that Fe(OH)$_3$ has much lower catalytic activity than goethite and this should be the main contribution to poorer performance of the 101st-cycle iron-coated CS as compared to goethite (α-FeOOH).
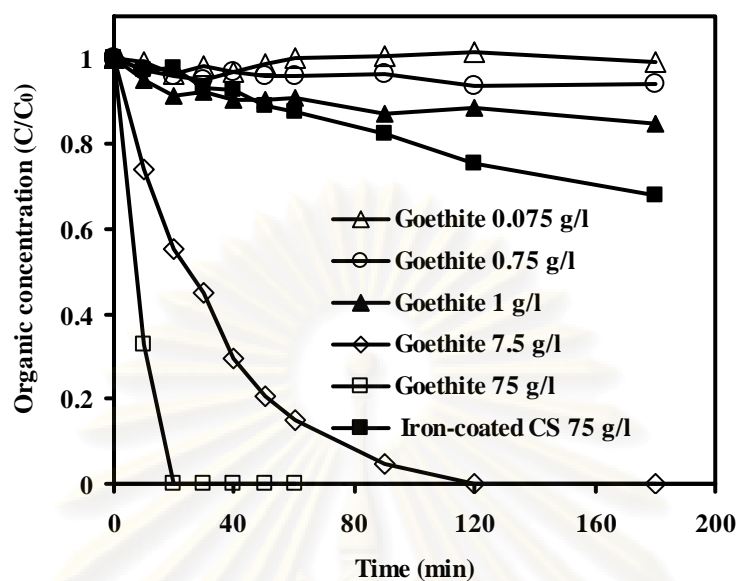
(a) Aniline
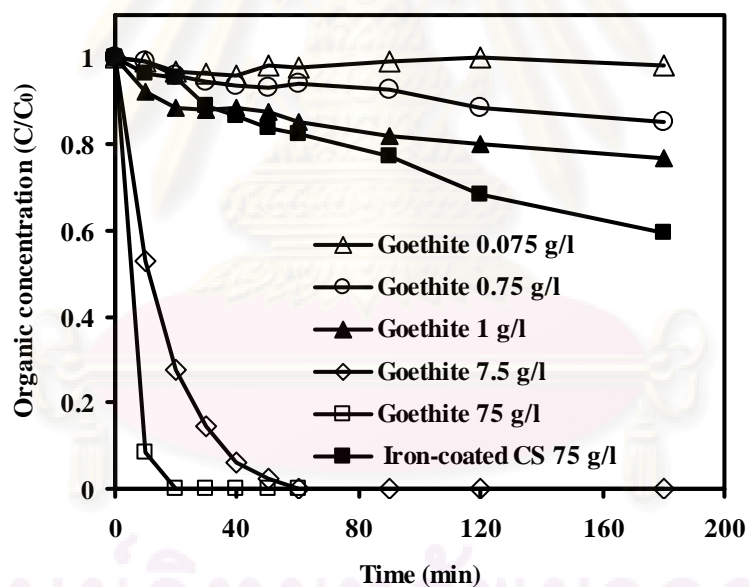
(b) 2,6-DMA

Figure 4.28 Catalytic activity of iron-coated CS on organic degradation in heterogeneous Fenton process as compare to commercial goethite with the initial conditions as follows: 1 mM of 2,6-DMA, 1 mM of AN, 20 mM of H_2O_2 at pH 3 and 25 °C.

Certain amounts of iron in the forms of Fe^{2+} and Fe^{3+} were leaching out into the mixture as shown in Figure 4.29 indicating that the reductive dissolution of iron oxide also happened in the mixture as suggested by Lu (2000). Nonetheless, further analysis for the determination of the rate constant between 2,6-DMA and $OH^•$ by using competitive rate kinetics with AN as a reference compound as shown in Figure 4.30 (as an example plot) provided the slope, which is the ratio of $k_{2,6\text{-DMA}}$ to k_{AN}, of 1.2725. This value was significantly different from the average of 3.5462 obtained from previous part where Fe^{2+} was added as illustrated in Section 4.1. This indicates that the degradation mechanism of 2,6-DMA and AN in the heterogeneous Fenton reaction was different from those in homogeneous Fenton reaction. As proposed by Lin and Gurol (1998), the decomposition of H_2O_2 occurred at the iron oxide surface. Hence, the oxidation of 2,6-DMA and AN in the heterogeneous Fenton reaction might involve the surface reaction resulting in different apparent rate constant from those of homogeneous reaction.
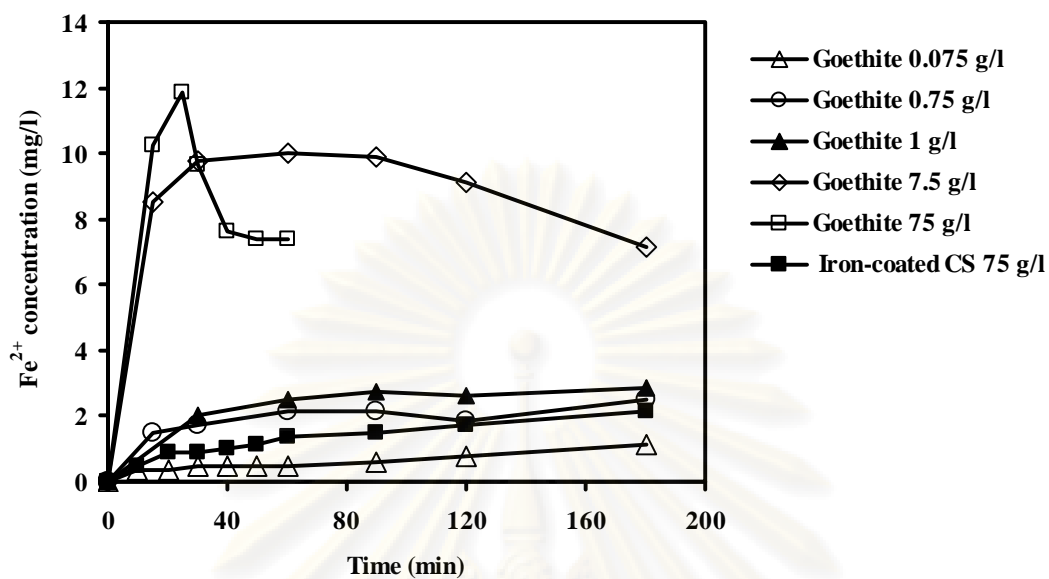
(a) Ferrous
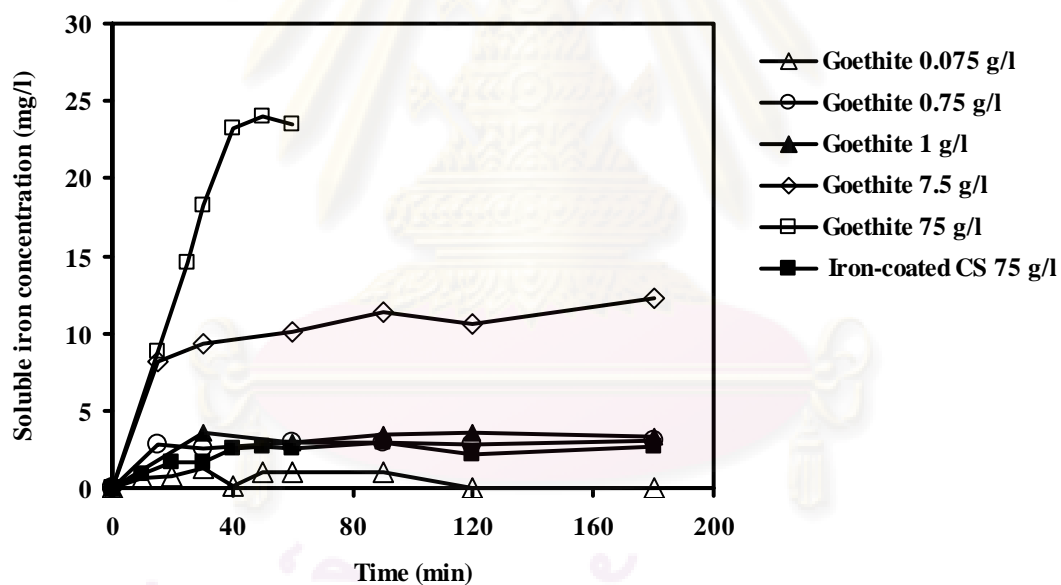
(b) Soluble iron

Figure 4.29 Iron leach ability of iron-coated CS and commercial goethite during the heterogeneous Fenton process with the initial conditions as follows: 1 mM of 2,6-DMA, 1 mM of AN, 20 mM of H_2O_2 at pH 3 and 25 °C.
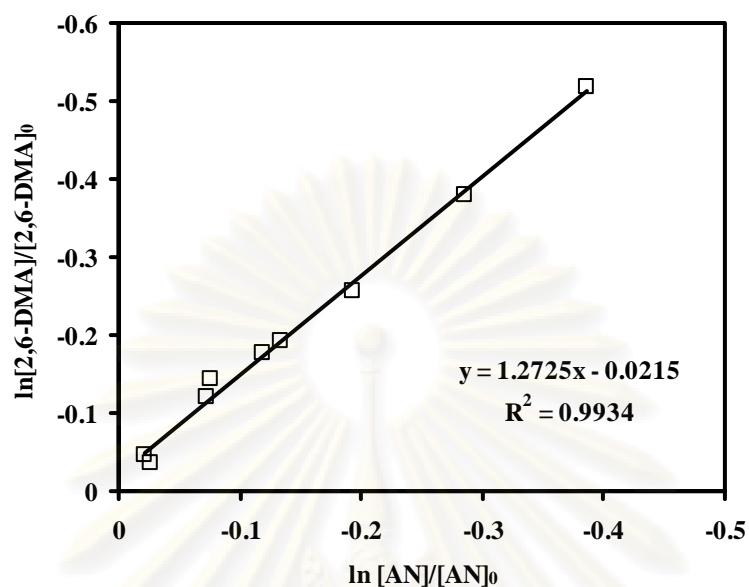
Figure 4.30 Relationship between $\ln([2,6\text{-DMA}]/[2,6\text{-DMA}]_0)$ versus $\ln([AN]/[AN]_0)$ using the data from the experiment with 75 g/l of 101st-cycle iron-coated CS with the initial conditions as follows: 1 mM of AN, 1 mM of 2,6-DMA, 20 mM of H_2O_2 at pH 3 and 25 °C.

CHAPTER V
CONCLUSIONS

5.1 Conclusions

5.1.1 Kinetics of 2,6-Dimethyl-aniline Degradation

The reaction between 2,6-DMA and OH• has been investigated by using Fenton reaction under various conditions, i.e., batch versus continuous operations, presence versus absence of solid media, and different Fenton's reagent. The following conclusions could be drawn from this part:

- Under the studied conditions, Fe^{2+} was the limiting reagent for organic oxidation.

- Competitive kinetics technique was proven to be an efficient and reliable method to determine the rate constant between organic compounds and hydroxyl radicals.

- Intrinsic 2nd-order rate constants between 2,6-dimethyl-aniline and hydroxyl radicals under various conditions were in between 1.59×10^{10} and 1.80×10^{10} $M^{-1} s^{-1}$ with an average and 95% confidence interval of $1.70 \pm 0.04 \times 10^{10} M^{-1} s^{-1}$.

- Intermediates from 2,6-DMA oxidation by hydroxyl radicals were 2,6-dimethyl-nitrobenzene, 2,6-dimethy-phenol, 2,6-dimethyl-nitrophenol, 2,6-dimethyl-hydroquinone, 2,6-dimethyl-benzoquinone, 2,6-dimethyl-3-hydroxy-benzoquinone, maleic, lactic, oxalic, acetic, and formic acids. The degradation pathway of 2,6-DMA was also proposed in this study.

5.1.2 Iron Crystallization

Iron precipitation and crystallization mechanisms were thoroughly investigated which could provide a better understanding on iron removal in the

fluidized-bed Fenton process. The outcomes of this part could be concluded as follows:

- Solubility of ferric is much less than those of ferrous; hence, after the initiation of Fenton reaction, ferric from ferrous oxidation should precipitate out in the form of ferric hydroxide even in the acidic solution.

- Saturation degree is the major factor controlling the precipitation process. Solid phase will be formed via the homogeneous nucleation if the precipitation occurs in the labile zone; iron removal in the fluidized-bed Fenton reactor will be sequentially unimpressive because the crystallization rate of iron onto fluidized media is very slow. On the other hand, if the precipitation happens within the metastable zone, heterogeneous nucleation will become predominate and the removal of iron in the fluidized-bed Fenton reactor will be rapid and exceptional.

- Newly formed crystallite has higher affinity with the foreign solid surface than aging or ripening crystallites; hence, the crystallization should occur simultaneously with the Fenton reaction in the fluidized-bed reactor in order to obtain the highest iron removal rate.

- Under the studied conditions, the crystallization process was controlled by the transport step rather than the surface-interaction step. Rate of crystal growth under turbulent condition followed the 2nd-order rate with respect to iron concentration (orthokinetic flocculation). In contrast, the growth rate under stagnant condition could be sufficiently explained by the transport mechanism both at the molecular and crystallite (perikinetic flocculation) levels.

- Presence of organic compounds/intermediates which can form complex with ferric such as oxalic acid will increase the solubility of ferric; hence, deteriorate the crystallization process. As a result, to obtain the significant iron removal in a full-scale fluidized-bed Fenton reactor, the oxidation reaction should proceed intensively toward complete mineralization.

- The rate of iron crystallization in the fluidized-bed Fenton reactor will gradually decrease with time; hence, to maintain the crystallization rate, a portion of coated-media has to be continuously replaced with fresh media.

- Catalytic activity of 75 g of the 101st-cycle iron-coated construction sands (>3.5% iron by weight) was approximately equivalent to 3 g of commercial goethite in term of aniline and 2,6-dimethyl-aniline degradation.

5.2 Recommendations for Further Studies

- Determine the rate constant of 2,6-dimethyl-aniline with hydroxyl radicals by using the competitive kinetics technique with different reference compounds and compare with the values obtained from this study.

- Determine the rate constant of 2,6-dimethyl-aniline with hydroxyl radicals by using other advanced oxidation processes such as TiO_2/UV, H_2O_2/UV and O_3/UV and compare with the values obtained from this study.

- Determine the effect of pH on the rate constant between 2,6-dimethyl-aniline and hydroxyl radicals and compare with the values obtained from this study.

- Determine the effect of temperature on the rate constant between 2,6-dimethyl-aniline and hydroxyl radicals via Arrhenius equation so that the rate constant can be applied in field practice for every required temperature.

- Investigate into more details on the factors affecting iron crystallization in the fluidized-bed Fenton process such as bed expansion, upflow velocity, pH, and temperature to obtain necessary information for scale up the fluidized-bed reactor for real application.

- Optimize the fluidized-bed Fenton process in term of organic and iron removals and compare the outcomes with the proposed mechanisms in this study.

REFERENCES

APHA (1992) Standard methods for the examination of water and wastewater, 18th Edition, American Public Health Association, Washington D.C.

Balci, B., Oturan, N., Cherrier, R. and Oturan, M.A. (2009) Degradation of atrazine in aqueous medium by electrocatalytically generated hydroxyl radicals. A kinetic and mechanistic study. Water Research 43: 1924-1934.

Baldrian, P., Merhautova, V., Gabriel, J., Nerud, F., Stopka, P., Hruby, M. And Benes, M.J. (2006) Decolorization of synthetic dyes by hydrogen peroxide with heterogeneous catalysis by mixed iron oxides. Applied Catalysis B: Environmental 66: 258–264

Brillas, E., Mur, E., Sauleda, R., Sanchez, L., Peral, J., Domenech, X. and Casadi J. (1998) Aniline mineralization by AOP's: anodic oxidation, photocatalysis, electro-Fenton and photoelectro-Fenton processes. Applied Catalysis B: Environmental 16(1): 31-42.

Buxton, G.V., Greenstock, C.L., Helman, W.P. and Ross, A.B. (1988) Critical review of rate constants for reactions of hydrated electrons, hydrogen atoms and hydroxyl radical ($^{\bullet}OH/^{\bullet}O^{-}$) in aqueous solution. Journal of Physical and Chemical Reference Data 17: 513-886.

Chen, G., Hoag, G.E., Chedda, P., Nadim, F., Woody, B.A. and Dobbs, G.M. (2001) The mechanism and applicability of in situ oxidation of trichloroethelene with Fenton's reagent. Journal of Hazardous Materials B87: 171-186.

Chou, S. and Huang, C. (1998) Application of a supported iron oxyhydroxide catalyst in oxidation of benzoic acid by hydrogen peroxide. Chemosphere 38(12): 2719-2731

Chou, S. and Huang, C. (1999) Effect of Fe^{2+} on catalytic oxidation in a fluidized bed reactor. Chemosphere 39, 2: 1997-2006.

Chou, S., Huang, C. and Huang, Y.H. (2001) Heterogeneous and homogeneous oxidation by supported γ-FeOOH in a fluidized-bed reactor: kinetic approach. Environmental Science and Technology 35: 1247-1251.

Chou, S., Huang, G.H., Liao, C.C., Hsu, S.F. and Huang, Y.H. (2003) Fenton family-advanced oxidation technologies for wastewater treatment. Asian Pacific Regional Conference on Practical Environmental Technologies, Tainan, Taiwan. (18-21 December 2003): (A2-17)-(A2-24).

Chou, S., Liao, C.C., Perng, S.H. and Chang, S.H. (2004) Factors influencing the preparation of supported iron oxide in fluidized-Bed crystallization. Chemosphere 54: 859-866.

Christopher, K.D., William, J.C. and T.David Waite. (2005) Fenton-Mediated oxidation in the presence and absence of oxygen. Environmental Science & Technology 39: 5052-5058.

Daniel, W.W. (1991) Biostatistics: A foundation for analysis in the health sciences. 5th-Edition, John Wiley & Sons, Inc., New York.

Dantas, T.L.P., Mendonca, V.P., Jose, H.J., Rodrigues, A.E. and Moreira, R.F.P.M. (2006) Treatment of textile wastewater by heterogeneous Fenton process using a new composite Fe_2O_3/carbon. Chemical Engineering Journal 118: 77–82

Einschlag, F. S. G., Carlos, L. And Capparelli, A. L. (2003) Conpetition kinetics using the UV/H_2O_2 process: a structure reactivity correlation for the rate constants of hydroxyl radicals toward nitroaromatic compounds. Chemosphere 53: 1-7.

Ewa, L.K. (1991) Degradation of aqueous nitrophenol and nitrobenzene by means of the Fenton reaction. Chemospere 22: 529-536.

Fenton, H.J.H. (1894) Oxidative properties of the H_2O_2/Fe^{2+} system and its application. Journal of Chemical Sources 65: 889-899.

Flores, Y., Flores, R. and Gallegos, A.A. (2008) Heterogeneous catalysis in the Fenton-type system reactive black 5/H_2O_2. Journal of Molecular Catalysis A: Chemical 281: 184–191

Glaze, W.H., Kang, J.W. and Chapin, D.H. (1987) The chemistry of water treatment processed involving ozone, hydrogen peroxide and ultraviolet radiation. Ozone Science & Engineering 9: 335-352.

Hoigné, J. (1998) Chemistry of aqueous ozone and transformation of pollutants by ozonation and advanced oxidation processes. Hutzinger, O. (Ed.). Handbook of Environmental Chemistry 5, Springer-Verlag, Berlin 5, pp. 83-141 (Part C).

Homanee, S. (2005) Iron pelletization with various seeding materials. Master's Thesis, Department of Environmental Management (Inter-Department), Graduate School, Chulalongkorn University.

Hsueh, C.L., Huang, Y.H., Wang, C.C. and Chen, C.Y. (2006) Photoassisted fenton degradation of nonbiodegradable azo-dye (Reactive Black 5) over a novel supported iron oxide catalyst at neutral pH. Journal of Molecular Catalysis A: Chemical 245: 78–86

Huang, C.P., Dong, C. and Tang, Z. (1993) Advanced chemical oxidation: its present role and potential future in hazardous waste treatment. Water Management 13: 361-377.

Huang, H.H., Lu, M.C. and Chen, J.N. (2001) Catalytic decomposition of hydrogen peroxide and 2-chlorophenol with iron oxides. Water Research 35(9): 2291-2299

IARC, Monographs on the Evaluation of Carcinogenic Risks to Humans, 57, 1993.

Kwon, B.G., Ryu, S. and Yoon, J. (2009) Determination of hydroxyl radical rate constant in a continuous flow system using competition kinetics. Journal of Industrial and Engineering Chemistry 15: 809-812.

Leitner, N.K.V. and Roshani, B. (2010) Kinetic of benzotriazole oxidation by ozone and hydroxyl radical. Water Research 44: 2058-2066.

Lin, S.S. and Gural, M.D. (1996) Heterogeneous catalytic oxidation of organic compounds by hydrogen peroxide. Water Science and Technology 34(9): 57-64.

Lin, S.S. and Gurol, M.D. (1998) Catalytic decomposition of hydrogen peroxide on iron oxide: kineics, mechanisms, and implications. Environmental Science and Technology 32: 1417-1423.

Lo, S.L. and Chen, T.Y. (1997) Adsorption of Se (IV) and Se (VI) on am iron coated sand from water. Journal of Chemosphere: 919-930.

Lunar, L., Sicilia, D., Rubio, S., Perez-Bendito, D. and Nickel, U. (2000) Degradation of photographic developers by Fenton's reagent: condition optimization and kinetics for metal oxidation. Water Research 34, 6: 1791-1802.

Lu, M.C. (2000) Oxidation of chlorophenols with hydrogen peroxide in the presence of goethite. Chemosphere 40: 125-130

Lu, M.C., Chen, J.N. and Chang, C.P. (1999) Oxidation of dichlorvos with hydrogen peroxide using ferrous ion as catalyst. Journal of Hazardous Materials B65: 277-288.

Lu, M.C., Chen, J.N. and Huang, H.H. (2002) Role of Goethite Dissolution in the oxidation of 2-chlorophenol with hydrogen peroxide. Chemosphere 46: 131-136

Masomboon, N., Ratanatamskul, C. and Lu, M.C. (2009) Chemical oxidation of 2,6-dimethylaniline in the Fenton process. Environmental Science and Technology 43: 8629-8634.

Masomboon, N., Ratanatamskul, C. and Lu, M.C. (2010) Chemical oxidation of 2,6-dimethylaniline by electrochemically generated Fenton's reagent. Journal of Hazardous Materials 176: 92-98.

Masten, S. and Davies, S. (1994) The use of ozonation to degrade organic contaminants in wastewater. Environmental Science and Technology 28: 180A-185A.

Mazellier, P., Busset, C., Delmont, A. and Laat, J.D. (2007) A comparison of fenuron degradation by hydroxyl and carbonate radicals in aqueous solution. Water Research 41: 4585-4594.

Morel F.M.M. and Hering J.G. (1993) Principles and applications of aquatic chemistry, John Wiley & Sons, Inc., New York.

Munter, R. (2001) Advanced oxidation processes-current status and prospects. Process Estinian Acadamic Science Chemistry 50(2): 59-80.

NTP, National Toxicology Program. Toxicology and Carcinogenesis Studies of 2,6-Xylidine (2,6-dimethyl-aniline) in Charles River CS Rats (Feed Studies), TR 278 U.S. Department of Health and Human Services, Public Health Service, (online) 1990. Available from: http://ntp.niehs.nih.gov/ntp/htdocs/LT rpts/tr278.pdf (accessed April 2009)

Oliviero, L., Barbier, Jr. J., Duprez, D., Wahyu, H., Ponton, J.W., Metcalfe, I.S. and Mantzavinos, D. (2001) Wet air oxidation of aqueous solutions of maleic acid over Ru/CeO$_2$ catalysts. Applied Catalysis B: Environmental 35(1): 1-1.

Oliviero, L., Wahyu, H., Barbier, Jr. J., Duprez, D., Ponton, J.W., Metcalfe, I.S. and Mantzavinos, D. (2003) Experimental and predictive approach for determining wet air oxidation reaction pathways in synthetic wastewaters. Chemical Engineering Research and Design 81(3): 384-392.

O'Melia, C.R., and Tiller, C.L. (1993) Physicochemical aggregation and deposition in aquatic environments. In Environmental Particles, Vol. 2, J. Buffle and H.P. van Leeuwen, Eds., Lewis, Boca Raton, FL.

Parsons, S. (2004) Advance oxidation processes for water and wastewater treatment, No.1, IWA Publishing, U.S.A. 130-145.

Peres, A.J., Heredia, D.J. and Dominguez, R.J. (2003) Integrated Fenton's Reagent Coagulation/Flocculation Process for the Treatment of cork processing wastewater. Journal of Hazardous Materials B107: 115-121.

Pignatello, J.J. (1992) Dark and photoassisted Fe^{3+}-catalyzed degradation of chlorophenoxy herbicides by hydrogen peroxide. Environmental Science and Technology 26: 944-951.

Prengle, H.W., Symos, M.J. and Bellhateche, D. (1978) H$_2$O$_2$/vis UV process for photo-oxidation of waterborne hazardous substances C$_1$-C$_6$ chlorinated hydrocarbons. Waste Management 16: 326-333.

Rodgers, J.D. and Bunce, N.J. (2001) Review paper, treatment methods for the remediation of nitroaromatic explosives. Water Research 35(9): 2101-2111.

Sauleda, R. and Brillas, E. (2001) Mineralization of aniline and 4-chlorophenol in acidic solution by ozonation catalyzed with Fe^{2+} and UVA light. Applied Catalysis B: Environmental 29(2): 135-145.

Skoumal, M., Arias, C., Cabot, P.L., Centellas, F., Garrido, J.A., Rodriguez, R.M. and Brillas, E. (2008) Mineralization of the biocide chloroxylenol by electrochemical advanced oxidation processes. Chemosphere 71: 1718-1729.

Spanggord, R.J., Yao, D. and Mill, T. (2000) Kinetics of aminodinitrotoluene oxidations with ozone and hydroxyl radical. Environmental Science and Technology 34: 450-454.

Shen, J.M., Chen, Z.L., Xu, Z.Z., Li, X.Y., Xu, B.B. and Qi, F. (2008) Kinetics and mechanism of degradation of p-chloronitrobenzene in water by ozonation. Journal of Hazardous Materials 152: 1325-1331.

Stumm, W. and Morgan, J.J. (1996) Aquatic chemistry: Chemical equilibria and rates in natural waters. 3rd Edition, John Wiley & Sons, Inc., New York.

Tai, C.Y. (1999) Crystal growth kinetics of two-step growth process in liquid fluidized-bed crystallizer. Journal of Crystal Growth 206: 109-108.

Tchobanoglous, G., Burton, F.L. and Stensel, H.D. (2003) Wastewater engineering treatment and reuse. 4th edition. New York: McGraw-Hill.

Ting, W.P., Lu, M.C. and Huang, Y.H. (2009) Kinetics of 2,6-dimethylaniline degradation by electro-Fenton process. Journal of Hazardous Materials 161: 1484-1490.

Zelmanov, G. and Semiat, R. (2008) Iron(3) oxide-based nanoparticles as catalysts in advanced organic aqueous oxidation. Water Research 42: 492 – 498.

APPENDICES
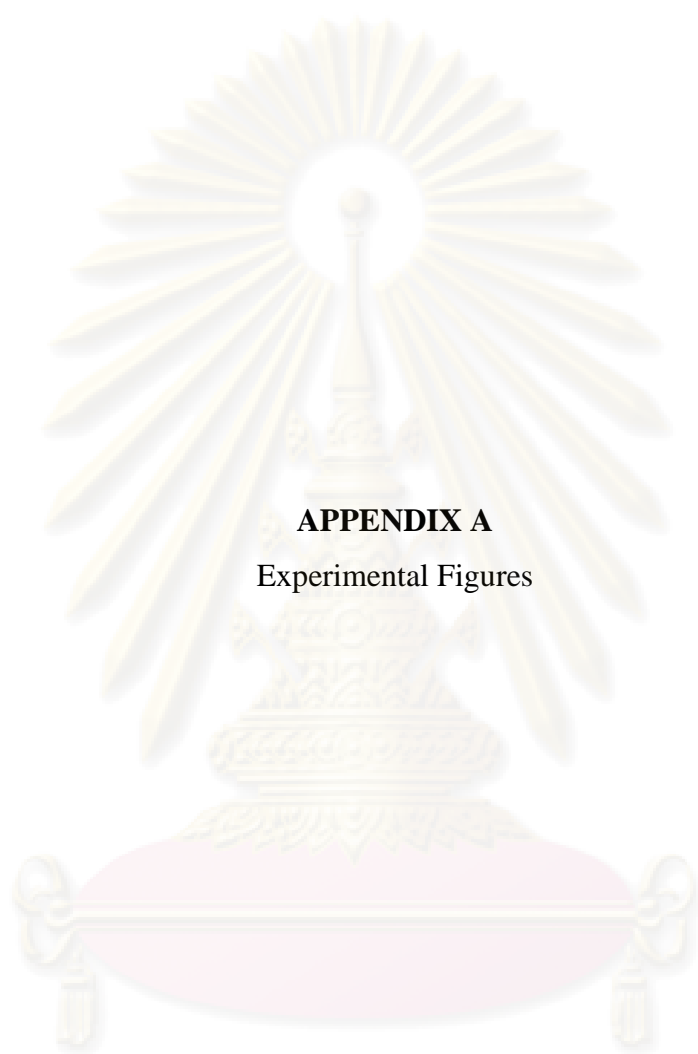
APPENDIX A

Experimental Figures

Figure A.1 Fenton experiment in the batch mode operation for determination of intrinsic rate constant of 2,6-DMA and OH$^\bullet$.

Figure A.2 Fenton experiment in the continuous mode operation for determination of intrinsic rate constant of 2,6-DMA and OH$^\bullet$.

Figure A.3 Fluidized-bed Fenton experiment.

| Goethite 0.75 g/l | Goethite 1 g/l | Goethite 7.5 g/l | Iron-coated 75 g/l |
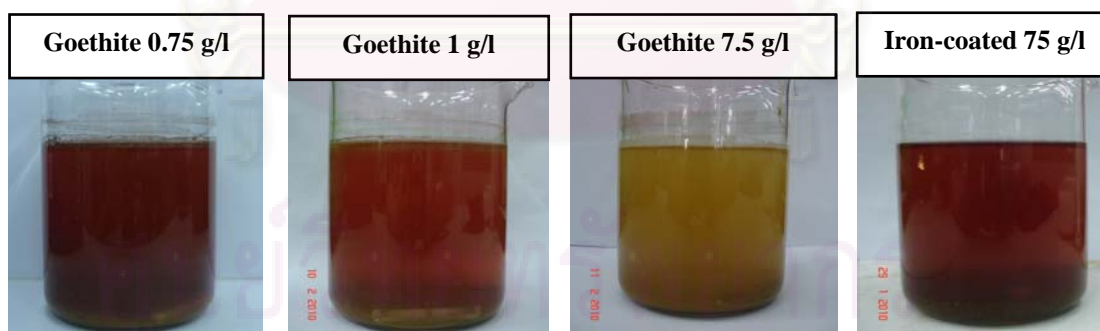
Figure A.4 Treated effluents from heterogeneous Fenton reaction under various catalytic conditions with the initial conditions of 1 mM of AN, 1 mM of 2,6-DMA, 20 mM of H_2O_2 at pH 3 and 25 °C.
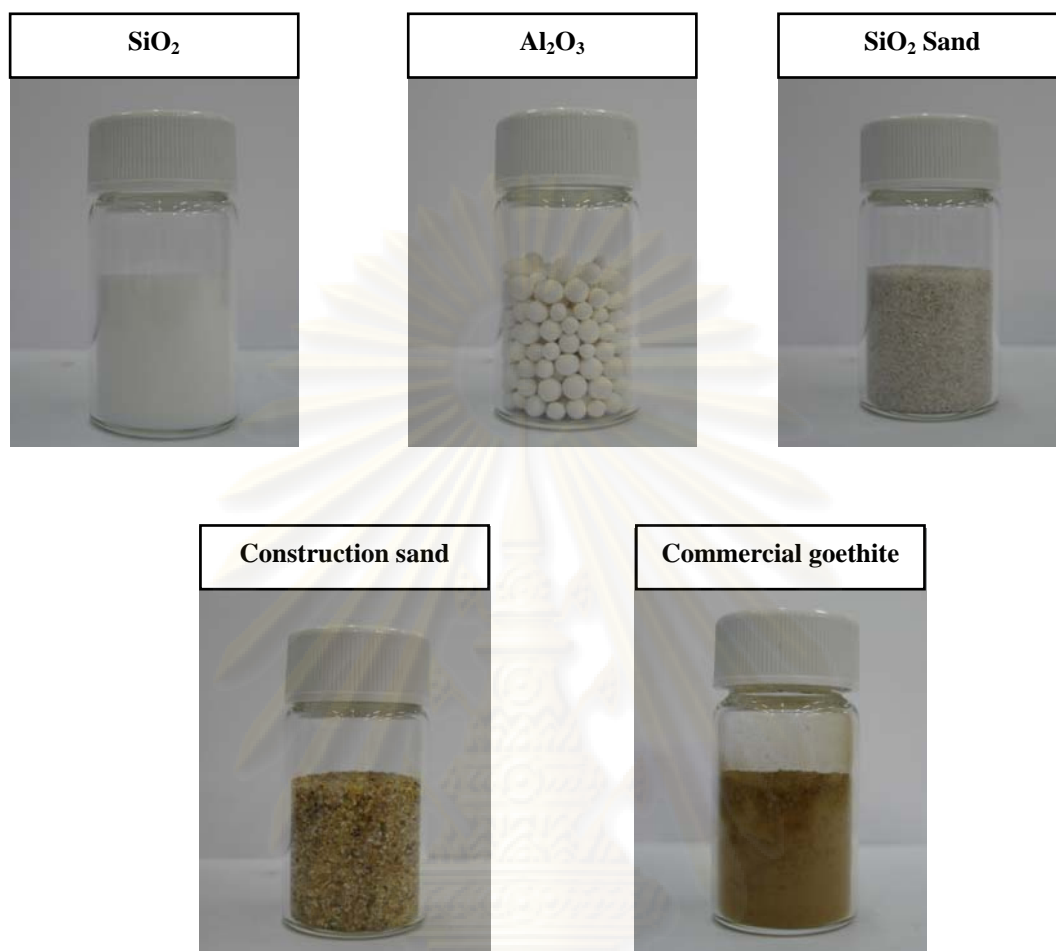
Figure A.5 Physical appearance of the fluidized materials.

Figure A.6 Physical appearance of the iron-coated construction sand after 101-cycle crystallization.

| Purge O$_2$ gas | Purge air | Purge N$_2$ gas |

(a) Fe^{3+} = 1 mM and pH = 3

| Neutralization to pH 7 after Fenton reaction | Fenton-like process |
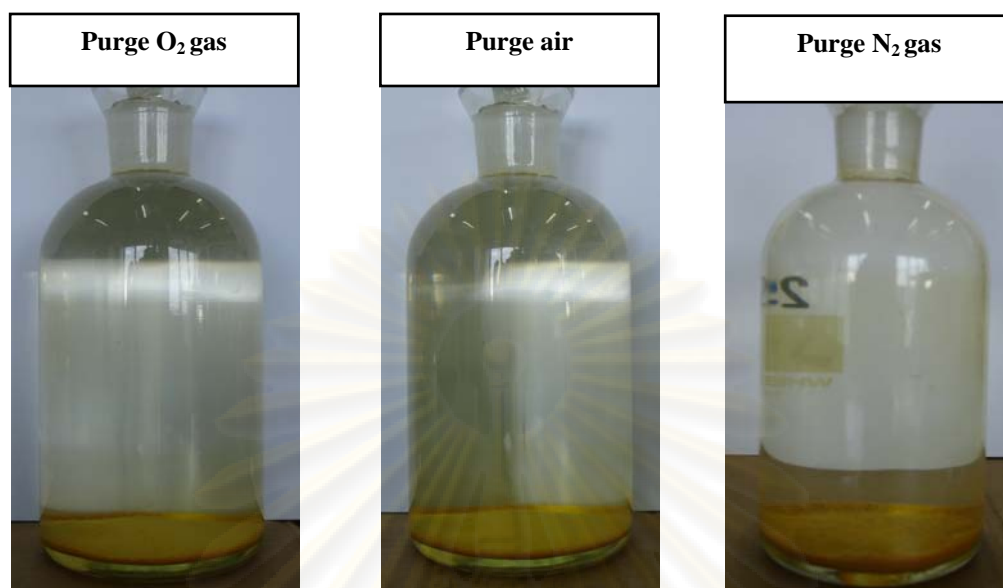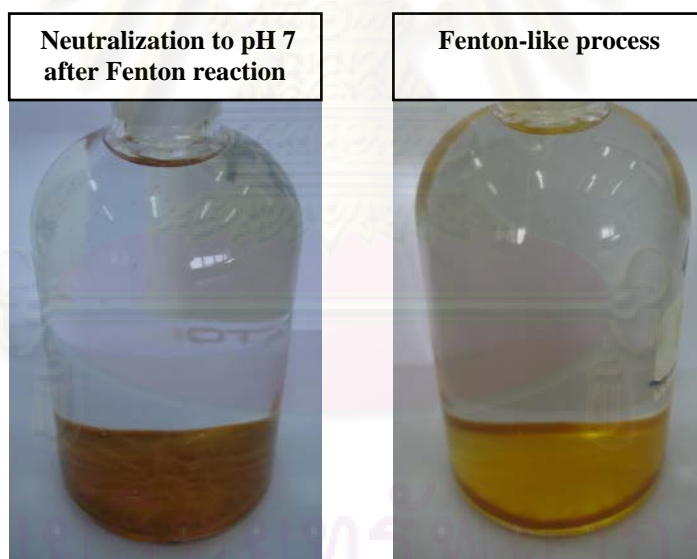
(b) Fe^{2+} = 1 mM and
H$_2$O$_2$ = 20 mM and pH = 3

(c) Fe^{3+} = 1 mM and
H$_2$O$_2$ = 20 mM and pH = 3

Figure A.7 Ferric precipitation under various turbulence conditions at 25°C.

Figure A.8 UV-visible spectrophotometer.

Figure A.9 Gas chromatography (GC-FID).

Figure A.10 Ion chromatography (IC).

Figure A.11 Total organic carbon analyzer.

Figure A.12 Gas chromatography mass spectrometry (GC-MS).
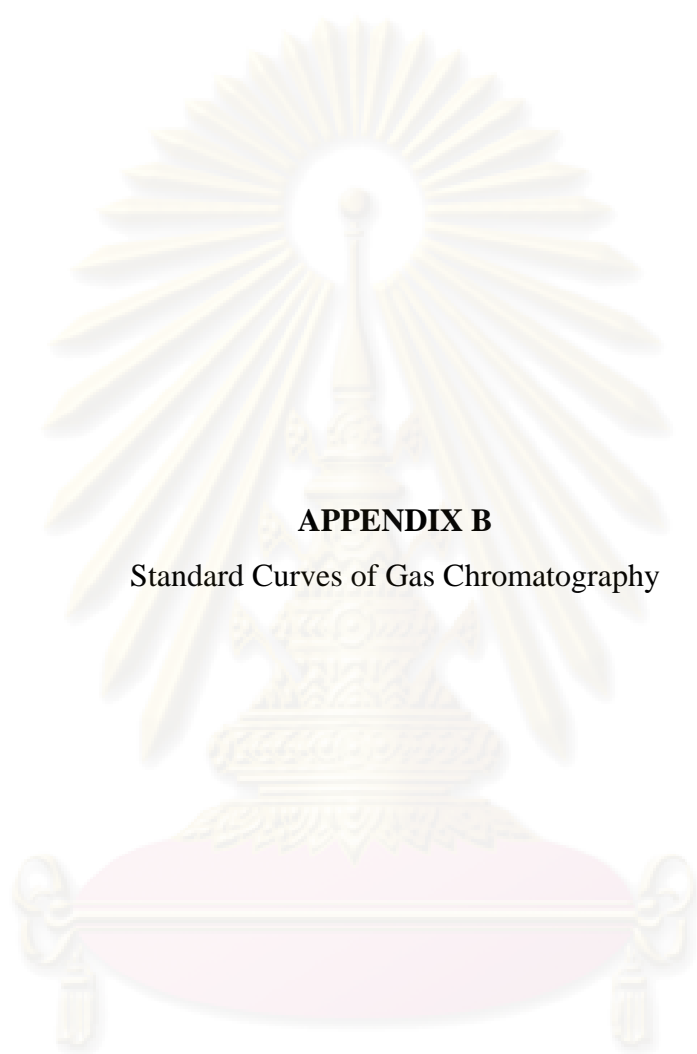
APPENDIX B

Standard Curves of Gas Chromatography
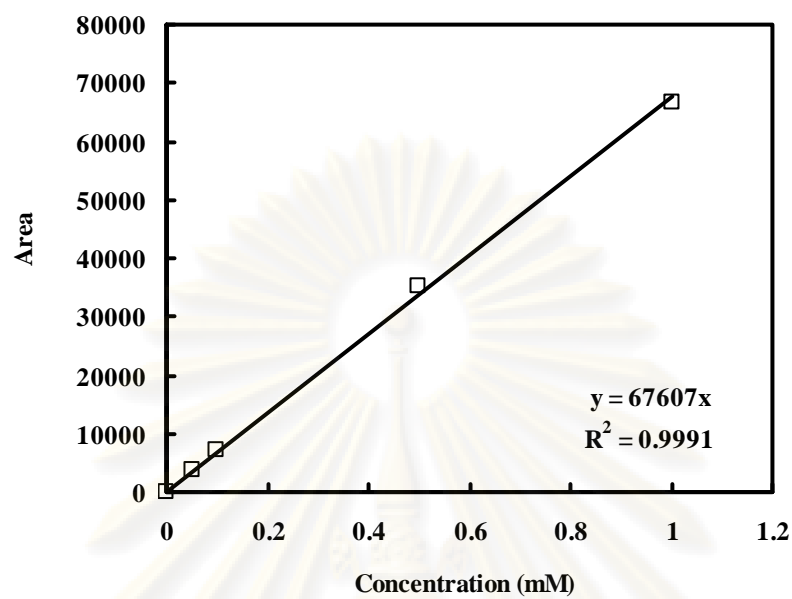
Figure B.1 Standard curve for 2,6-DMA.
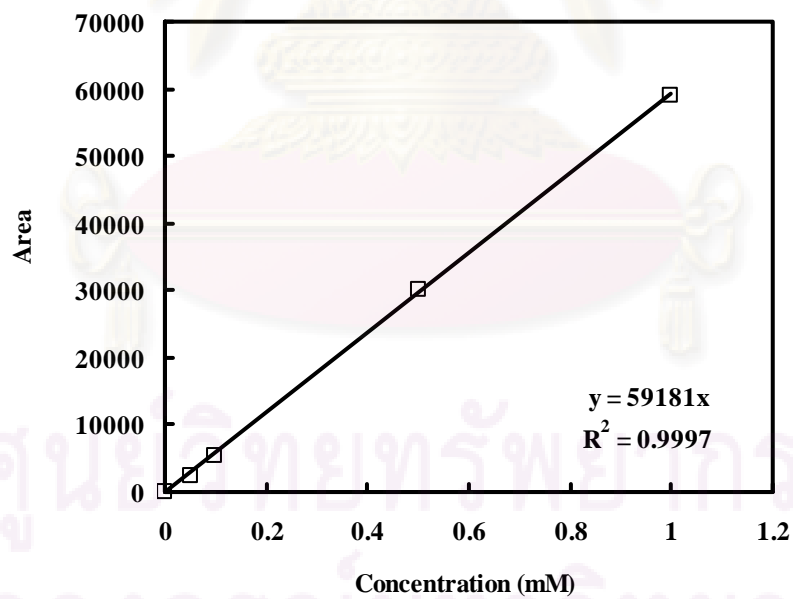
Figure B.2 Standard curve for n,n-DMA.
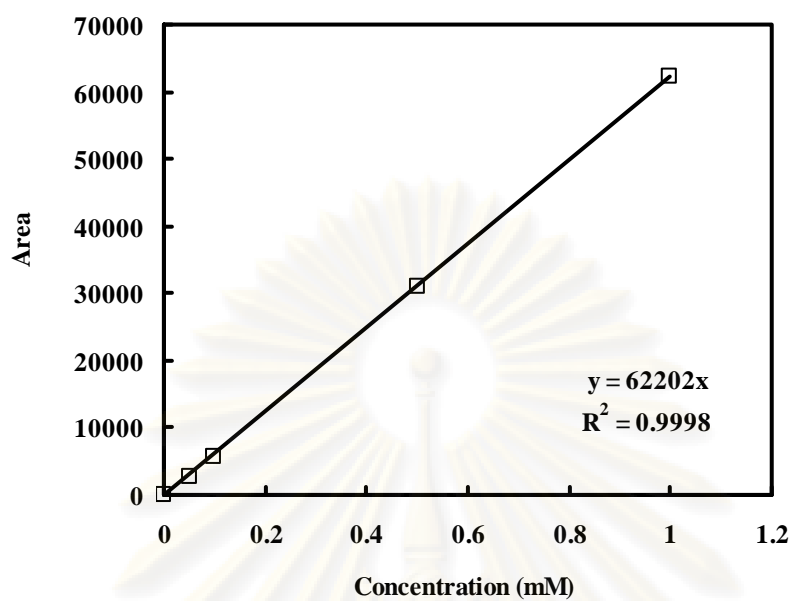
Figure B.3 Standard curve for aniline.
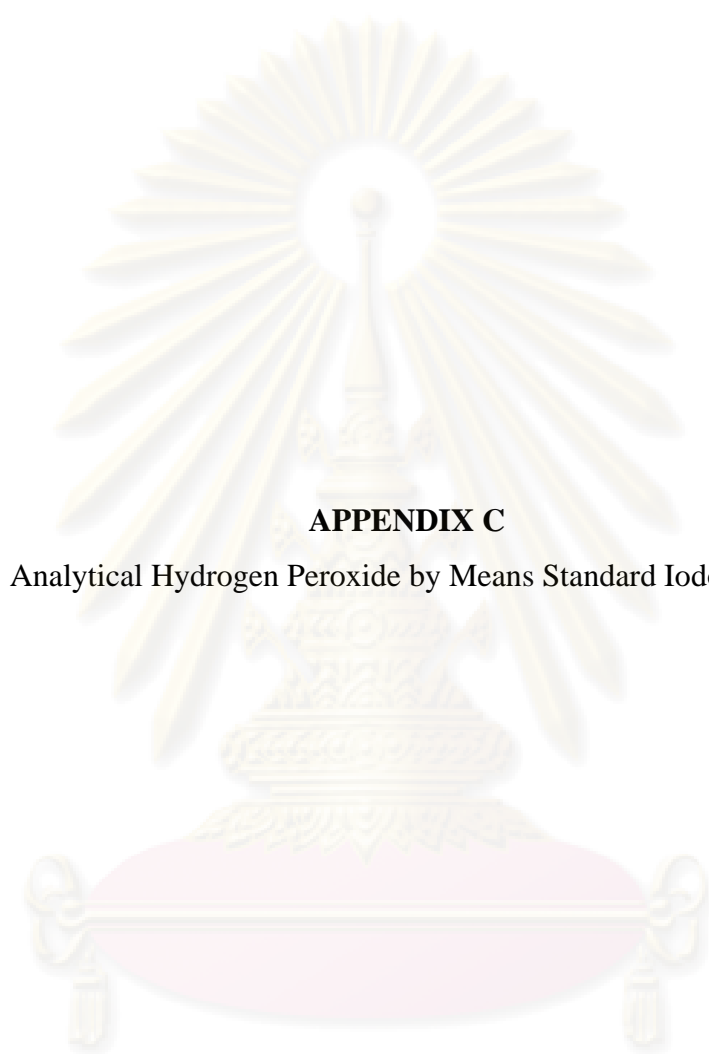
APPENDIX C

Analytical Hydrogen Peroxide by Means Standard Iodometric

C.1 Principle

Hydrogen peroxide oxidized iodine to iodine in the presence of acid and molybdate catalyst. The iodine formed is titrated with thiosulfate solution, incorporating a starch indicator as demonstrated in the following equation:

$$H_2O_2 + 2KI + H_2SO_4 \quad \Rightarrow \quad I_2 + K_2SO_4 + 2H_2O \quad \quad (C.1)$$

$$I_2 + 2Na_2S_2O_3 \quad \Rightarrow \quad Na_2S_4O_6 + 2NaI \quad \quad (C.2)$$

C.2 Interferences

Other oxidizing agents will also produce iodine, whereas reducing agents (and unsaturated organics) will react with the liberated iodine. The contribution from other oxidizing agents can be determined by omitting the acid and molybdate catalyst.

C.3 Reagents

1. Potassium iodine solution (1% w/v): dissolve 10 g of KI into 1 liter of DI water
2. Ammonium molybdate solution: dissolve 9 g of ammonium molybdate in 10 ml of 6 N NH_4OH, add 24 g of NH_4NO_3 and dilute to 100 ml with DI water.
3. Sulfuric acid solution (1+3 H_2SO_4): carefully add one part H_2SO_4 98% to three parts DI water.
4. Starch indicator: 2 g of starch and dilute to 100 ml by DI water.
5. Sodium thiosulfate solution (0.0125 N)

C.4 Apparatus

1. Analytical balance (+/- mg/l)
2. Small weighing bottle (<5 ml)
3. 250 Erlenmeyer flask
4. 50 ml burette (class A)

C.5 Procedure

1. Transfer sample to Erlenmeyer flask.
2. Add 50 ml of DI water to Erlenmeyer flask. Next, 10 ml of sulfuric acid solution and 15 ml of potassium iodide were added. Then two drops ammonium molybdate solution was added.
3. Titrate with 0.0125 N sodium thiosulfate to faint yellow or straw color. Swirl or stir gently during titration to minimize iodine loss
4. Add about 2 ml starch indicator, and continue titration until the blue color just disappears.
5. Repeat steps 2-4 on a blank sample of water.
6. Note ml of 0.0125 N $Na_2S_2O_3$ for samples and blank analysis.

C.6 Calculation

$$H_2O_2, mg/l = \frac{(A - B) \times N \times 17 \times 1000}{ml.sample}$$

Where:

A   =   ml of ml of $Na_2S_2O_3$ for sample

B   =   ml of $Na_2S_2O_3$ for blank

N   =   Normality of $Na_2S_2O_3$ for sample
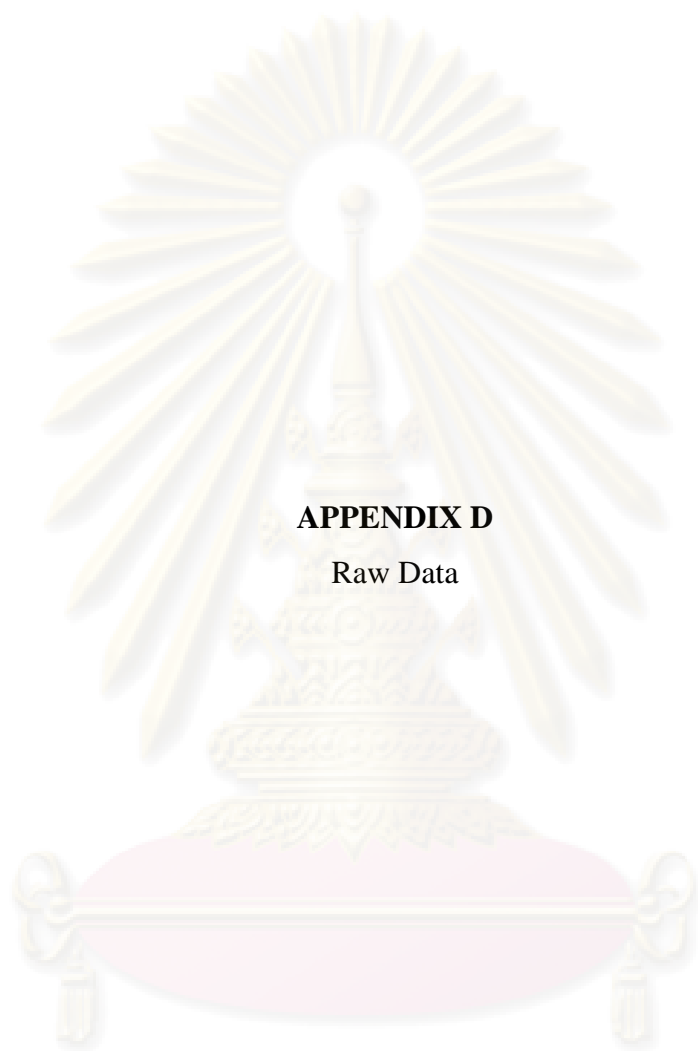
APPENDIX D
Raw Data

D.1 Kinetics of 2,6-Dimethyl-aniline Degradation

D.1.1 Experimental Control

Table D.1 Disappearance of AN, 2,6-DMA, and n,n-DMA by direct H_2O_2 oxidation and volatilization.

Time (min)	Organic concentration (C/C_0)		
	Aniline	**2,6-DMA**	**n,n-DMA**
0	1.0000	1.0000	1.0000
30	0.9774	1.0122	0.9758
60	0.9827	1.0138	0.9633

Note: 1 mM of AN, 1 mM of 2,6-DMA, 1 mM of n,n-DMA, 20 mM of H_2O_2 at pH 3, and 25 °C.

Table D.2 *o*-toluidine oxidation by direct H_2O_2.

Time (min)	*o*-toluidine (C/C_0)
0	1.0000
30	0.9863
60	1.0023

Note: 0.1 mM of OT, 2 mM of H_2O_2 at pH 11.

D.1.2 Verification of Competitive Kinetics Technique

Table D.3 Competitive oxidation of aniline and n,n-DMA by Fenton reaction (Run No. 1).

Time (min)	Organic concentration (C/C_0)	
	Aniline	**n,n-DMA**
0	1.0000	1.0000
0.5	0.6442	0.7663
1	0.6138	0.7323
5	0.2956	0.4515

Note: 1 mM of AN, 1 mM of n,n-DMA, 1 mM of Fe^{2+}, 20 mM of H_2O_2 at pH 3 and 25 °C.

Table D.4 Competitive oxidation of aniline and n,n-DMA by Fenton reaction (Run No. 2).

Time (min)	Organic concentration (C/C_0)	
	Aniline	**n,n-DMA**
0	1.000	1.000
0.5	0.678	0.740
1	0.662	0.711
1.5	0.654	0.708
2	0.629	0.675
3	0.580	0.649
4	0.512	0.564
5	0.372	0.515
7.5	0.129	0.256
10	0.000	0.071
20	0.000	0.017

Note: 1 mM of AN, 1 mM of n,n-DMA, 1 mM of Fe^{2+}, 20 mM of H_2O_2 at pH 3 and 25 °C.

Table D.5 Competitive oxidation of aniline and n,n-DMA by Fenton reaction (Run No. 3).

Time	Organic concentration (C/C_0)	
(min)	**Aniline**	**n,n-DMA**
0	1.0000	1.0000
0.5	0.6480	0.7212
1	0.6117	0.7125
1.5	0.5843	0.6874
2	0.5293	0.6352
3	0.4666	0.5367
4	0.3750	0.4832
5	0.3167	0.4229
7.5	0.0868	0.1909
10	0.0000	0.0476
20	0.0000	0.0167

Note: 1 mM of AN, 1 mM of n,n-DMA, 1 mM of Fe^{2+}, 20 mM of H_2O_2 at pH 3 and 25 °C.

D.1.3 Intrinsic Rate Constant of 2,6-DMA with Hydroxyl Radical

D.1.3.1 Batch Study in the Absence of Media

Table D.6 Competitive oxidation of aniline and 2,6-DMA by Fenton reaction in the batch reactor without media (Run No. 1).

Time	Organic concentration (C/C_0)	
(min)	Aniline	2,6-DMA
0	1.0000	1.0000
0.5	0.8362	0.5833
1	0.8824	0.5880
2	0.8711	0.5697
5	0.7542	0.4581
10	0.7611	0.4109
15	0.7592	0.3625
20	0.6792	0.2818
25	0.6561	0.2301
30	0.6305	0.1796
60	0.0000	0.0000

Note: 1 mM of AN, 1 mM of 2,6-DMA, 1 mM of Fe^{2+}, 20 mM of H_2O_2 at pH 3 and 25 °C.

Table D.7 Competitive oxidation of aniline and 2,6-DMA by Fenton reaction in the batch reactor without media (Run No. 2).

Time	Organic concentration (C/C_0)	
(min)	**Aniline**	**2,6-DMA**
0	1.0000	1.0000
0.5	0.7960	0.5330
1	0.7931	0.5557
2	0.7726	0.5141
5	0.7661	0.4655
10	0.7086	0.3948
15	0.6759	0.3365
20	0.6747	0.2904
25	0.6766	0.2523
30	0.5736	0.1817
45	0.4220	0.0534
60	0.0882	0.0000

Note: 1 mM of AN, 1 mM of 2,6-DMA, 1 mM of Fe^{2+}, 20 mM of H_2O_2 at pH 3 and 25 °C.

Table D.8 Competitive oxidation of aniline and 2,6-DMA by Fenton reaction in the batch reactor without media (Run No. 3).

Time (min)	Organic concentration (C/C_0)	
	Aniline	**2,6-DMA**
0	1.0000	1.0000
0.5	0.7788	0.5459
1	0.7277	0.4847
2	0.7027	0.4587
5	0.6992	0.4229
10	0.6898	0.3725
15	0.6591	0.3168
20	0.6315	0.2622
25	0.5793	0.2057
30	0.5050	0.1468
45	0.3554	0.0292
60	0.0000	0.0000

Note: 1 mM of AN, 1 mM of 2,6-DMA, 1 mM of Fe^{2+}, 20 mM of H_2O_2 at pH 3 and 25 °C.

Table D.9 Competitive oxidation of aniline and 2,6-DMA by Fenton reaction in the batch reactor without media (Run No. 4).

Time (min)	Organic concentration (C/C_0)	
	Aniline	**2,6-DMA**
0	1	1
0.5	0.8126	0.4607
1	0.7879	0.4283
2	0.7410	0.3799
5	0.7407	0.3157
10	0.6341	0.1917

Note: 1 mM of AN, 0.5 mM of 2,6-DMA, 1 mM of Fe^{2+}, 20 mM of H_2O_2 at pH 3 and 25 °C.

Table D.10 Competitive oxidation of aniline and 2,6-DMA by Fenton reaction in the batch reactor without media (Run No. 5).

Time	Organic concentration (C/C_0)	
(min)	Aniline	2,6-DMA
0	1.0000	1.0000
2	0.8788	0.5652
5	0.8774	0.5276
10	0.8221	0.4488
15	0.8067	0.4024
20	0.7653	0.3499
25	0.7593	0.3089
30	0.7312	0.2721
45	0.6681	0.1646
60	0.4638	0.0701

Note: 0.5 mM of AN, 1 mM of 2,6-DMA, 1 mM of Fe^{2+}, 20 mM of H_2O_2 at pH 3, and 25 °C.

Table D.11 Competitive oxidation of aniline and 2,6-DMA by Fenton reaction in the batch reactor without media (Run No. 6).

Time	Organic concentration (C/C_0)	
(min)	Aniline	2,6-DMA
0	1.0000	1.0000
0.5	0.7363	0.3720
1	0.7636	0.3711
2	0.7163	0.3329
5	0.7320	0.2782
10	0.6489	0.1831
20	0.4793	0.0818
25	0.3999	0.0000

Note: 0.5 mM of AN, 0.5 mM of 2,6-DMA, 1 mM of Fe^{2+}, 20 mM of H_2O_2 at pH 3, and 25 °C.

Table D.12 Competitive oxidation of aniline and 2,6-DMA by Fenton reaction in the
batch reactor without media (Run No. 7).

Time	Organic concentration (C/C_0)	
(min)	Aniline	2,6-DMA
0	1.0000	1.0000
0.5	0.7629	0.4585
1	0.7531	0.4394
5	0.6738	0.3145
10	0.6004	0.2079
15	0.5265	0.1181
20	0.3760	0.0361
25	0.1485	0.0000

Note: 1 mM of AN, 1 mM of 2,6-DMA, 1.5 mM of Fe^{2+}, 30 mM of H_2O_2 at
pH 3, and 25 °C.

Table D.13 Competitive oxidation of aniline and 2,6-DMA by Fenton reaction in the
batch reactor without media (Run No. 8).

Time	Organic concentration (C/C_0)	
(min)	Aniline	2,6-DMA
0	1.0000	1.0000
0.5	0.6519	0.3523
1	0.6392	0.3188
2	0.5702	0.2484
5	0.5083	0.1552
10	0.3026	0.0211
15	0.0302	0.0000

Note: 1 mM of AN, 1 mM of 2,6-DMA, 2 mM of Fe^{2+}, 40 mM of H_2O_2 at
pH 3, and 25 °C.

Table D.14 Competitive oxidation of aniline and 2,6-DMA by Fenton reaction in the batch reactor without media (Run No. 9).

Time (min)	Organic concentration (C/C_0)	
	Aniline	**2,6-DMA**
0	1.0000	1.0000
0.5	0.8410	0.5621
1	0.8278	0.5521
5	0.7922	0.4735
15	0.7198	0.3397
20	0.6770	0.2831
25	0.6584	0.2259
30	0.6226	0.1872
60	0.0228	0.0000

Note: 1 mM of AN, 1 mM of 2,6-DMA, 1 mM of Fe^{2+}, 30 mM of H_2O_2 at pH 3, and 25 °C.

ศูนย์วิทยทรัพยากร

จุฬาลงกรณ์มหาวิทยาลัย

D.1.3.2 Batch Study in the Presence of Media

Table D.15 Competitive oxidation of aniline and 2,6-DMA by Fenton reaction in the batch reactor with media.

Time (min)	Organic concentration (C/C_0)	
	Aniline	**2,6-DMA**
0	1.0000	1.0000
2	0.8434	0.6254
5	0.8340	0.6085
10	0.8159	0.5935
15	0.8220	0.5825
25	0.8023	0.5546
30	0.7986	0.5456
45	0.7988	0.5216
60	0.7889	0.4880

Note: 1 mM of AN, 1 mM of 2,6-DMA, 1 mM of Fe^{2+}, 20 mM of H_2O_2, 37.04 g/l of SiO_2 at pH 3, and 25 °C.

D.1.3.3 Batch Study in the Fluidized-bed Reactor

Table D.16 Competitive oxidation of aniline and 2,6-DMA by fluidized-bed Fenton process (Run No. 1).

Time (min)	Organic concentration (C/C_0)	
	Aniline	**2,6-DMA**
0	1.0000	1.0000
1	0.7433	0.5904
2	0.7269	0.5471
5	0.6966	0.4732
10	0.6193	0.3755
15	0.6173	0.3295
20	0.5805	0.2746
25	0.5454	0.2186
30	0.5208	0.1771
45	0.3906	0.0629
60	0.2228	0.0000

Note: 1 mM of AN, 1 mM of 2,6-DMA, 1 mM of Fe^{2+}, 20 mM of H_2O_2, 230.77 g/l of CS at pH 3, and 25 °C.

Table D.17 Competitive oxidation of aniline and 2,6-DMA by fluidized-bed Fenton process (Run No. 2).

Time	Organic concentration (C/C_0)	
(min)	Aniline	2,6-DMA
0	1.0000	1.0000
1	0.7553	0.5919
2	0.7499	0.5500
5	0.7218	0.4695
10	0.6602	0.3696
15	0.5955	0.3004
20	0.5736	0.2334
25	0.5411	0.1853
30	0.5196	0.1450
45	0.3632	0.0389
60	0.1484	0.0000

Note: 1 mM of AN, 1 mM of 2,6-DMA, 1 mM of Fe^{2+}, 20 mM of H_2O_2, 230.77 g/l of CS at pH 3, and 25 °C.

D.1.3.4 Continuous Study in the Absence of Media

Table D.18 Competitive oxidation of aniline and 2,6-DMA by Fenton reaction in the continuous reactor without media (Run No. 1).

Time	Organic concentration (C/C_0)	
(min)	Aniline	2,6-DMA
0	1.0000	1.0000
30	0.3594	0.1589
60	0.3401	0.1384
90	0.3692	0.1489
120	0.3624	0.1447
150	0.3750	0.1559

Note: 1 mM of AN, 1 mM of 2,6-DMA, 1 mM of Fe^{2+}, 20 mM of H_2O_2 at pH 3, and 25 °C.

Table D.19 Competitive oxidation of aniline and 2,6-DMA by Fenton reaction in the continuous reactor without media (Run No. 2).

Time	Organic concentration (C/C_0)	
(min)	**Aniline**	**2,6-DMA**
0	1.0000	1.0000
30	0.3516	0.1437
60	0.3547	0.1444
90	0.3578	0.1437
120	0.3651	0.1440
150	0.3647	0.1435

Note: 1 mM of AN, 1 mM of 2,6-DMA, 1 mM of Fe^{2+}, 20 mM of H_2O_2 at pH 3, and 25 °C.

D.1.4 Effect of Fenton's Reagent on Organic Degradation

Table D.20 Co-oxidation of aniline and 2,6-DMA under various Fenton's reagent.

Time (min)	Organic concentration (C/C_0)							
	Fe^{2+}1 mM H$_2$O$_2$ 20 mM		Fe^{2+}1.5 mM H$_2$O$_2$ 30 mM		Fe^{2+}2 mM H$_2$O$_2$ 40 mM		Fe^{2+}1 mM H$_2$O$_2$ 30 mM	
	AN	2,6-DMA	AN	2,6-DMA	AN	2,6-DMA	AN	2,6-DMA
0	1.0000	1.0000	1.0000	1.0000	1.0000	1.0000	1.0000	1.0000
0.5	0.7960	0.5330	0.7629	0.4585	0.6519	0.3523	0.8410	0.5621
1	0.7931	0.5557	0.7531	0.4394	0.6392	0.3188	0.8278	0.5521
2	0.7726	0.5141	-	-	0.5702	0.2484	-	-
5	0.7661	0.4655	0.6738	0.3145	0.5083	0.1552	0.7922	0.4735
10	0.7086	0.3948	0.6004	0.2079	0.3026	0.0211	-	-
15	0.6759	0.3365	0.5265	0.1181	0.0302	0.0000	0.7198	0.3397
20	0.6747	0.2904	0.3760	0.0361	-	-	0.6770	0.2831
25	0.6766	0.2523	0.1485	0.0000	-	-	0.6584	0.2259
30	0.5736	0.1817	-	-	-	-	0.6226	0.1872
45	0.4220	0.0534	-	-	-	-	-	-
60	0.0882	0.0000	-	-	-	-	0.0228	0.0000

Note: 1 mM of AN, 1 mM of 2,6-DMA at pH 3, and 25 °C.

D.1.5 Degradation Intermediates and Pathway

Table D.21 Time-profile of intermediate products from 2,6-DMA oxidation by Fenton process.

Time (min)	Carboxylic acid concentration (mM)			Organic intermediate concentration (mM)		
	Acetic acid	Formic acid	Oxalic acid	2,6-DMA	2,6-DMNB	2,6-DMP
0	0.000	0.000	0.000	10.000	0.000	0.000
5	3.200	17.200	23.390	1.696	0.010	0.014
10	4.000	20.000	17.940	1.273	0.008	0.013
15	4.000	21.100	0.000	1.130	0.007	0.010
20	3.900	22.200	0.000	-	-	-
30	4.300	23.500	0.000	0.557	0.003	0.006
45	4.600	30.800	0.000	-	-	-
60	4.800	26.400	0.000	0.242	0.000	0.000

Note: 10 mM of 2,6-DMA, 10 mM of Fe^{2+}, 200 mM of H_2O_2 at pH 3, and 25 °C.

Table D.22 Time-profile of the calculated total organic carbon of the intermediate products from 2,6-DMA oxidation by Fenton process.

Time (min)	Carboxylic acid concentration (mM)			Organic intermediate concentration (mM)			TOC calculated (mM)	TOC Measured (mM)
	Acetic acid	Formic acid	Oxalic acid	2,6-DMA	2,6-DMNB	2,6-DMP		
0	0.000	0.000	0.000	80.000	0.000	0.000	80.000	80.000
5	6.400	17.200	46.780	13.568	0.080	0.112	84.140	-
10	8.000	20.000	35.880	10.184	0.064	0.104	74.232	-
15	8.000	21.100	0.000	9.040	0.056	0.080	38.276	72.508
20	7.800	22.200	0.000	-	-	-	30.000	70.550
30	8.600	23.500	0.000	4.456	0.024	0.048	36.628	66.308
45	9.200	30.800	0.000	-	-	-	40.000	-
60	9.600	26.400	0.000	1.936	0.000	0.000	37.936	55.000

Note: 10 mM of 2,6-DMA, 10 mM of Fe^{2+}, 200 mM of H_2O_2 at pH 3, and 25 °C.

ศูนย์วิทยทรัพยากร

จุฬาลงกรณ์มหาวิทยาลัย

D.2 Iron Crystallization

D.2.1 Iron Solubility

Table D.23 Effect of pH on Fe^{2+} solubility.

Fe^{2+} 1 mM with NaClO$_4$		Fe^{2+} 1 mM without NaClO$_4$		Fe^{2+} 2 mM with NaClO$_4$	
pH	Sol. iron (mg/l)	pH	Sol. iron (mg/l)	pH	Sol. iron (mg/l)
2.10	59.700	1.96	59.700	2.11	118.810
2.93	59.858	3.09	60.684	3.01	117.100
4.93	60.401	4.94	60.834	4.44	117.490
5.24	16.592	5.35	6.134	5.11	111.420
5.51	5.444	6.82	0.000	5.91	7.440
6.75	0.000	7.17	0.000	6.80	0.000
7.55	0.085	9.24	0.000	8.20	0.000
9.12	0.000	10.54	0.000	9.22	0.000
10.19	0.000	11.25	0.000	10.03	0.000
11.15	0.000	12.05	0.000	11.03	0.000
12.01	0.000	-	-	12.03	0.000

Note: Operating at 25 °C.

Table D.24 Effect of pH on Fe^{3+} solubility.

Fe^{2+} 2 mM		Fe^{2+} 1 mM	
pH	Sol. iron (mg/l)	pH	Sol. iron (mg/l)
2.59	118.650	2.42	59.700
2.64	115.799	2.64	51.769
2.69	86.120	2.80	52.702
2.78	33.470	2.96	42.344
3.02	10.300	4.24	0.000
3.32	0.082	5.18	0.000
4.53	0.000	7.05	0.000
5.23	0.000	9.06	0.000
6.42	0.000	12.04	0.000
7.11	0.000		
8.33	0.000		
8.98	0		
10.22	0		
11.12	0		
12.04	0		

Note: 1 and 2 mM of Fe^{3+} with 0.1 M of $NaClO_4$ and operation at 25 °C.

Table D.25 Ferric precipitation under various turbulence conditions.

Time (min)	O_2 gas		Air		Stagnant (BOD bottle)	
	Tot. iron (mg/l)	Sol. iron (mg/l)	Tot. iron (mg/l)	Sol. iron (mg/l)	Tot. iron (mg/l)	Sol. iron (mg/l)
0	56.125	55.000	57.750	55.125	56.625	47.000
5	0.000	43.875	0.000	45.250	-	-
10	0.000	39.250	0.000	38.625	-	-
15	0.000	34.875	0.000	33.125	-	-
30	52.500	21.500	57.125	22.125	55.500	42.375
60	54.500	11.250	57.875	14.125	53.875	40.125
120	55.000	7.625	56.875	8.500	55.375	34.750
180	53.750	6.500	56.625	6.375	54.500	32.750
1140	-	-	-	-	0.000	15.875

Note: 1 mM of Fe^{3+} at pH 3 and 25 °C.

D.2.2 Fe(OH)$_3$ Crystallization in Fluidized-bed Reactor (FBR)

Table D.26 Effect of material type on ferric removal in the FBR at pH 7.

Time (min)	Total iron at pH 7 (mg/l)		
	CS	Al$_2$O$_3$	SiO$_2$
0	56.850	57.250	56.250
10	57.296	-	-
20	57.048	-	-
30	57.098	-	56.293
40	54.866	-	-
50	54.816	-	-
60	55.411	53.696	55.139
120	-	53.665	56.606
180	-	53.619	55.225

Note: 1 mM of Fe^{3+}, 230.77 g/l of media at 25 °C.

Table D.27 Total and soluble iron removal in the FBR at pH 3 using construction sand as the media.

Time (min)	Tot. iron (mg/l)	Sol. iron (mg/l)
0	58.000	40.375
5	34.125	19.750
10	33.125	17.750
15	28.625	17.125
30	21.750	15.250
60	18.125	12.375
120	13.375	9.875
180	11.250	9.250

Note: 1 mM of Fe^{3+}, 230.77 g/l of CS at 25 °C.

D.2.3 Fe(OH)₃ Crystallization in Fluidized-bed Fenton Process

Table D.28 Total iron removal in the FBR with different media.

Time (min)	SiO₂ pass #30 remained #40 (mg/l)	CS pass #30 (mg/l)	CS pass #30 remained #40 Run #1 (mg/l)	CS pass #30 remained #40 Run #2 (mg/l)	Fenton-like (mg/l)
0	57.875	57.875	56.625	58.250	57.875
5	52.250	24.875	23.125	25.000	40.375
10	48.500	22.000	22.375	24.125	25.125
15	44.125	19.000	17.750	21.500	21.250
30	31.875	15.625	15.625	16.500	18.250
60	21.500	11.750	11.750	13.000	17.000
120	15.125	10.250	10.000	10.875	13.625
180	10.625	9.625	9.000	9.125	12.750

Note: 1 mM of Fe^{2+} (for Fenton) or Fe^{3+} (for Fenton-like), 20 mM of H_2O_2, 230.77 g/l of media at pH 3 and 25 °C.

Table D.29 Soluble iron removal in the FBR with different media.

Time (min)	SiO$_2$ pass #30 remained #40 (mg/l)	CS pass #30 (mg/l)	CS pass #30 remained #40 Run #1 (mg/l)	CS pass #30 remained #40 Run #2 (mg/l)	Fenton-like (mg/l)
0	57.750	57.875	58.375	58.125	54.875
5	51.500	21.625	20.000	21.250	27.625
10	43.375	19.375	19.125	20.750	16.250
15	38.125	17.375	18.000	19.750	14.500
30	25.000	17.000	11.625	14.375	12.750
60	14.500	11.000	12.250	11.875	11.500
120	9.750	9.375	9.250	9.500	9.000
180	7.875	7.500	8.125	6.625	8.500

Note: 1 mM of Fe^{2+} (for Fenton) or Fe^{3+} (for Fenton-like), 20 mM of H$_2$O$_2$, 230.77 g/l of media at pH 3 and 25 °C.

Table D.30 Ferrous removal in the FBR with different media.

Time (min)	SiO$_2$ pass #30 remained #40 (mg/l)	CS pass #30 (mg/l)	CS pass #30 remained #40 Run #1 (mg/l)	CS pass #30 remained #40 Run #2 (mg/l)	Fenton-like (mg/l)
0	56.750	57.875	56.625	56.875	-
5	0.375	0.750	0.500	0.875	-
10	0.250	0.375	0.500	0.000	-
15	0.625	0.625	0.875	0.000	-
30	0.375	0.875	1.250	0.000	-
60	0.000	1.000	1.000	1.000	-
120	0.000	0.000	0.500	1.125	-
180	0.875	0.625	0.375	1.250	-

Note: 1 mM of Fe^{2+} or Fe^{3+}, 20 mM of H$_2$O$_2$, 230.77 g/l of media at pH 3 and 25 °C.

Table D.31 Hydrogen peroxide remaining in the FBR with different media.

Time (min)	SiO$_2$ pass #30 remained #40 (mg/l)	CS pass #30 (mg/l)	CS pass #30 remained #40 Run #1 (mg/l)	CS pass #30 remained #40 Run #2 (mg/l)	Fenton-like (mg/l)
0	680.200	680.200	680.200	680.200	680.200
5	523.077	513.423	537.755	553.220	654.966
10	523.077	530.537	503.061	553.220	628.767
15	505.641	504.866	477.041	527.288	602.568
30	401.026	462.081	442.347	484.068	558.904
60	348.718	393.624	364.286	397.627	489.041
120	322.564	316.611	277.551	276.610	349.315
180	270.256	222.483	190.816	181.525	244.521

Note: 1 mM of Fe^{2+} or Fe^{3+}, 20 mM of H_2O_2, 230.77 g/l of media at pH 3 and 25 °C.

D.2.4 Effect of Fe(OH)$_3$ Crystallites

Table D.32 Total and soluble iron removal in the FBR under various concentrations of Fenton's reagent.

Time (min)	Total iron (mg/l)			Soluble iron (mg/l)		
	Fe^{2+}:H_2O_2 1:20 mM	Fe^{2+}:H_2O_2 2:40 mM	Fe^{2+}:H_2O_2 3:60 mM	Fe^{2+}:H_2O_2 1:20 mM	Fe^{2+}:H_2O_2 2:40 mM	Fe^{2+}:H_2O_2 3:60 mM
0	56.625	111.750	172.000	58.375	117.000	173.500
5	23.125	63.000	112.750	20.000	56.500	39.500
10	22.375	52.500	102.250	19.125	42.750	31.250
15	17.750	45.000	92.000	18.000	31.000	26.000
30	15.625	28.500	80.000	11.625	17.250	16.250
60	11.750	16.250	64.750	12.250	7.750	10.500
120	10.000	11.500	39.750	9.250	3.750	7.500
180	9.000	7.750	18.000	8.125	3.500	6.750

Note: 230.77 g/l of CS at pH 3 and 25 °C.

Table D.33 Ferrous and hydrogen peroxide remaining in the FBR reactor under various concentrations of Fenton's reagent.

Time (min)	Fe^{2+} (mg/l)			H_2O_2 (mg/l)		
	$Fe^{2+}:H_2O_2$ 1:20 mM	$Fe^{2+}:H_2O_2$ 2:40 mM	$Fe^{2+}:H_2O_2$ 3:60 mM	$Fe^{2+}:H_2O_2$ 1:20 mM	$Fe^{2+}:H_2O_2$ 2:40 mM	$Fe^{2+}:H_2O_2$ 3:60 mM
0	56.625	114.750	175.500	680.200	1360.400	2040.600
5	0.500	1.500	1.750	537.755	1060.949	843.885
10	0.500	-	-	503.061	1005.109	788.849
15	0.875	-	-	477.041	856.204	742.986
30	1.250	-	-	442.347	949.270	697.122
60	1.000	1.250	1.750	364.286	725.912	614.568
120	0.500	1.500	2.500	277.551	614.234	495.324
180	0.375	1.250	1.500	190.816	521.168	476.978

Note: 230.77 g/l of CS at pH 3 and 25 °C.

Table D.34 Total and soluble iron removal by 1-hr pre-CMR+FBR under various concentrations of Fenton's reagent.

Time (min)	Total iron (mg/l)			Soluble iron (mg/l)		
	$Fe^{2+}:H_2O_2$ 1:20 mM	$Fe^{2+}:H_2O_2$ 2:40 mM	$Fe^{2+}:H_2O_2$ 3:60 mM	$Fe^{2+}:H_2O_2$ 1:20 mM	$Fe^{2+}:H_2O_2$ 2:40 mM	$Fe^{2+}:H_2O_2$ 3:60 mM
0	56.875	113.750	172.500	57.500	115.500	172.750
5	-	-	-	37.875	43.000	24.750
10	-	-	-	29.750	31.500	16.500
15	-	-	-	24.500	21.750	13.250
30	57.000	114.250	172.250	15.375	14.000	8.750
60	57.500	114.750	172.750	8.750	9.000	6.000
65	45.125	114.250	165.500	3.375	6.250	4.000
70	37.250	107.750	163.250	3.625	6.750	5.250
75	31.125	100.000	159.000	3.375	7.500	3.750
90	22.375	90.750	150.500	4.000	6.000	4.000
120	16.125	81.250	137.250	4.500	9.000	5.000
180	9.750	64.000	123.250	3.750	5.750	4.750
240	7.500	42.500	111.250	3.875	9.250	4.750

Note: 230.77 g/l of CS at pH 3 and 25 °C.

ศูนย์วิทยทรัพยากร

จุฬาลงกรณ์มหาวิทยาลัย

Table D.35 Ferrous and hydrogen peroxide remaining in the 1-hr pre-CMR+FBR under various concentrations of Fenton's reagent.

Time (min)	Fe^{2+} (mg/l)			H_2O_2 (mg/l)		
	$Fe^{2+}:H_2O_2$ 1:20 mM	$Fe^{2+}:H_2O_2$ 2:40 mM	$Fe^{2+}:H_2O_2$ 3:60 mM	$Fe^{2+}:H_2O_2$ 1:20 mM	$Fe^{2+}:H_2O_2$ 2:40 mM	$Fe^{2+}:H_2O_2$ 3:60 mM
0	58.625	116.250	173.500	680.200	1360.400	2040.600
5	1.625	0.500	0.750	577.007	1154.015	1706.115
60	1.125	1.750	0.750	428.102	912.044	1449.280
120	1.625	1.750	1.250	381.569	763.139	1265.827
180	2.500	1.250	1.000	325.730	595.620	1155.755
240	1.875	2.000	1.250	260.584	595.620	1082.374

Note: 230.77 g/l of CS at pH 3 and 25 °C.

Table D.36 Total and soluble iron removal by 5-min pre-CMR+FBR

Time (min)	Total iron (mg/l)	Soluble iron (mg/l)
0	172.000	173.000
5	172.000	22.750
10	162.750	22.000
15	156.000	11.000
20	152.000	9.750
35	141.250	7.750
65	125.500	6.500
125	105.250	6.250
185	76.500	5.500

Note: 3 mM of Fe^{2+}, 60 mM of H_2O_2, 230.77 g/l of CS at pH 3 and 25 °C.

Table D.37 Ferrous and hydrogen peroxide remaining in the 5-min pre-CMR+FBR.

Time (min)	Fe^{2+} (mg/l)	H_2O_2 (mg/l)
0	171.750	2040.600
5	0.750	1687.770
65	0.750	1375.899
125	0.750	1192.446
185	0.750	1155.755

Note: 3 mM of Fe^{2+}, 60 mM of H_2O_2, 230.77 g/l of CS at pH 3 and 25 °C.

D.2.5 Effect of Iron Concentration (all the raw data used in the discussions of this part are similar to those of "D.2.4 Effect of Fe(OH)$_3$ Crystallites")

Table D.32 Total and soluble iron removal in the FBR under various concentrations of Fenton's reagent.

Time (min)	Total iron (mg/l)			Soluble iron (mg/l)		
	Fe^{2+}:H_2O_2 1:20 mM	Fe^{2+}:H_2O_2 2:40 mM	Fe^{2+}:H_2O_2 3:60 mM	Fe^{2+}:H_2O_2 1:20 mM	Fe^{2+}:H_2O_2 2:40 mM	Fe^{2+}:H_2O_2 3:60 mM
0	56.625	111.750	172.000	58.375	117.000	173.500
5	23.125	63.000	112.750	20.000	56.500	39.500
10	22.375	52.500	102.250	19.125	42.750	31.250
15	17.750	45.000	92.000	18.000	31.000	26.000
30	15.625	28.500	80.000	11.625	17.250	16.250
60	11.750	16.250	64.750	12.250	7.750	10.500
120	10.000	11.500	39.750	9.250	3.750	7.500
180	9.000	7.750	18.000	8.125	3.500	6.750

Note: 230.77 g/l of CS at pH 3 and 25 °C.

Table D.33 Ferrous and hydrogen peroxide remaining in the FBR reactor under various concentrations of Fenton's reagent.

Time (min)	Fe^{2+} (mg/l)			H_2O_2 (mg/l)		
	$Fe^{2+}:H_2O_2$ 1:20 mM	$Fe^{2+}:H_2O_2$ 2:40 mM	$Fe^{2+}:H_2O_2$ 3:60 mM	$Fe^{2+}:H_2O_2$ 1:20 mM	$Fe^{2+}:H_2O_2$ 2:40 mM	$Fe^{2+}:H_2O_2$ 3:60 mM
0	56.625	114.750	175.500	680.200	1360.400	2040.600
5	0.500	1.500	1.750	537.755	1060.949	843.885
10	0.500	-	-	503.061	1005.109	788.849
15	0.875	-	-	477.041	856.204	742.986
30	1.250	-	-	442.347	949.270	697.122
60	1.000	1.250	1.750	364.286	725.912	614.568
120	0.500	1.500	2.500	277.551	614.234	495.324
180	0.375	1.250	1.500	190.816	521.168	476.978

Note: 230.77 g/l of CS at pH 3 and 25 °C.

Table D.34 Total and soluble iron removal by 1-hr pre-CMR+FBR under various concentrations of Fenton's reagent.

Time (min)	Total iron (mg/l)			Soluble iron (mg/l)		
	$Fe^{2+}:H_2O_2$ 1:20 mM	$Fe^{2+}:H_2O_2$ 2:40 mM	$Fe^{2+}:H_2O_2$ 3:60 mM	$Fe^{2+}:H_2O_2$ 1:20 mM	$Fe^{2+}:H_2O_2$ 2:40 mM	$Fe^{2+}:H_2O_2$ 3:60 mM
0	56.875	113.750	172.500	57.500	115.500	172.750
5	-	-	-	37.875	43.000	24.750
10	-	-	-	29.750	31.500	16.500
15	-	-	-	24.500	21.750	13.250
30	57.000	114.250	172.250	15.375	14.000	8.750
60	57.500	114.750	172.750	8.750	9.000	6.000
65	45.125	114.250	165.500	3.375	6.250	4.000
70	37.250	107.750	163.250	3.625	6.750	5.250
75	31.125	100.000	159.000	3.375	7.500	3.750
90	22.375	90.750	150.500	4.000	6.000	4.000
120	16.125	81.250	137.250	4.500	9.000	5.000
180	9.750	64.000	123.250	3.750	5.750	4.750
240	7.500	42.500	111.250	3.875	9.250	4.750

Note: 230.77 g/l of CS at pH 3 and 25 °C.

Table D.35 Ferrous and hydrogen peroxide remaining in the 1-hr pre-CMR+FBR under various concentrations of Fenton's reagent.

Time (min)	Fe^{2+} (mg/l)			H_2O_2 (mg/l)		
	$Fe^{2+}:H_2O_2$ 1:20 mM	$Fe^{2+}:H_2O_2$ 2:40 mM	$Fe^{2+}:H_2O_2$ 3:60 mM	$Fe^{2+}:H_2O_2$ 1:20 mM	$Fe^{2+}:H_2O_2$ 2:40 mM	$Fe^{2+}:H_2O_2$ 3:60 mM
0	58.625	116.250	173.500	680.200	1360.400	2040.600
5	1.625	0.500	0.750	577.007	1154.015	1706.115
60	1.125	1.750	0.750	428.102	912.044	1449.280
120	1.625	1.750	1.250	381.569	763.139	1265.827
180	2.500	1.250	1.000	325.730	595.620	1155.755
240	1.875	2.000	1.250	260.584	595.620	1082.374

Note: 230.77 g/l of CS at pH 3 and 25 °C.

Table D.36 Total and soluble iron removal by 5-min pre-CMR+FBR

Time (min)	Total iron (mg/l)	Soluble iron (mg/l)
0	172.000	173.000
5	172.000	22.750
10	162.750	22.000
15	156.000	11.000
20	152.000	9.750
35	141.250	7.750
65	125.500	6.500
125	105.250	6.250
185	76.500	5.500

Note: 3 mM of Fe^{2+}, 60 mM of H_2O_2, 230.77 g/l of CS at pH 3 and 25 °C.

Table D.37 Ferrous and hydrogen peroxide remaining in the 5-min pre-CMR+FBR

Time (min)	Fe^{2+} (mg/l)	H_2O_2 (mg/l)
0	171.750	2040.600
5	0.750	1687.770
65	0.750	1375.899
125	0.750	1192.446
185	0.750	1155.755

Note: 3 mM of Fe^{2+}, 60 mM of H_2O_2, 230.77 g/l of CS at pH 3 and 25 °C.

D.2.6 Effect of Turbulence (some raw data used in the discussions of this part are similar to those of "D.2.1 Iron Solubility")

Table D.25 Ferric precipitation under various turbulence conditions.

Time (min)	O_2 gas		Air		Stagnant (BOD bottle)	
	Tot. iron (mg/l)	Sol. iron (mg/l)	Tot. iron (mg/l)	Sol. iron (mg/l)	Tot. iron (mg/l)	Sol. iron (mg/l)
0	56.125	55.000	57.750	55.125	56.625	47.000
5	0.000	43.875	0.000	45.250	-	-
10	0.000	39.250	0.000	38.625	-	-
15	0.000	34.875	0.000	33.125	-	-
30	52.500	21.500	57.125	22.125	55.500	42.375
60	54.500	11.250	57.875	14.125	53.875	40.125
120	55.000	7.625	56.875	8.500	55.375	34.750
180	53.750	6.500	56.625	6.375	54.500	32.750
1140	-	-	-	-	0.000	15.875

Note: 1 mM of Fe^{3+} at pH 3 and 25 °C.

Table D.38 Ferric precipitation under Fenton experiment.

Time (min)	Total iron (mg/l)	Soluble iron (mg/l)	Fe^{2+} (mg/l)	H_2O_2 (mg/l)
0	56.250	56.250	57.000	680.200
5	57.125	45.750	0.750	567.637
10	56.750	39.250	-	523.973
15	56.750	33.125	-	523.973
30	56.125	22.000	-	462.842
60	56.500	12.375	0.375	401.712
120	56.625	8.500	0.500	314.384
180	58.125	6.125	1.000	279.452

Note: 1 mM of Fe^{2+}, 20 mM of H_2O_2 at pH 3 and 25 °C.

D.2.7 Effect of Organic Compounds

Table D.39 Effect of organo-ferric complex on iron crystallization in FBR.

Time (min)	Absence of VFA		Presence of VFA	
	Sol. iron (mg/l)	Tot. iron (mg/l)	Sol. iron (mg/l)	Tot. iron (mg/l)
0	40.375	58.000	59.000	59.000
5	19.750	34.125	56.500	59.000
10	17.750	33.125	55.375	59.000
15	17.125	28.625	55.375	59.375
30	15.250	21.750	54.500	59.375
60	12.375	18.125	54.125	59.375
120	9.875	13.375	54.125	58.750
180	9.250	11.250	53.625	58.625

Note: 1 mM of Fe^{3+}, 230.77 g/l of CS at pH 3 and 25 °C, VFA consisted of 2 mM of formic acid, 0.5 mM of acetic acid and 2 mM of oxalic acid.

Table D.40 Effect of organo-ferric complex on total iron removal in fully fluidized-bed Fenton process.

Time (min)	Total iron (mg/l)			
	Free org.	Org. 0.1 mM Run #1	Org. 0.1 mM Run #2	Org. 1 mM
0	56.625	57.250	57.250	57.375
5	23.125	41.250	36.125	41.125
10	22.375	38.500	34.750	34.125
15	17.750	37.375	33.875	31.875
30	15.625	36.625	33.125	28.750
60	11.750	35.750	30.750	27.625
120	10.000	34.375	28.250	42.250
180	9.000	30.375	27.625	46.000

Note: 1 mM of Fe^{2+}, 20 mM of H_2O_2, 230.77 g/l of CS at pH 3 and 25 °C.

Table D.41 Effect of organo-ferric complex on soluble iron removal in fully fluidized-bed Fenton process.

Time (min)	Soluble iron (mg/l)			
	Free org.	Org. 0.1 mM Run #1	Org. 0.1 mM Run #2	Org. 1 mM
0	58.375	57.250	57.375	59.625
5	20.000	35.375	34.500	35.625
10	19.125	35.500	32.375	34.000
15	18.000	34.875	31.625	30.875
30	11.625	33.250	30.000	27.500
60	12.250	32.375	28.000	27.250
120	9.250	29.750	26.000	41.250
180	8.125	27.750	24.250	45.750

Note: 1 mM of Fe^{2+}, 20 mM of H_2O_2, 230.77 g/l of CS at pH 3 and 25 °C.

Table D.42 Effect of organo-ferric complex on ferrous removal in fully fluidized-bed Fenton process.

Time (min)	Fe^{2+} remaining (mg/l)			
	Free org.	Org. 0.1 mM Run #1	Org. 0.1 mM Run #2	Org. 1 mM
0	56.625	57.250	57.500	58.500
5	0.500	1.750	3.000	11.625
10	0.500	-	-	10.125
15	0.875	-	-	9.500
30	1.250	-	-	7.250
60	1.000	-	2.250	12.000
120	0.500	-	1.500	7.500
180	0.375	-	1.500	6.500

Note: 1 mM of Fe^{2+}, 20 mM of H_2O_2, 230.77 g/l of CS at pH 3 and 25 °C.

Table D.43 Effect of organo-ferric complex on H_2O_2 consumption in fully fluidized-bed Fenton process.

Time (min)	H_2O_2 remaining (mg/l)			
	Free org.	Org. 0.1 mM Run #1	Org. 0.1 mM Run #2	Org. 1 mM
0	680.200	680.200	680.200	680.200
5	537.755	534.831	534.831	604.927
10	503.061	467.978	458.427	558.394
15	477.041	410.674	382.022	567.701
30	442.347	305.618	257.865	530.474
60	364.286	181.461	143.258	409.489
120	277.551	57.303	38.202	46.533
180	190.816	9.551	19.101	0.000

Note: 1 mM of Fe^{2+}, 20 mM of H_2O_2, 230.77 g/l of CS at pH 3 and 25 °C.

Table D.44 Effect of organo-ferric complex on total and soluble iron removal in 1-hr pre-CMR+FBR.

Time (min)	Total iron (mg/l)		Soluble iron (mg/l)	
	Org. 0.1 mM	Org. 1 mM	Org. 0.1 mM	Org. 1 mM
0	57.875	57.125	57.875	57.125
60	57.875	57.000	47.625	30.125
65	42.000	53.625	38.750	26.875
70	40.250	53.500	36.500	27.250
75	38.625	54.500	28.875	30.250
80	-	54.750	-	29.875
90	32.750	53.875	27.375	31.000
120	29.125	53.125	24.750	34.250
180	23.125	55.125	20.500	37.500
240	22.750	55.625	20.000	39.125

Note: 1 mM of Fe^{2+}, 20 mM of H_2O_2, 230.77 g/l of CS at pH 3 and 25 °C.

Table D.45 Effect of organo-ferric complex on Fe^{2+} removal and H_2O_2 consumption in 1-hr pre-CMR+FBR.

Time (min)	Fe^{2+} remaining (mg/l)		H_2O_2 remaining (mg/l)	
	Org. 0.1 mM	Org. 1 mM	Org. 0.1 mM	Org. 1 mM
0	58.125	58.250	680.200	680.200
60	1.750	10.875	112.373	363.051
65	0.000	0.000	112.373	259.322
70	0.000	0.000	86.441	250.678
75	0.000	7.875	77.797	216.102
80	-	7.000	-	207.458
90	0.000	6.500	60.508	146.949
120	0.000	5.875	34.576	60.508
180	0.000	4.750	8.644	25.932
240	0.000	4.125	0.000	0

Note: 1 mM of Fe^{2+}, 20 mM of H_2O_2, 230.77 g/l of CS at pH 3 and 25 °C.

ศูนย์วิทยทรัพยากร
จุฬาลงกรณ์มหาวิทยาลัย

D.2.8 Reusability of Iron-coated Construction Sand for Iron Crystallization

Table D.46 Reusability of iron-coated CS for iron crystallization.

Cycle	Total iron @ 60 min (mg/l)	Cycle	Total iron @ 60 min (mg/l)	Cycle	Total iron @ 60 min (mg/l)	Cycle	Total iron @ 60 min (mg/l)
1	9.875	26	33.500	51	37.500	76	40.000
2	6.875	27	21.000	52	33.750	77	36.500
3	7.875	28	22.500	53	40.250	78	37.000
4	8.125	29	26.750	54	31.250	79	35.250
5	9.250	30	29.750	55	30.750	80	37.750
6	24.750	31	24.750	56	34.750	81	39.250
7	30.250	32	28.750	57	38.000	82	41.250
8	32.250	33	30.750	58	28.000	83	37.750
9	28.500	34	35.750	59	32.750	84	35.000
10	29.500	35	30.500	60	31.750	85	38.500
11	27.750	36	31.750	61	31.000	86	44.750
12	17.750	37	32.500	62	30.500	87	41.500
13	20.750	38	34.000	63	30.500	88	45.500
14	31.000	39	34.500	64	31.000	89	41.750
15	21.500	40	31.250	65	30.750	90	46.500
16	21.250	41	33.750	66	35.750	91	50.750
17	25.500	42	26.750	67	29.750	92	35.500
18	26.750	43	33.000	68	34.250	93	38.250
19	26.250	44	29.000	69	38.250	94	33.750
20	34.000	45	30.750	70	39.250	95	39.000
21	27.500	46	33.250	71	41.250	96	35.500
22	31.000	47	27.500	72	32.250	97	43.000
23	25.250	48	24.500	73	31.750	98	39.750
24	26.750	49	26.500	74	34.000	99	44.750
25	26.250	50	34.750	75	36.500	100	44.750
						101	44.250

Note: 1 mM of Fe^{2+}, 20 mM of H_2O_2 at Cycle 1st -5th

2 mM of Fe^{2+}, 40 mM of H_2O_2 at Cycle 6th-101st , 230.77 g/l of CS

at pH 3 and 25 °C.

Table D.47 Comparison of total and soluble iron removal between the 1st cycle and 101st cycle.

Time	Total iron (mg/l)		Soluble iron (mg/l)	
(min)	1st cycle	101st cysle	1st cycle	101st cysle
0	111.750	132.500	117.000	116.500
5	63.000	102.500	56.500	14.250
10	52.500	74.250	42.750	14.000
15	45.000	69.500	31.000	10.000
30	28.500	56.500	17.250	10.000
60	16.250	44.250	7.750	5.000
120	11.500	38.250	3.750	3.250
180	7.750	31.500	3.500	3.500

Note: 2 mM of Fe^{2+}, 40 mM of H_2O_2, 230.77 g/l of CS at pH 3 and 25 °C.

Table D.48 Comparison of Fe^{2+} removal and H_2O_2 consumption between the 1st cycle and 101st cycle.

Time	Fe^{2+} (mg/l)		H_2O_2 (mg/l)	
(min)	1st cycle	101st cycle	1st cycle	101st cycle
0	114.750	115.750	1360.400	1360.400
5	1.500	0.500	1060.949	1069.930
10	-	-	1005.109	-
15	-	-	856.204	-
30	-	-	949.270	980.769
60	1.250	0.250	725.912	838.112
120	1.500	0.750	614.234	748.951
180	1.250	0.500	521.168	677.622

Note: 2 mM of Fe^{2+}, 40 mM of H_2O_2, 230.77 g/l of CS at pH 3 and 25 °C.

D.2.9 Catalytic Activity of Iron-coated Construction Sand

Table D.49 Aniline removal in the system with H_2O_2 and catalyst.

Time (min)	Aniline concentration (C/C_0)					
	Goethite 0.075 g/l	Goethite 0.75 g/l	Goethite 1 g/l	Goethite 7.5 g/l	Goethite 75 g/l	Iron-coated CS 75 g/l
0	1.0000	1.0000	1.0000	1.0000	1.0000	1.0000
10	0.9901	0.9742	0.9524	0.7415	0.3294	0.9736
20	0.9663	0.9611	0.9130	0.5534	0.0000	0.9784
30	0.9814	0.9524	0.9222	0.4488	0.0000	0.9296
40	0.9687	0.9688	0.9054	0.2951	0.0000	0.9272
50	0.9881	0.9598	0.9048	0.2047	0.0000	0.8886
60	1.0004	0.9615	0.9079	0.1498	0.0000	0.8754
90	1.0080	0.9662	0.8697	0.0474	0.0000	0.8244
120	1.0159	0.9356	0.8856	0.0000	0.0000	0.7516
180	0.9919	0.9402	0.8477	0.0000	0.0000	0.6796

Note: 1 mM of AN, 1 mM of 2,6-DMA, 20 mM of H_2O_2 at pH 3 and 25 °C.

Table D.50 2,6-DMA removal in the system with H_2O_2 and catalyst.

Time (min)	2,6-DMA concentration (C/C$_0$)					
	Goethite 0.075 g/l	Goethite 0.75 g/l	Goethite 1 g/l	Goethite 7.5 g/l	Goethite 75 g/l	Iron-coated CS 75 g/l
0	1.0000	1.0000	1.0000	1.0000	1.0000	1.0000
10	0.9925	0.9910	0.9209	0.5299	0.0857	0.9653
20	0.9709	0.9618	0.8833	0.2780	0.0000	0.9543
30	0.9664	0.9464	0.8822	0.1467	0.0000	0.8874
40	0.9581	0.9378	0.8833	0.0590	0.0000	0.8662
50	0.9807	0.9293	0.8749	0.0249	0.0000	0.8387
60	0.9779	0.9400	0.8519	0.0000	0.0000	0.8260
90	0.9934	0.9245	0.8193	0.0000	0.0000	0.7732
120	1.0040	0.8834	0.7987	0.0000	0.0000	0.6848
180	0.9822	0.8542	0.7657	0.0000	0.0000	0.5963

Note: 1 mM of AN, 1 mM of 2,6-DMA, 20 mM of H_2O_2 at pH 3 and 25 °C.

ศูนย์วิทยทรัพยากร
จุฬาลงกรณ์มหาวิทยาลัย

Table D.51 Soluble iron removal in the system with H_2O_2 and catalyst.

Time (min)	Soluble iron (mg/l)					
	Goethite 0.075 g/l	Goethite 0.75 g/l	Goethite 1 g/l	Goethite 7.5 g/l	Goethite 75 g/l	Iron-coated CS 75 g/l
0	0.000	0.000	0.000	0.000	0.000	0.000
10	0.625	-	-	-	-	0.875
15	-	2.750	-	8.125	8.750	-
20	0.750	-	-	-	-	1.625
25	-	-	-	-	14.500	-
30	1.250	2.500	3.625	9.375	18.250	1.625
40	0.125	-	-	-	23.250	2.500
50	1.000	-	-	-	24.000	2.625
60	1.000	3.000	2.875	10.125	23.500	2.500
90	1.000	2.875	3.500	11.375	-	2.875
120	0.000	2.750	3.625	10.625	-	2.125
180	0.000	3.125	3.375	12.250	-	2.625

Note: 1 mM of AN, 1 mM of 2,6-DMA, 20 mM of H_2O_2 at pH 3 and 25 °C.

Table D.52 Ferrous removal in the system with H_2O_2 and catalyst.

Time (min)	Fe^{2+} (mg/l)					
	Goethite 0.075 g/l	Goethite 0.75 g/l	Goethite 1 g/l	Goethite 7.5 g/l	Goethite 75 g/l	Iron-coated CS 75 g/l
0	0.000	0.000	0.000	0.000	0.000	0.000
10	0.375	-	-		-	0.500
15	-	1.500	-	8.500	10.250	-
20	0.375	-	-	-	-	0.875
25	-	-	-	-	11.875	-
30	0.500	1.750	2.000	9.750	9.625	0.875
40	0.500	-	-	-	7.625	1.000
50	0.500	-	-	-	7.375	1.125
60	0.500	2.125	2.500	10.000	7.375	1.375
90	0.625	2.125	2.750	9.875	-	1.500
120	0.750	1.875	2.625	9.125	-	1.750
180	1.125	2.500	2.875	7.125	-	2.125

Note: 1 mM of AN, 1 mM of 2,6-DMA, 20 mM of H_2O_2 at pH 3 and 25 °C.

Table D.53 Relationship between $\ln([2,6\text{-DMA}]/[n2,6\text{-DMA}]_0)$ and $\ln([AN]/[AN]_0)$ of the system with H_2O_2 and iron-coated CS.

Time	Organic concentration (C/C_0)	
(min)	**Aniline**	**2,6-DMA**
0	1.0000	1.0000
10	0.9736	0.9653
20	0.9784	0.9543
30	0.9296	0.8874
40	0.9272	0.8662
50	0.8886	0.8387
60	0.8754	0.8260
90	0.8244	0.7732
120	0.7516	0.6848
180	0.6796	0.5963

Note: 1 mM of AN, 1 mM of 2,6-DMA, 20 mM of H_2O_2, 75 g/l of iron-coated CS at pH 3 and 25 °C.

APPENDIX E

Determination of the Rate Constant Ratio Using the Competitive Kinetics Technique

E.1 Verification of Competitive Kinetics Technique
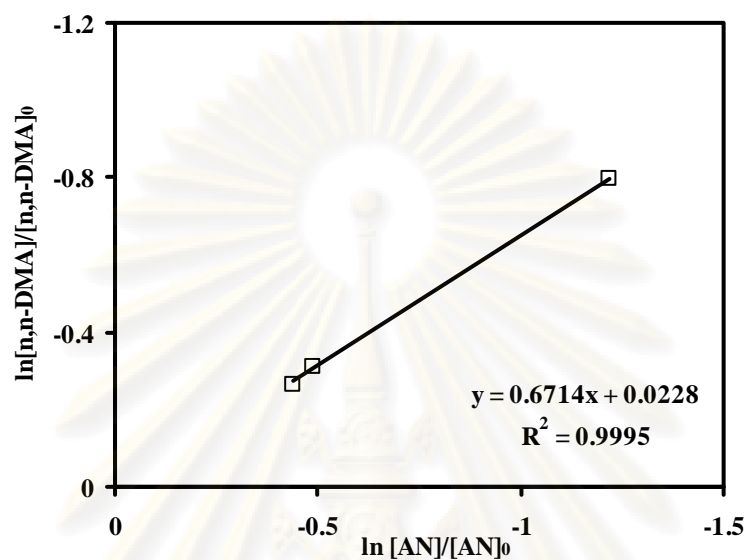
Figure E.1 Relationship between $\ln([n,n\text{-DMA}]/[n,n\text{-DMA}]_0)$ versus $\ln([AN]/[AN]_0)$ (Run No. 1) with the initial conditions as follows: 1 mM of AN, 1 mM of n,n-DMA, 1 mM of Fe^{2+}, 20 mM of H_2O_2 at pH 3 and 25 °C.
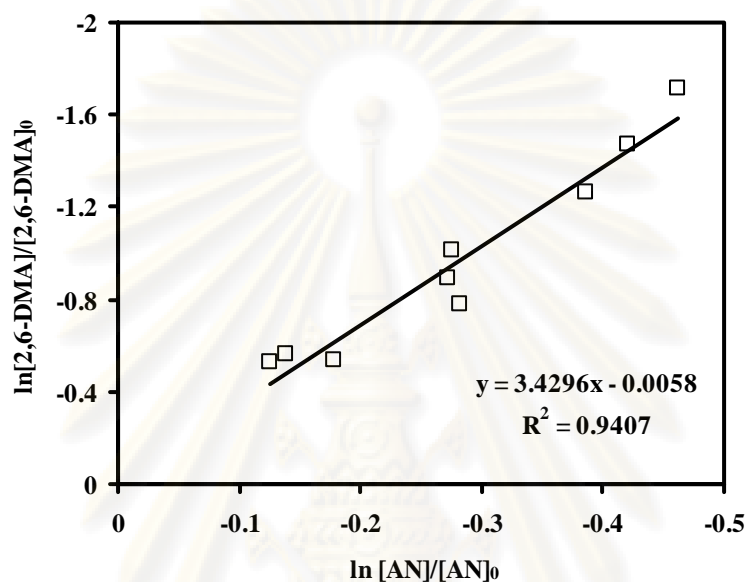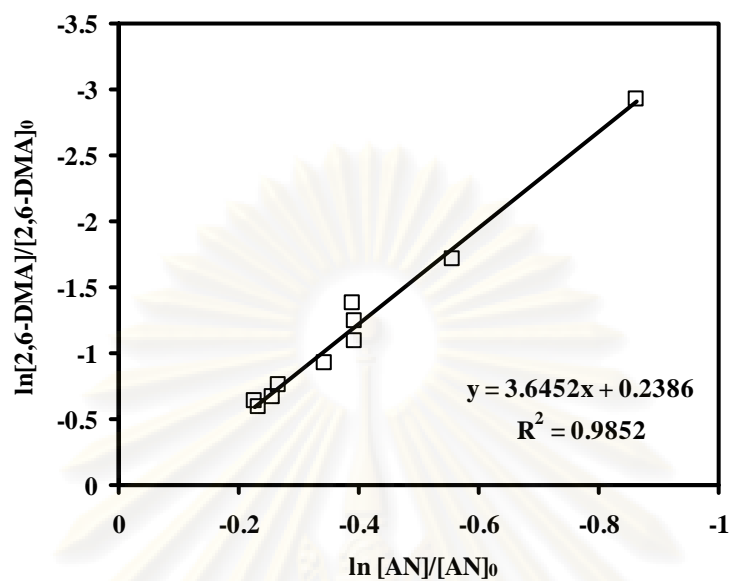
ศูนย์วิทยทรัพยากร

จุฬาลงกรณ์มหาวิทยาลัย
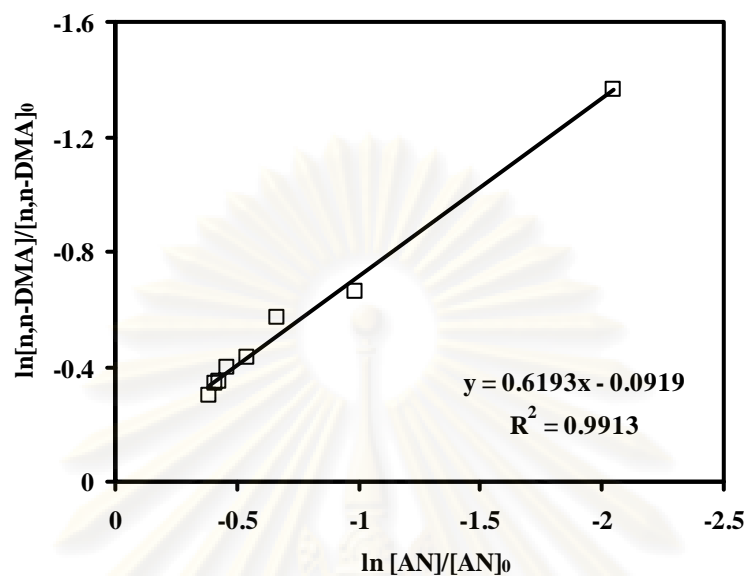
Figure E.2 Relationship between $\ln([n,n\text{-}DMA]/[n,n\text{-}DMA]_0)$ versus $\ln([AN]/[AN]_0)$ (Run No. 2) with the initial conditions as follows: 1 mM of AN, 1 mM of n,n-DMA, 1 mM of Fe^{2+}, 20 mM of H_2O_2 at pH 3 and 25 °C.
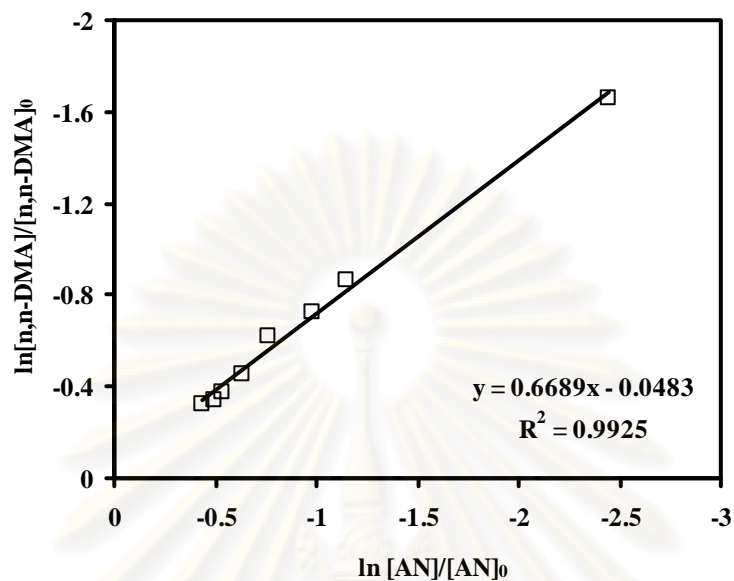
Figure E.3 Relationship between $\ln([n,n\text{-DMA}]/[n,n\text{-DMA}]_0)$ versus $\ln([AN]/[AN]_0)$ (Run No. 3) with the initial conditions as follows: 1 mM of AN, 1 mM of n,n-DMA, 1 mM of Fe^{2+}, 20 mM of H_2O_2 at pH 3 and 25 °C.

E.2 Intrinsic Rate Constant of 2,6-DMA with Hydroxyl Radical
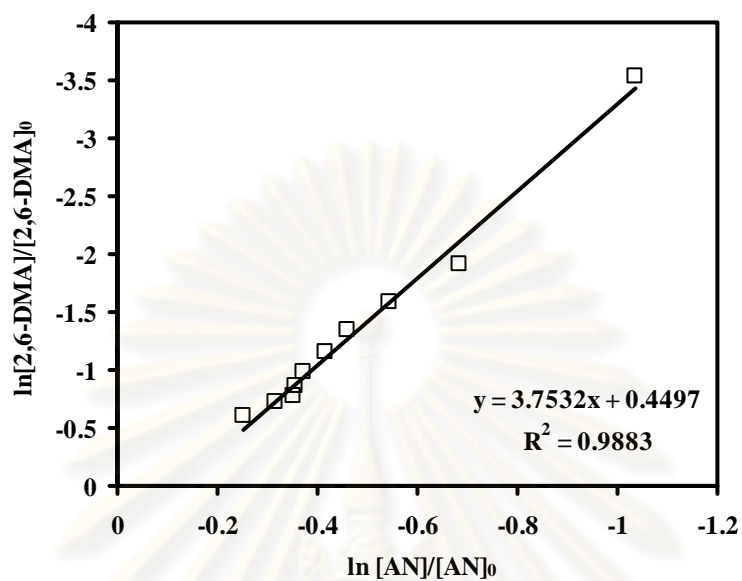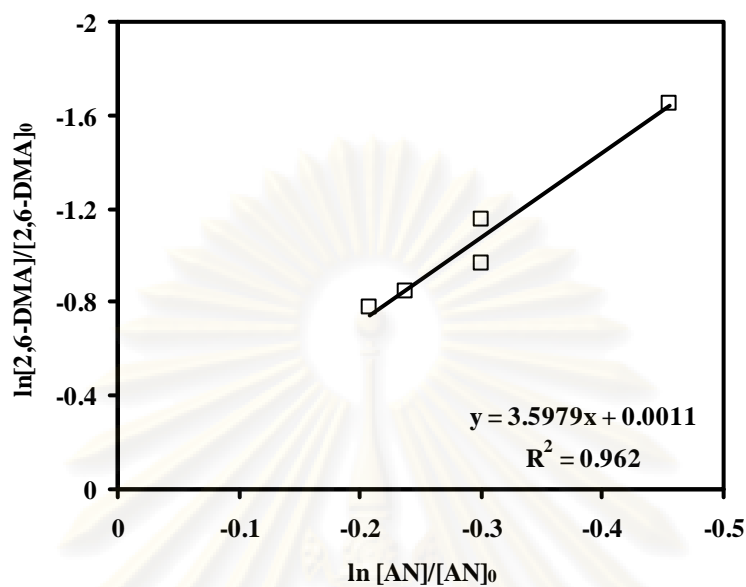
E.2.1 Batch Study in the Absence of Media

Figure E.4 Relationship between $\ln([2,6\text{-DMA}]/[2,6\text{-DMA}]_0)$ versus $\ln([AN]/[AN]_0)$ (Run No. 1) with the initial conditions as follows: 1 mM of AN, 1 mM of 2,6-DMA, 1 mM of Fe^{2+}, 20 mM of H_2O_2 at pH 3 and 25 °C.
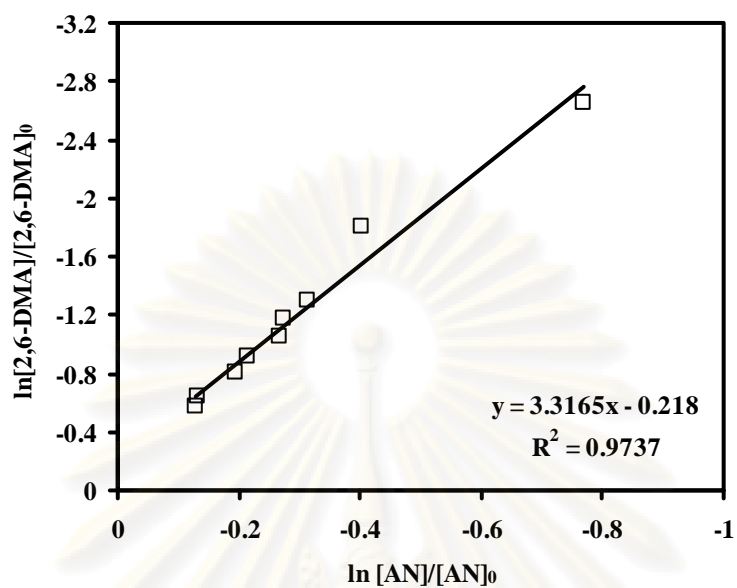
Figure E.5 Relationship between $\ln([2,6\text{-DMA}]/[2,6\text{-DMA}]_0)$ versus $\ln([AN]/[AN]_0)$ (Run No. 2) with the initial conditions as follows: 1 mM of AN, 1 mM of 2,6-DMA, 1 mM of Fe^{2+}, 20 mM of H_2O_2 at pH 3 and 25 °C.

Figure E.6 Relationship between $\ln([2,6\text{-DMA}]/[2,6\text{-DMA}]_0)$ versus $\ln([AN]/[AN]_0)$ (Run No. 3) with the initial conditions as follows: 1 mM of AN, 1 mM of 2,6-DMA, 1 mM of Fe^{2+}, 20 mM of H_2O_2 at pH 3 and 25 °C.
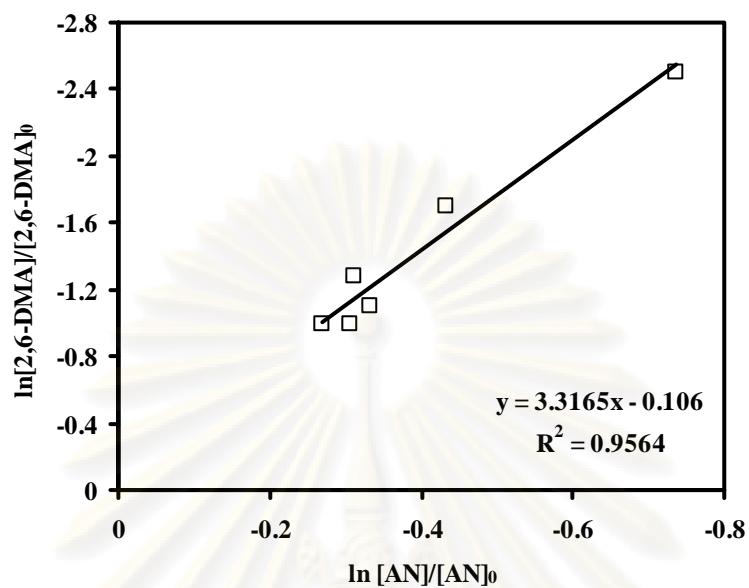
ศูนย์วิทยทรัพยากร

จุฬาลงกรณ์มหาวิทยาลัย

Figure E.7 Relationship between $\ln([2,6\text{-DMA}]/[2,6\text{-DMA}]_0)$ versus $\ln([AN]/[AN]_0)$ (Run No. 4) with the initial conditions as follows: 1 mM of AN, 0.5 mM of 2,6-DMA, 1 mM of Fe^{2+}, 20 mM of H_2O_2 at pH 3 and 25 °C.
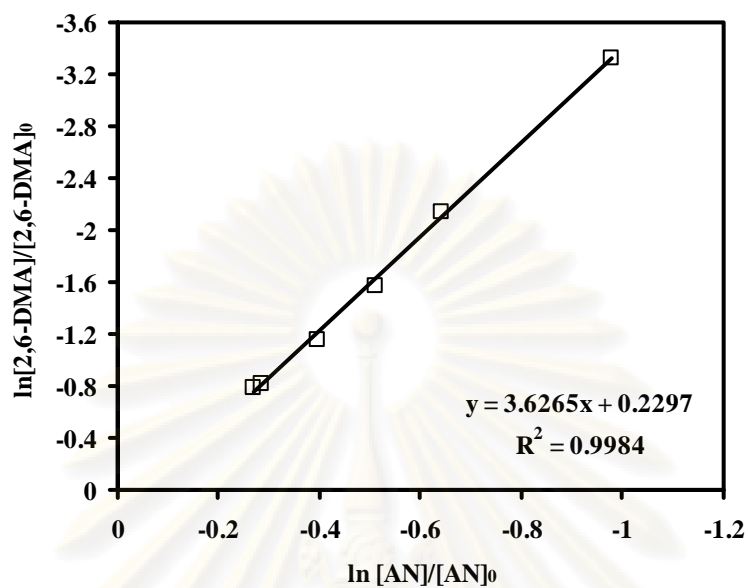
Figure E.8 Relationship between $\ln([2,6\text{-DMA}]/[2,6\text{-DMA}]_0)$ versus $\ln([AN]/[AN]_0)$ (Run No. 5) with the initial conditions as follows: 0.5 mM of AN, 1 mM of 2,6-DMA, 1 mM of Fe^{2+}, 20 mM of H_2O_2 at pH 3 and 25 °C.

Figure E.9 Relationship between $\ln([2,6\text{-}DMA]/[2,6\text{-}DMA]_0)$ versus $\ln([AN]/[AN]_0)$ (Run No. 6) with the initial conditions as follows: 0.5 mM of AN, 0.5 mM of 2,6-DMA, 1 mM of Fe^{2+}, 20 mM of H_2O_2 at pH 3 and 25 °C.

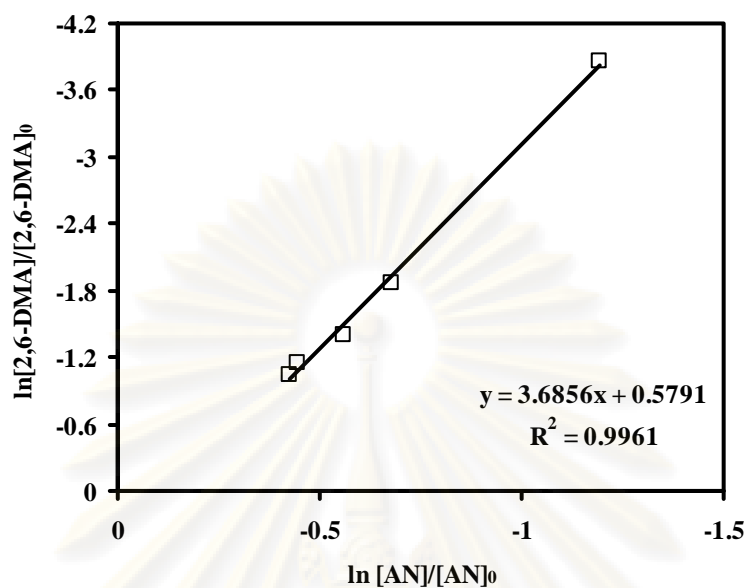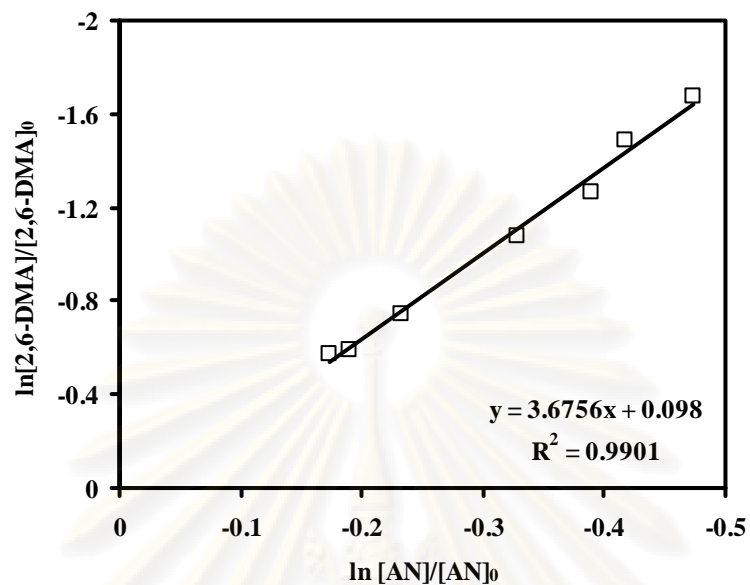**Figure E.10** Relationship between $\ln([2,6\text{-DMA}]/[2,6\text{-DMA}]_0)$ versus $\ln([AN]/[AN]_0)$ (Run No. 7) with the initial conditions as follows: 1 mM of AN, 1 mM of 2,6-DMA, 1.5 mM of Fe^{2+}, 30 mM of H_2O_2 at pH 3 and 25 °C.

Figure E.11 Relationship between $\ln([2,6\text{-DMA}]/[2,6\text{-DMA}]_0)$ versus $\ln([AN]/[AN]_0)$ (Run No. 8) with the initial conditions as follows: 1 mM of AN, 1 mM of 2,6-DMA, 2 mM of Fe^{2+}, 40 mM of H_2O_2 at pH 3 and 25 °C.

Figure E.12 Relationship between $\ln([2,6\text{-DMA}]/[2,6\text{-DMA}]_0)$ versus $\ln([AN]/[AN]_0)$ (Run No. 9) with the initial conditions as follows: 1 mM of AN, 1 mM of 2,6-DMA, 1 mM of Fe^{2+}, 30 mM of H_2O_2 at pH 3 and 25 °C.
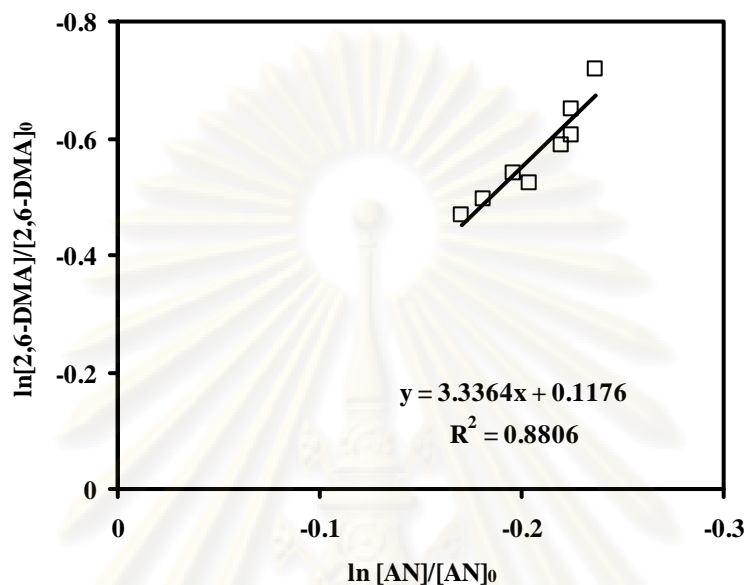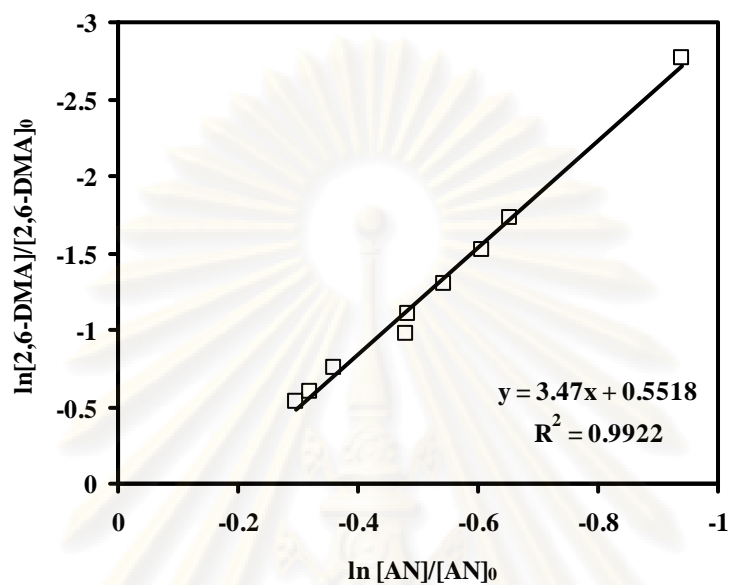
E.2.2 Batch Study in the Presence of Media

Figure E.13 Relationship between $\ln([2,6\text{-}DMA]/[2,6\text{-}DMA]_0)$ versus $\ln([AN]/[AN]_0)$ (Run No. 10) with the initial conditions as follows: 1 mM of AN, 1 mM of 2,6-DMA, 1 mM of Fe^{2+}, 20 mM of H_2O_2, 37.04 g/l of SiO_2 at pH 3 and 25 °C.

E.2.3 Batch Study in the Fluidized-bed Reactor

Figure E.14 Relationship between $\ln([2,6\text{-DMA}]/[2,6\text{-DMA}]_0)$ versus $\ln([AN]/[AN]_0)$ (Run No. 11) with the initial conditions as follows: 1 mM of AN, 1 mM of 2,6-DMA, 1 mM of Fe^{2+}, 20 mM of H_2O_2, 230.77 g/l of CS at pH 3 and 25 °C.
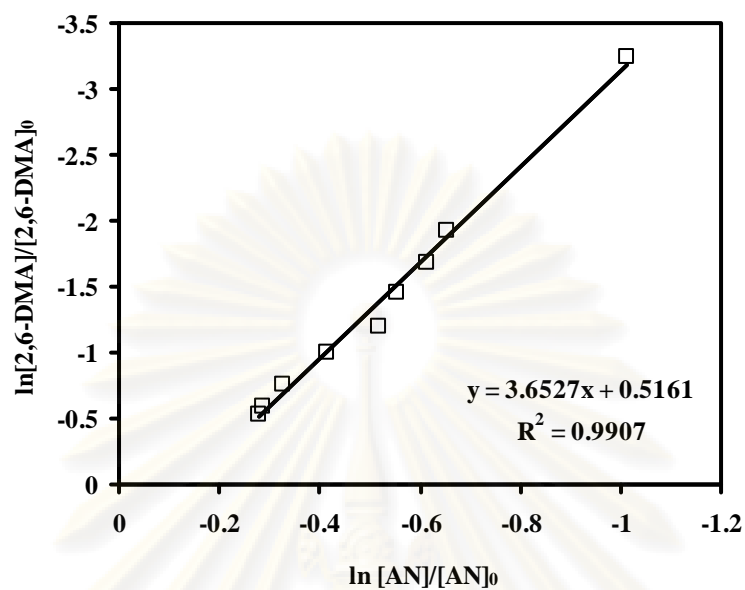
Figure E.15 Relationship between $\ln([2,6\text{-DMA}]/[2,6\text{-DMA}]_0)$ versus $\ln([AN]/[AN]_0)$ (Run No.12) with the initial conditions as follows: 1 mM of AN, 1 mM of 2,6-DMA, 1 mM of Fe^{2+}, 20 mM of H_2O_2, 230.77 g/l of CS at pH 3 and 25 °C.

APPENDIX F

Calculation for the construction of "log C - pH Diagram" for Fe^{3+} Solubility

Calculate for ideal solution at 25°C and neglecting the ionic strength

Step 1: Species → H^+, OH^-, Fe^{3+}, $Fe(OH)^{2+}$, $Fe(OH)_2^+$, $Fe(OH)_{3(aq)}$, $Fe(OH)_4^-$, $Fe(OH)_{3(s)}$

Step 2: Equilibrium equation:

$$[H^+][OH^-] \quad = \quad K_w \quad = \quad 10^{-14} \rightarrow pH + pOH = \quad 14$$

$$[Fe(OH)_i^{3-i}] \quad = \quad \beta_i[Fe^{3+}][OH^-]^i \qquad (F.1) \rightarrow (F.4)$$

$$\beta_1 = 10^{11.81}, \beta_2 = 10^{22.33}, \beta_3 = 10^{28.40}, \beta_4 = 10^{34.30}$$

$$[Fe^{3+}][OH^-]^3 \quad = \quad K_{sp} \quad = \quad 10^{-37.11} \text{ for } Fe(OH)_{3(s)} \qquad (F.5)$$

From (5)

$$\log[Fe^{3+}] + 3\log[OH^-] \quad = \quad -37.11$$

$$\log[Fe^{3+}] \quad = \quad -3\log[OH^-] - 37.11$$

$$= \quad 3pOH - 37.11$$

$$= \quad 3(14-pH) - 37.11$$

$$\log[Fe^{3+}] \quad = \quad -3pH + 4.89 \qquad (F.6)$$

$$\log[Fe(OH)_i^{3-i}] \quad = \quad \log\beta_i + \log[Fe^{3+}] + i\log[OH^-]$$

$$\log[Fe(OH)_i^{3-i}] \quad = \quad \log\beta_i + (-3pH + 4.89) - i(14-pH)$$

$$= \quad (\log\beta_i + 4.89 - 14i) + (i-3)pH$$

$$\therefore \log[Fe(OH)^{2+}] \quad = \quad (11.81 + 4.89 - 14) - 2pH$$

$$= \quad 2.7 - 2pH \qquad (F.7)$$

$$\log[Fe(OH)_2^+] \quad = \quad (22.33 + 4.89 - 28) - pH$$

$$= \quad -0.78 - pH \qquad (F.8)$$

$$\log[Fe(OH)_3^0] \quad = \quad (28.4 + 4.89 - 4.2)$$

$$= \quad -8.71 \qquad (F.9)$$

$$\log[Fe(OH)_4^-] \quad = \quad (34.4 + 4.89 - 56) + pH$$

$$= \quad -16.71 + pH \qquad (F.10)$$

BIOGRAPHY

NAME   Miss Nonglak Boonrattanakij

DATE OF BIRTH   1 August 1980

EDUCATIONAL RECORD

Bachelor Degree   Bachelor of Engineering (Environmental Engineering)
                       King Mongkut's University of Technology Thonburi, Bangkok,
                       Thailand, 2002

Master Degree   Master of Engineering (Environmental Engineering)
                       King Mongkut's University of Technology Thonburi, Bangkok,
                       Thailand, 2006

Doctoral Degree   Doctor of Philosophy (Environmental Management)
                       International Postgraduate Program in Environmental
                       Management (Hazardous Waste Management), Inter-
                       Department of Environmental Management
                       Chulalongkorn University, Bangkok, Thailand, 2009

SCHOLARSHIP   Royal Golden Jubilee Ph.D. Program
                       Grant No. PHD/0056/2549, Thailand Research Fund

JOURNAL PUBLICATIONS
1. Jin Anotai, Pasootah Sakulkittimasak, <u>Nonglak Boonrattanakij</u>, Ming-Chun Lu
    (2009) Kinetics of nitrobenzene oxidation and iron crystallization in fluidized-bed
    Fenton process. *Journal of Hazardous Materials*, 165, 874-880.
2. <u>Nonglak Boonrattanakij</u>, Jin Anotai, and Ming-Chun Lu (2009) Kinetics and
    mechanism of 2,6-dimethyl-aniline degradation by hydroxyl radicals. *Journal of
    Hazardous Materials*, 172, 952-957.

CONFERENCE PUBLICATIONS
1.   Jin Anotai, Pasootah Sakulkittimasak, <u>Nonglak Boonrattanakij</u>, and Ming-Chun
    Lu (2008) Kinetics of nitrobenzene oxidation in fluidized-bed Fenton process. *The
    2008- International Conference on Environmental Quality Concern, Control and
    Conservation*, Tainan, TAIWAN, May 23, 2008
2. <u>Nonglak Boonrattanakij</u>, Jin Anotai and Ming-Chun Lu (2009) Kinetics study on
    2,6-dimethyl-aniline degradation by Fenton oxidation process. *Royal Golden
    Jubilee (RGJ)–Ph.D. Congress X*, Chonburi, THAILAND, April 3-5, 2009.
3. <u>Nonglak Boonrattanakij</u>, Jin Anotai and Ming-Chun Lu (2009) Determination of
    the reaction rate constant of hydroxyl radicals in aqueous solution using Fenton
    process and competitive oxidation technique. *The 3rd IWA-ASPIRE Conference
    and Exhibition*, Taipei, TAIWAN, October 18-22, 2009.
4. Jin Anotai, Nakorn Panchanawaporn, <u>Nonglak Boonrattankij</u>, Ming-Chun Lu
    (2010) Kinetics of o-toluidine and 2,6-dimethyl-aniline oxidation by Fenton
    process. *The 2010 International Advanced Oxidation Processes (AOPs)
    Conference,* Taichung, TAIWAN, March 29-30, 2010.